ผลของการบดต่อการเกิดไคอะลูมินาจากกิบบ์ไซต์และการประยุกต์ใช้เป็นตัวรองรับสำหรับตัวเร่งปฏิกิริยาโคบอลต์

นายวสุ ไชยตรี

วิทยานิพนธ์นี้เป็นส่วนหนึ่งของการศึกษาตามหลักสูตรปริญญาวิศวกรรมศาสตรมหาบัณฑิต
สาขาวิชาวิศวกรรมเคมี ภาควิชาวิศวกรรมเคมี
คณะวิศวกรรมศาสตร์ จุฬาลงกรณ์มหาวิทยาลัย
ปีการศึกษา 2552

EFFECT OF MILLING ON THE FORMATION OF CHI-ALUMINA FROM GIBBSITE AND ITS APPLICATION AS COBALT CATALYST SUPPORT

Mr. Wasu Chaitree

A Thesis Submitted in Partial Fulfillment of the Requirements
for the Degree of Master of Engineering Program in Chemical Engineering
Department of Chemical Engineering
Faculty of Engineering
Chulalongkorn University
Academic Year 2009

Thesis Title	EFFECT OF MILLING ON THE FORMATION OF CHI-ALUMINA FROM GIBBSITE AND ITS APPLICATION AS COBALT CATALYST SUPPORT
By	Mr. Wasu Chaitree
Field of Study	Chemical Engineering
Thesis Advisor	Assistant Professor Joongjai Panpranot, Ph.D.
Thesis Co-Advisor	Assistant Professor Sirithan Jiemsirilers, Ph.D.

Accepted by the Faculty of Engineering, Chulalongkorn University in Partial Fulfillment of the Requirements for the Master's Degree

..... Dean of the Faculty of Engineering

(Associate Professor Boonsom Lerdhirunwong, Dr.Ing)

THESIS COMMITTEE

..... Chairman

(Professor Piyasan Praserthdam, Dr.Ing.)

..... Thesis Advisor

(Assistant Professor Joongjai Panpranot, Ph.D.)

..... Thesis Co-Advisor

(Assistant Professor Sirithan Jiemsirilers, Ph.D.)

..... Examiner

(Associate Professor Bunjerd Jongsomjit, Ph.D.)

..... External Examiner

(Assistant Professor Okorn Mekasuwandumrong, D.Eng.)

วสุ ไชยตรี: ผลของการบดต่อการเกิดไคอะลูมินาจากกิบบ์ไซต์และการประยุกต์ใช้เป็นตัวรองรับสำหรับตัวเร่งปฏิกิริยาโคบอลต์. (EFFECT OF MILLING ON THE FORMATION OF CHI-ALUMINA FROM GIBBSITE AND ITS APPLICATION AS COBALT CATALYST SUPPORT) อ. ที่ปรึกษาวิทยานิพนธ์หลัก :ผศ.ดร. จูงใจ ปั้นประณต,อ. ที่ปรึกษาวิทยานิพนธ์ร่วม:ผศ.ดร. ศิริธันว์ เจียมศิริเลิศ, 106หน้า.

วัตถุประสงค์ในงานวิจัยนี้คือการศึกษาผลของการบดต่อการเกิดไคอะลูมินาจากกิบบ์ไซต์และการประยุกต์ใช้เป็นตัวรองรับสำหรับตัวเร่งปฏิกิริยาโคบอลต์ บดกิบบ์ไซต์ขนาดละเอียด (เส้นผ่านจุดศูนย์กลางเฉลี่ย 13 ไมโครเมตร) เป็นเวลา 12 และ 24 ชั่วโมง และเผาที่อุณหภูมิที่แตกต่างกัน ระหว่าง 350 ถึง 600 องศาเซลเซียส ไคอะลูมินาบริสุทธิ์เกิดที่อุณหภูมิ 350 องศาเซลเซียส สำหรับกิบบ์ไซต์บด 24 ชั่วโมง ในกรณีที่ไม่บด โดยปกติอะลูมินาจะเกิดขึ้นเป็นเฟสผสมระหว่างแกมมาและไคอะลูมินา และค่าคงที่ของปฏิกิริยา (k) สำหรับการเปลี่ยนเฟสเพิ่มขึ้นในขณะที่ขนาดของอนุภาคของกิบบ์ไซต์ขนาดละเอียดลดลง สำหรับปฏิกิริยาไฮโดรจิเนชันของคาร์บอนมอนอกไซด์ ศึกษาไคอะลูมินาที่เตรียมจากวิธีข้างต้น วิธีโซลโวเทอร์มอล และแกมมาอะลูมินา ใช้เป็นตัวรองรับสำหรับตัวเร่งปฏิกิริยาโคบอลต์ ที่ภาวะเริ่มต้น โคบอลต์บนไคอะลูมินาเตรียมจากกิบบ์ไซต์ขนาดละเอียด ให้ค่าความว่องไวที่สูงกว่าตัวเร่งปฏิกิริยาอื่นๆ อย่างไรก็ตาม โคบอลต์บนไคอะลูมินาเตรียมจากวิธีโซลโวเทอร์มอล ให้ค่าความว่องไวที่สูงกว่าที่ภาวะคงตัว เนื่องจากอันตรกิริยาระหว่างอนุภาคโคบอลต์และตัวรองรับแข็งแรงกว่า และอนุภาคโคบอลต์มีความเสถียรบนพื้นผิวที่สูงกว่าซึ่งสังเกตได้จากการรีดักชันแบบโปรแกรมอุณหภูมิ และกล้องจุลทรรศน์อิเลคตรอนแบบส่องผ่าน นอกจากนี้ ค่าความว่องไวของตัวเร่งปฏิกิริยาโคบอลต์บนไคอะลูมินาให้ค่าสูงกว่าโคบอลต์บนแกมมาอะลูมินา

ภาควิชา.....วิศวกรรมเคมี..... ลายมือชื่อนิสิต.....วสุ ไชยตรี.....

สาขาวิชา.....วิศวกรรมเคมี..... ลายมือชื่อ อ.ที่ปรึกษาวิทยานิพนธ์หลัก.....

ปีการศึกษา .....2552..... ลายมือชื่อ อ.ที่ปรึกษาวิทยานิพนธ์ร่วม.....

#5170621721: MAJOR CHEMICAL ENGINEERING

KEYWORDS : MILLING/ GIBBSITE/ CHI-ALUMINA/ COBALT CATALYST/ CARBON MONOXIDE HYDROGENATION

WASU CHAITREE: EFFECT OF MILLING ON THE FORMATION OF CHI-ALUMINA FROM GIBBSITE AND ITS APPLICATION AS COBALT CATALYST SUPPORT. THESIS ADVISOR: ASST. PROF. JOONGJAI PANPRANOT, Ph.D., THESIS CO-ADVISOR: ASST. PROF. SIRITHAN JIEMSIRILERS, Ph.D., 106 pp.

The objective of this study is to investigate the effect of milling on formation χ-alumina from gibbsite and its application as cobalt catalyst support. Fine gibbsite (d_{50}=13μm) was milled in an attrition mill for 12 and 24 h and calcined at different temperatures in the range of 350 to 600°C. Pure χ-alumina was obtained at 350°C for the 24h-milled fine gibbsite. Without milling, the obtained alumina normally contained the mixed phases between γ and χ-phase alumina. The rate constant (k) for phase transformation increased as the particle size of fine gibbsite decreased. For CO hydrogenation, χ-alumina prepared from the above-mentioned method, solvothermal method, and γ-Al_2O_3 were used as support for cobalt catalyst. At initial conditions, the cobalt on χ-alumina prepared from fine gibbsite showed higher catalytic activity than other catalysts. However, the cobalt on χ-solvothermal performed higher activity at steady state conditions. It was due to stronger interaction between cobalt particles and support as well as more stable cobalt particles on the surface, which was observed by TPR and TEM. Additionally, the catalytic activity of both of Co/χ-Al_2O_3 was higher than that of Co/γ-Al_2O_3.

Department :	Chemical Engineering	Student's Signature	Wasu Chaitree
Field of Study :	Chemical Engineering	Advisor's Signature	Joongjai Pr
Academic Year :	2009	Co-Advisor's Signature	Sirithan J.

ACKNOWLEDGEMENTS

The author would like to express greatest gratitude to his advisor and co-advisor, Associate Professor Joongjai Panpranot for her invaluable suggestion and guidance throughout this study. Without the continuous guidance and comments from his co-advisor, Assistant Professor Sirithan Jiemsirilers, this work would never have been achieved. In addition, I would be also grateful to thank to Professor Piyasan Praserthdam who has been the chairman of the committee for this thesis, and Associate Professor Bunjerd Jongsomjit, Assistant Professor Okorn Mekasuwandamrong, members of the thesis committee for their kind cooperation. Moreover, I would be grateful to thank to Associate Professor Thawatchai Charinpanitkul who gives assistance in using a laser diffraction-based size analyzer.

Most of all, the author would like to express his highest gratitude to his parents who always pay attention to his all the times for their suggestions and have provided support and encouragements. The most success of graduation is devoted to his parents.

Moreover, the author wishes to thank all my friends and members of the Center of Excellent on Catalysis & Catalytic Reaction Engineering, Department of Chemical Engineering, Chulalongkorn University for their assistance and friendly encouragement. To the others, not specifically named, who have provided his with support and encouragement, please be assured that he thinks of you

.

Finally, the author would like to thank the Thailand Research Fund (TRF), as well as the Graduate School of Chulalongkorn University for their financial supports.

CONTENTS

Page

CHAPTER

Page

CHAPTER

Page

LIST OF TABLES

LIST OF FIGURES

CHAPTER I

INTRODUCTION

1.1 Rationale

Alumina (Al_2O_3) is one of the most common crystalline materials used as catalysts, catalyst supports, sorbent, coating and ceramics (Zolotovskii, 1983; Gitzen, 1970; Lacroix, 1986; Church, 1993). Compared to the other oxides, alumina has high surface area, good catalytic activity, high mechanical resistance, good thermal stability, high strength and toughness (Mekasuwandumrong, 2004, 2008; Pansanga, 2008). There are many methods to synthesize alumina such as solvothermal (Mekasuwandumrong, 2004; Pansanga, 2008), molten salt synthesis (He, 2005), shock wave action (Tsvigunov, 1999), sol-gel (Ahmad, 2007), spray pyrolysis (Kim, 2010) and thermal decomposition of aluminum hydroxide (boehmite and gibbsite) (Jang, 2000; Boumaza, 2009).

χ-Al_2O_3 is a crystallographic form of series of alumina which is normally obtained by dehydration of gibbsite (<200 nm) (Brindley, 1961; Stumpf, 1950). When it is fired, χ-Al_2O_3 will transform to κ-Al_2O_3 at temperature in range 650-750 $^{\circ}$C and consequently form α-Al_2O_3 at temperature around 1000 $^{\circ}$C. In our previous works, χ-Al2O3 has been used as catalysts and catalyst supports, which showed the interesting results. Khom-in *et al.* prepared nanocrystalline pure γ-Al_2O_3, χ-Al_2O_3 and mixed-phase Al_2O_3 and used it as the catalysts in dehydration reaction of methanol to dimethyl ether. Pansanga *et al.* used mixed γ- and χ- phase Al_2O_3, pure phases (γ) as supports and studied catalytic activities for CO hydrogenation of Co/Al_2O_3. Meephoka *et al.* prepared mixed (γ,χ) and pure phases of Al_2O_3 as supports, Pt/ Al_2O_3 catalysts were used in CO oxidation reaction. Nevertheless, the alumina in the mention above was prepared by solvothermal method. This technique required high pressure reactor and long reaction time.

The Fischer-Tropsch synthesis (FTS) was successfully carried out for future alternative resource instead of coal or crude oil. There are many active metals that can be used for hydrogenation of carbon monoxide (CO) to hydrocarbon such as ruthenium (Ru), iron (Fe), cobalt (Co), palladium (Pd), and etc. The cobalt catalysts have used for FTS because they can obtain high activity and selectivity and they have high resistance toward deactivation (Bae, 2009; Rojanapipatkul, 2008). Several researchers would like to increase activities for cobalt catalysts, thus, it is deposited on a high surface area support in order to obtain high dispersion. Many supports such as SiO_2 (Okabe, 2004), Al_2O_3 (Kogelbauer, 1996), TiO_2 (Tauster, 1978) have been studied for supported Co catalyst.

Gibbsite (α-$Al(OH)_3$) is widely used in transformation aluminas because it can be dehydrated to various phases ($\chi,\gamma,\theta,\kappa,\alpha$) (Samtos, 2000) and cheap starting material (Ogata, 2006). Figure 1.1 shows diagram of phase transformation from gibbsite. The transformation route is depended on temperature, heating environment, particle size of staring gibbsite and heating rate (I. N. Bhattacharya, 2004). For small particles (<1μm), the phase transformation process takes place by route 1 and gave χ-Al_2O_3 (Brindley, 1961). To reduce the particle sizes, many attentions have been paid to the grinding method because it is a simple process, presenting minimal environmental problems, convenient operation and absence of wastes.

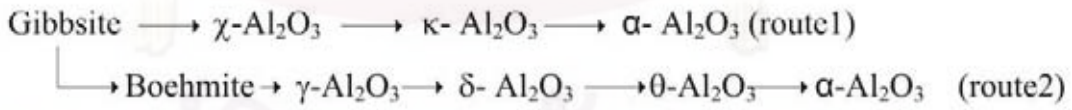

Figure 1.1. Transformation aluminas from gibbsite to α-alumina

Several researchers studied the crystallization of χ-Al_2O_3 from gibbsite. For examples, Jang *et al.* studied the effect of grinding on transition of gibbsite, they ground gibbsite (64.2μm) for 0.5 to 12 h in a planetary mill. For a sample milled for 30 min, the decomposition reaction of gibbsite occurred by route 2 (Figure 1), however, the ground

samples (9.7μm) for 5 h, χ-Al_2O_3 was observed at 450 °C and completed at around 910 °C. According to Bhattacharya *et al.* presented thermal decomposition of fine (1.5μm) gibbsite. At 500 °C, χ-Al_2O_3 formation was observed and its crystal remained form at around 800 °C.

In this study, χ-Al_2O_3 was synthesized by thermal decomposition of gibbsite because it spent short time producing product and gave the large amount of product. Effect of milling time and starting particle sizes of gibbsite on the properties of χ-Al2O3 were investigated by a laser diffraction-based size analyzer, XRD, TGA/DTA, N_2 physisorption, TEM and isothermal kinetic measurement. The properties of cobalt as a catalytic phase for CO hydrogenation reaction were investigated. The samples were prepared and characterized by several techniques, such as BET, XRD, TEM, TPR, XPS and CO chemisorption. The reaction study of CO hydrogenation was carried out in order to measure activity and product selectivity under methanation condition.

1.2 Objective

The objective of this research is to investigate the effect of milling on the formation of χ-Al_2O_3 from gibbsite and cobalt based χ-Al_2O_3 support catalyst for CO hydrogenation regarding CO conversion and selectivity.

1.3 Research scopes

- Preparation of χ-Al_2O_3 from 12h-milled, 24h-milled and unmilled fine gibbsite.
- Characterization of the χ-Al_2O_3 sample by BET surface area, X-ray diffraction (XRD), transmission electron spectroscopy (TEM), laser diffraction-based size analyzer, thermogravimetric and differential thermal analysis (TG-DTA).
- Measurement of isothermal kinetic for phase transformation from gibbsite to χ-Al_2O_3

- Preparation of supported Co catalyst on the χ-Al_2O_3 supports (20 wt% Co) using the incipient wetness impregnation method.
- Characterization of the catalyst samples using BET surface area, X-ray diffraction (XRD), temperature programmed reduction (TPR), carbon monoxide chemisorptions, X-ray photoelectron spectroscopy (XPS) and transmission electron spectroscopy (TEM).
- Investigation of the catalytic activity of Co/χ-Al_2O_3 catalyst in the hydrogenation of carbon monoxide (CO) at 220°C and 1 atm and a H_2/CO ratio of 10 under methanation condition. The catalytic activity of Co/χ-Al_2O_3 compared with that of cobalt catalyst on χ-Al_2O_3 prepared from solvothermal method and cobalt catalyst on γ-Al_2O_3 (commercial).

1.4 Research Methodology

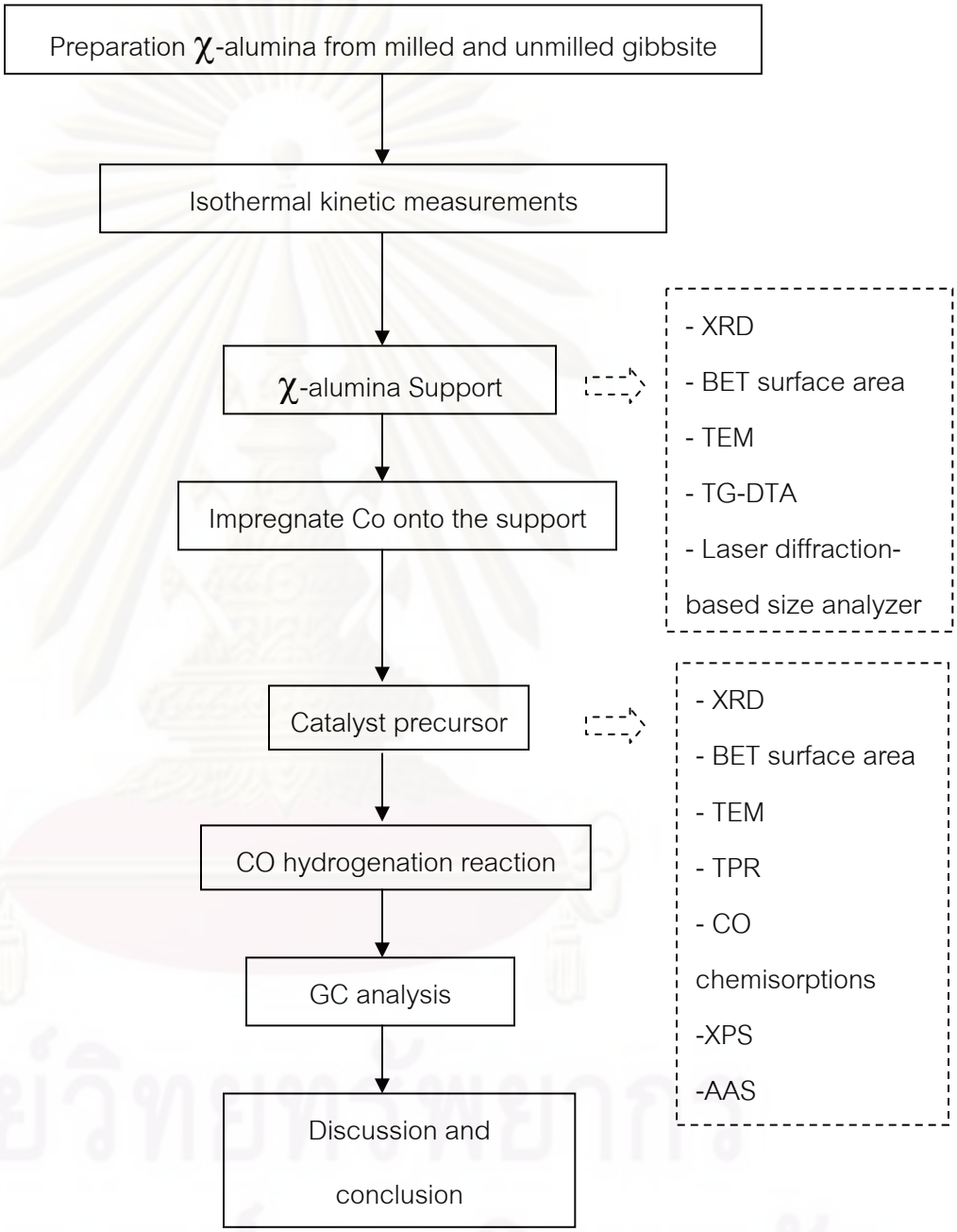

CHAPTER II

THEORY

2.1 Fischer-Tropsch synthesis (FTS)

Fischer-Tropsch synthesis (FTS) or CO hydrogenation reaction is important method to produce synthesis gases (CO and H_2) to liquid hydrocarbons, developing route for environmentally sound production of chemicals and fuels from coal and natural gas. This synthesis is basically the reductive polymerization (oligomerization) of carbon monoxide by hydrogen to form organic products containing mainly hydrocarbons and some oxygenated products in lesser amounts. The main reactions of FTS are:

$$CO + 3H_2 \rightarrow CH_4 + H_2O \quad (2.1)$$

$$CO + 2H_2 \rightarrow (\frac{1}{n})(C_nH_{2n}) + H_2O \quad (2.2)$$

$$CO + H_2O \rightarrow CO_2 + H_2 \quad (2.3)$$

$$2CO \rightarrow C + CO_2 \quad (2.4)$$

Equations (2.1) is the formation of methane, the equation (2.2) is the synthesis of hydrocarbons higher than methane, the equation (2.3) is the water-gas shift reaction, and the equation (2.4) is the Boudouard reaction resulting in which results in deposition of carbon. The reaction mechanism of methanation can be described by the following set of mechanism:

$$CO + * = CO^*$$

$$CO^* + * = C^* + O^*$$

$$H_2 + 2^* = 2H^*$$

$$C^* + H^* = CH^* + *$$

$$CH^* + H^* = CH_2^* + *$$

$$CH_2^* + H^* = CH_3^* + *$$

$$CH_3^* + H^* = CH_4(g) + 2^*$$

$$O^* + H^* = OH^* + *$$

$$OH^* + H^* = H_2O(g) + 2^*$$

Normally, catalysts used for FTS are group VIII metals. By nature, the hydrogenation activity increases in order of Fe < Co < Ni < Ru. Ru is the most active. Ni forms predominantly methane, while Co yields much higher ratios of paraffins to olefins and much less oxygenated products such as alcohols and aldehydes than Fe does.

Commercially, Entrained bed reactors or slurry bubble column reactors are used in FTS since they can remove heat from this exothermic synthesis, allowing better temperature control.

The current main goal in FTS is to obtain high molecular weight, straight chain hydrocarbons. However, methane and other light hydrocarbons are always present as less desirable products from the synthesis. According to the Anderson-Schulz-Flory (ASF) product distribution, typically 10 to 20% of products from the synthesis are usually light hydrocarbon (C_1-C_4). These light alkanes have low boiling points and exist in the gas phase at room temperature, which is inconvenient for transportation. Many attempts have been made to minimize these by-products and increase the yield of long chain liquid hydrocarbons by improving chain growth probability. It would be more efficient to be able to convert these less desirable products into more useful forms, rather than re-reforming them into syngas and recycling them (Farrauto and Bartholomew, 1997). Depending upon the type of catalyst used,

promoters, reaction conditions (pressure, temperature and H_2/CO ratios), and type of reactors, the distribution of the molecular weight of the hydrocarbon products can be noticeably varied.

2.2 Aluminium Oxides or Alumina (Al_2O_3)

Aluminum oxides, which are a term of alumina compounds, can exist in many metastable phase before transforming to the stable α-alumina (corundum from). There are six principle phase designated by The Greek letters Chi (χ), kappa (κ), eta (η), theta (θ), delta (δ) and gamma (γ). The nature of the product obtained by calcinations depends on the starting hydroxide (Gibbsite, boehmite and others) and on the heat treatment conditions. Normally, transition alumina starts to lose their surface area even at temperature below 800°C due to the elimination of micro-pores. However, drastic loss occurs at temperature higher than 1000°C when the crystallization to the thermodynamically stable α-alumina occurs (Dynys, 1982).

Several studies have been carried out on the direct phase transformation of alumina. Especially, the mechanism of direct phase transformation from gibbsite to α-alumina is widely studied. The phase transformation of alumina depends on starting material, the transition temperature, water vapor and impurity (Gitzen, 1970). Gibbsite has been used as starting material in order to form various alumina phases. **Figure 2.1** shows thermal transformation of different types of starting material.

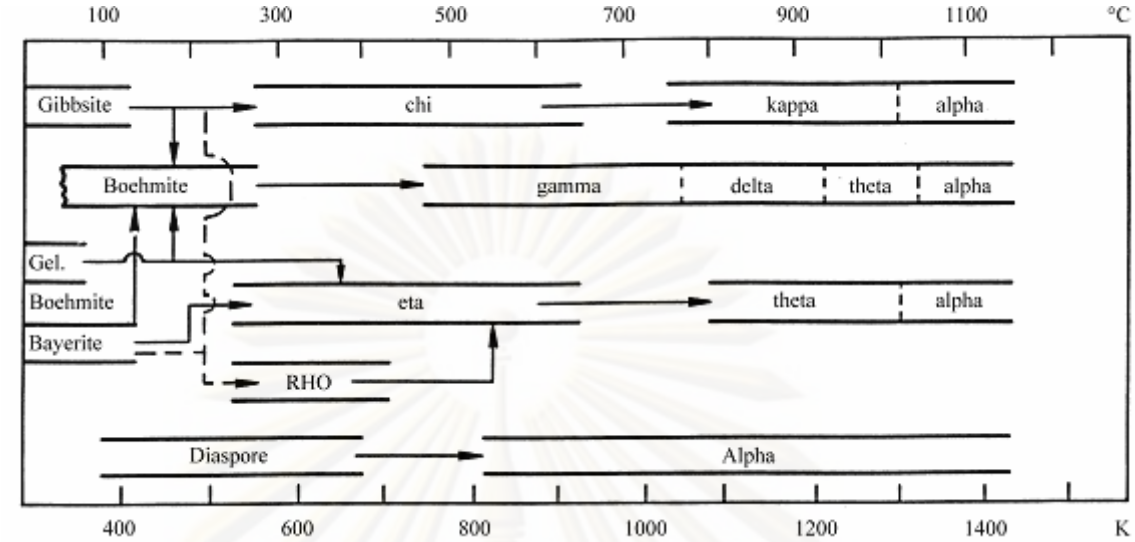

Figure 2.1 Thermal transformation of different types of starting material. (Santos, 2000)

In general, gibbsite can be dehydrated to χ-, κ-, θ-, δ-, γ-, and α-phase. The route of transformation to α-alumina is divided to two parts, route 1 is gibbsite to χ- to κ- to α-alumina and route 2 is gibbsite to boehmite to γ- to δ- to θ- to α-alumina. The transformation of structures depends on temperature, heating environment, particle size of staring gibbsite and heating rate (Bhattacharya, 2004). According to Gitzen, in vacuum, coarse or fine gibbsite transforms to rho (100-400°C), to eta (270-500°C), to theta (870-1150°C), to alpha alumina (1150°C). For instantaneous dehydration at 800°C, gibbsite forms to eta, to theta, to alpha alumina.

2.3 Cobalt (Young 1960; Othmer, 1991)

2.3.1 General

Cobalt, a transition series metallic element having atomic number 27, is similar to silver in appearance.

Cobalt and cobalt compounds have expended from use colorants in glasses and ground coat fits for pottery to drying agents in paints and lacquers, animal and human nutrients, electroplating materials, high temperature alloys, hard facing

alloys, high speed tools, magnetic alloys, alloys used for prosthetics, and used in radiology. Cobalt is also as a catalyst for hydrocarbon refining from crude oil for the synthesis of heating fuel.

2.3.2 Physical Properties

The electronic structure of cobalt is [Ar] $3d^7 4s^2$. At room temperature the crystalline structure of the α (or ε) form, is close-packed hexagonal (cph) and lattice parameters are a = 0.2501 nm and c = 0.4066 nm. Above approximately 417°C, a face-centered cubic (fcc) allotrope, the γ (or β) form, having a lattice parameter a = 0.3554 nm, becomes the stable crystalline form

The scale formed on unalloyed cobalt during exposure to air or oxygen at high temperature is double-layered. In the range of 300 to 900°C, the scale consists of a thin layer of mixed cobalt oxide, Co_3O_4, on the outside and cobalt (II) oxide, CoO, layer next to metal. Cobalt (III) oxide, Co_2O_3, may be formed at temperatures below 300°C. Above 900°C, Co_3O_4 decomposes and both layers, although of different appearance, are composed of CoO only. Scales formed below 600°C and above 750°C appear to be stable to cracking on colling, whereas those produced at 600-750°C crack and flake off the surface.

Cobalt forms numerous compounds and complexes of industrial importance. Cobalt, atomic weight 58.933, is one of the first transition series of Group 9 (VIIIB). There are thirteen know isotope, but only three are significant: ^{59}Co is the only stable and naturally occurring isotope; ^{60}Co has a half-life of 5.3 years and is a common source of γ-source for MÖssbauer spectroscopy.

Cobalt exists in the +2 or +3 valance states for the major of its compounds and complexes. A multitude of complexes of the cobalt (III) ion exists, but few stable simple salt are know. Octahedral stereochemistries are the most common for cobalt (II) ion as well as for cobalt (III). Cobalt (II) forms numerous simple compounds and complexes, most of which are octahedral or tetrahedral in nature; cobalt (II) forms more tetrahedral complex than other transition-metal ions. Because of the small stability

difference between octahedral and tetrahedral complexes of cobalt (II), both can be found equilibrium for a number of complexes. Typically, octahedral cobalt (II) salts and complexes are pink to brownish red; most of the tetrahedral Co (II) species are blue.

Table 2.1 Physical properties of cobalt (Othmer, 1991)

Property	Value
atomic number	27
atomic weight	58.93
transformation temperature, ^{o}C	417
heat of transformation, J/g[a]	251
melting point, ^{o}C	1493
latent heat of fusion, ΔH_{fus} J/g[a]	395
boiling point, , ^{o}C	3100
latent heat of vaporization at bp, ΔH_{vap} kJ/g[a]	6276
specific heat, J/(g·^{o}C)[a]	
15-100°C	0.442
molten metal	0.560
coefficient of thermalexpansion, $^{o}C^{-1}$	
cph at room temperature	12.5
fcc at 417°C	14.2
thermal conductivity at 25 ^{o}C, W/(m·K)	69.16

Table 2.1 Physical properties of cobalt (cont.)

Property		Value	
thermal neutron absorption, Bohr atom		34.8	
resistivity, at 20 °C[b], $10^{-8}\Omega\cdot m$		6.24	
Curie temperature, °C		1121	
saturation induction, $4\pi I_s$, T[c]		1.870	
permeability, μ			
initial		68	
max		245	
residual induction, T[c]		0.490	
coercive force, A/m		708	
Young's modulus, Gpac		211	
Poisson's ratio		0.32	
Hardness[f], diamond pyramid, of %Co		99.9	99.98[e]
At 20 °C		225	253
At 300 °C		141	145
At 600 °C		62	43
At 900 °C		22	17
strength of 99.99 %cobalt, MPa[g]	as cast	annealed	sintered
tensile	237	588	679
tensile yield	138	193	302
compressive	841	808	
compressive yield	291	387	

[a] To convert J to cal, divided by 4.184.

[b] conductivity = 27.6 % of International Annealed Copper Standard.

[c] To convert T to gauss, multiply by 10^4.

[d] To convert GPa to psi , multiply by 145,000.

[e] Zone refined.

[f] Vickers.

[g] To convert MPa to psi , multiply by 145.

2.3.3 Cobalt Oxides

Cobalt has three well-know oxides:

Cobalt (II) oxide, CoO, is an olive green, cubic crystalline material. Cobalt (II) oxide is the final product formed when the carbonate or the other oxides are calcined to a sufficiently high temperature, preferably in a neutral or slightly reducing atmosphere. Pure cobalt (II) oxide is a difficult substance to prepare, since it readily takes up oxygen even at room temperature to re-form a higher oxide. Above about 850°C, cobalt (II) oxide form is the stable oxide. The product of commerce is usually dark gray and contains 77-78 wt % cobalt. Cobalt (II) oxide is soluble in water, ammonia solution, and organic solvents, but dissolves in strong mineral acids. It is used in glass decorating and coloring and is a precursor for the production of cobalt chemical.

Cobalt (II) oxide, Co_2O_3, is form when cobalt compounds are heated at a low temperature in the presence of an excess of air. Some authorities told that cobalt (III) oxide exists only in the hydrate form. The lower hydrate may be made as a black power by oxidizing neutral cobalt solutions with substances like sodium hypochlorite. Co_2O_3 or $Co_2O_3.H_2O$ is completely converted to Co_3O_4 at temperatures above 265°C. Co_3O_4 will absorb oxygen in a sufficient quantity to correspond to the higher oxide Co_2O_3.

Cobalt oxide, Co_3O_4, is formed when cobalt compounds, such as the carbonate or the hydrated sesquioxide, are heated in air at temperatures above approximately 265°C and not exceeding 800°C.

2.4 Co-based catalysts

Supported cobalt (Co) catalysts are the preferred catalysts for the synthesis of heavy hydrocarbons from natural gas based syngas (CO and H_2) because of their high Fischer-Tropsch (FT) activity, high selectivity for linear hydrocarbons, and low activity for the water gas shift reaction. It is known that reduced cobalt metal, rather than its oxides or carbides, is the most active phase for CO hydrogenation in such catalysts. Investigations have been done to determine the nature of cobalt species on various supports such as alumina, silica, titania, magnesia, carbon, and zeolites. The influence of various types of cobalt precursors used was also investigated. It was found that the used of organic precursors such as Co (III) acetyl acetate resulting in an increase of CO conversion compared to that of cobalt nitrate (Kraum and Baerns, 1999).

2.5 Milling/Grinding

Size reduction of particulate solids by milling is an essential unit operation in many industrial sectors such as chemical, metallurgy, pharmaceutical, nuclear and food. Recently, the increasing use of powders with particle sizes smaller than those achieved by conventional production methods emphasizes the importance of milling in powder. Compared with other methods, ball milling has the advantages of being a cheap method, simple process, presenting minimal environmental problems, convenient operation and absence of wastes. Energy absorbed by the material on impact may result in a modification of the particle surfaces by introducing dislocations, point defects, and other structural defects. This leads to materials with increased surface free energy, which makes them more reactive.

In many last years, mechanical processing is a novel technique for preparation of nanostructured materials. This includes vibratory ball mills, attrition mills, tumbler ball mills, and rod and hammer mills. A choice between these is determined by the end results required, and the chemical and physical properties of the powder.

Stirred-ball attrition mills (**Figure 2.2**) are widely used for fine grinding of various materials in the industry as they are most efficient and effective in reducing particle size among grinding media-based compression shear type mills, moreover, they are ideally appropriate for the industrial process due to their high efficiency and availability in large scale. In addition, their superior advantages are the fast grinding, proficient temperature control and simple operation. The reduction of particle size by milling in liquids is a useful technique because fine grinding could be done effectively in wet atmosphere. It was found possible to reduce the grain size of particles to the nanometer range with the stirred-ball attrition mill. The feed material is comminuted among the moving media, the stirrer and the grinding chamber wall by friction, impact, and compression forces. The dominant breakage mechanism is based on the impact effect. Milling action is caused by a vertical rotating rod with horizontal arms or 'lifters' which stirs the balls causing them to lift up and fall back. There is thus a differential movement between the balls and the milled material, giving a high degree of surface contact. Milling, achieved by impact and shear forces, is very intensive because the force restoring the media downward is the weight of all media above it (PM technology focus, 1996).

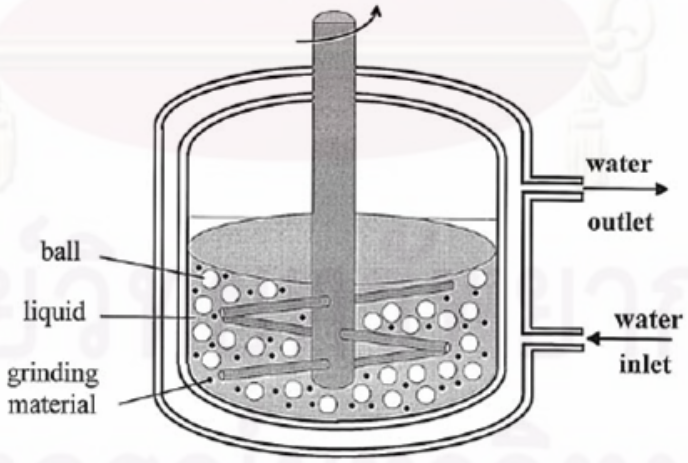

Figure 2.2 Schematic drawing of laboratory stirred-ball mill (Shinohara *et al.*, 2002)

Currently, ball milling is used in a variety of applications, including dispersed alloy materials, metallic refinery, ore treatment, waste disposal, and synthesis of organic materials.

CHAPTER III

LITERATURE REVIEW

CO hydrogenation is a well-known catalytic reaction used to produce hydrocarbon fuels. Generally, supported cobalt catalyst is employed for this process due to its good activity and selectivity. Moreover, several factors have shown to affect the performance of Co catalysts for CO hydrogenation such as preparation method, addition of a second metal, type of supports.

3.1 Phase transformation of alumina from gibbsite

Tonejc *et al.* (1994) presented transformation of boehmite and gibbsite by using high energy milling. The milling was performed in the planetary mill, using 10 tungsten carbide (WC) balls and a vial of the same material. XRD data indicated that ground gibbsite for 7 h and boehmite milled for 2.5 h can produce α-alumina.

MacKenzie *et.al* (1999) studied thermal decomposition of mechanically activated gibbsite to α-alumina. Gibbsite was ground for 20 h in a planetary mill. Gringing results in breaking a proportion of the Al-OH bonds. XRD patterns of unground gibbsite showed that α-alumina can be formed via γ and θ-alumina. In the other hand, for ground gibbsite, α-alumina took placed via γ-alumina at 900 $^{\circ}$C.

Jang *et al.* (2000) studied about effect of grinding on transition of gibbsite to α-Al_2O_3, they ground gibbsite for 0.5 to 12 h in a planetary mill and the sample was heated at temperature in range 450-1200 $^{\circ}$C. For a sample milled for 30 min was calcined, boehmite was observed after heating to 450 $^{\circ}$C and γ-Al_2O_3 after heating to 650 $^{\circ}$C. Beyond 910 $^{\circ}$C, a mixture of δ- Al_2O_3 and θ- Al_2O_3 took place.

However, the ground samples for 5 h, χ-alumina happened at 450 ^{o}C and completed at around 910 ^{o}C. For ground gibbsite for 8 h, χ-alumina started at 650 ^{o}C. At around 910 ^{o}C, the formation of κ-alumina was observed. Temperature of calcination in order to transform gibbsite to α-Al_2O_3 decreased from 1250°C before milling to about 1000 ^{o}C after milling 8 h.

Kano *et al.* (2000) studied effect of dry grinding of gibbsite powder, with and without fine α-alumina powder as a seed on reduction in transformation to alpha phase in a planetary mill for 15-120 min. The samples were heat at temperature in range 800-1200°C for 2h. The phase transformation temperature of samples was determined by DTA and XRD. The result showed that the transformation temperature to α-Al_2O_3 decreased from 1350 ^{o}C to 1100 ^{o}C when gibbsite was milled for 15 min. Besides, the sample was ground for 60 min, temperature decreased about to 1020 ^{o}C. Addition of the seed made an effect on reduction in transformation temperature. The temperature is reduced to 910 ^{o}C by milling gibbsite with 50% of seed powder.

Santos et al. (2000) studied standard transition aluminas from electron microscopy. The shape of six standard transition aluminas (chi, kappa, gamma, theta, delta) was investigated by TEM and SEM. XRD was used for confirmation of types of alumina. The six samples were supplied by ALCOA Central Laboratory. The result showed that (a). chi-alumina crystals are pseudomorphs from pseudohexagonal plates of gibbsite (b). kappa-alumina crystals are platy irregular crystals (c). gamma-alumina crystals are pseudomorphs from rhombs or lozenge platy crystals (d). delta-alumina crystals are pseudomorphs from rhombs of gamma-alumina (e). theta-alumina crystals are agglomerates of round particles (f). eta-alumina are agglomerates of small round particles.

Bhattacharya *et al.* (2004) studied thermal decomposition of fine and coarse gibbsite. The fine (1.5μm) and coarse (100μm) gibbsite were subjected to dehydration at various temperatures. XRD, DTA, FTIR were used in investigating

properties of transition aluminas. For fine gibbsite, boehmite phase started at 250 °C and completed its transformation at 400 °C. Beyond 400 °C, various phases were formed. At 500 °C, χ-alumina was observed; κ-alumina was formed at 900 °C and completed its phase at 1000 °C. α-alumina was found at 1400 °C. Coarser particle followed the similar trend. Moreover, α-alumina took place at 1200 °C. FTIR spectra showed the presence of molecular water and Al-O bonds in gibbsite. Wave length at 3098, 2099 and 1070 cm^{-1} was observed for boehmite phase at 400 °C.

Okata *et al.* (2006) studied structure transformation of gibbsite by calcination. Gibbsite was calcined in the temperature range from 200 to 1150 °C. TG-DTA experiment showed that the structure of gibbsite changed at 282.7 °C. In this temperature, it loses most of the molecular water. From XRD data, at 200 °C, the gibbsite is the same as that of original structure and its structure was destroyed when temperature was 300 °C. Boehmite and amorphous alumina was observed at 400 °C. Besides, the calcination temperature is higher than 1000 °C, gibbsite transformed to stable aluminum oxide. The specific surface area of sample becomes maximum when the calcination temperature is 400 °C. The specific surface area decreased as the calcination temperature is raised in the range over 400 °C.

Hill *et al.* (2007) studied calcination cycle from gibbsite to corundum. Gibbsite (98.7μm) was prepared by soak calcinations in flowing air for 2 h across the range of 100-1200 °C at 100 °C increment. XRD data indicated that the transition from gibbsite to boehmite is observed at 300 °C. The small amount of χ-phase took place at this point. At 500 °C, γ-alumina is formed and completed at around 800 °C. δ-, θ-phase becomes prominent above 900 °C. α-alumina starts at 1000 °C and becomes fully established by 1200 °C. The ^{27}Al MAS NMR showed that gibbsite structure contains two octahedrally coordinated (AlO_6). The structure of boehmite consists of one octahedrally coordinated aluminum site, the ^{7}Al spectra at 300 °C and 400 °C indicates

a 10-12% AlO_4. The γ-phase contains AlO_4 and AlO_6 (with maxima at 65 and 10 ppm shift, respectively).

Vieira *et al.* (2007) synthesized a new gibbsite by reaction between aluminum powder and water having iodine as activator. It formed gibbsite (called "I-gibbsite"). Gibbsite characterization was investigated by XRD, DTA, TEM and N_2 adsorption method. I-gibbsite (**Figure 3.1**) constituted by thin hexagonal plates, 0.2 to 0.6 μm in diameter, 32 nm thick which corresponds to 66 gibbsite layers and with specific areas of 29 m^2/g. The I-gibbsite was fired between 200-1500 ^{o}C, produced χ-alumina at 300 ^{o}C. The maximum value of 347 m^2/g of surface area was obtained in this temperature. χ-alumina can form in 200-900 ^{o}C, κ-alumina started at temperature in range 900-1000 ^{o}C and α-alumina can take place in 1000-1500 ^{o}C. In contrast, the gibbsite form Bayer process, produced χ-alumina, κ-alumina, α-alumina in 273, 753 and 1020 ^{o}C, respectively. **Figure 3.2** show thermal transformation series between Bayer gibbsite and I-gibbsite.

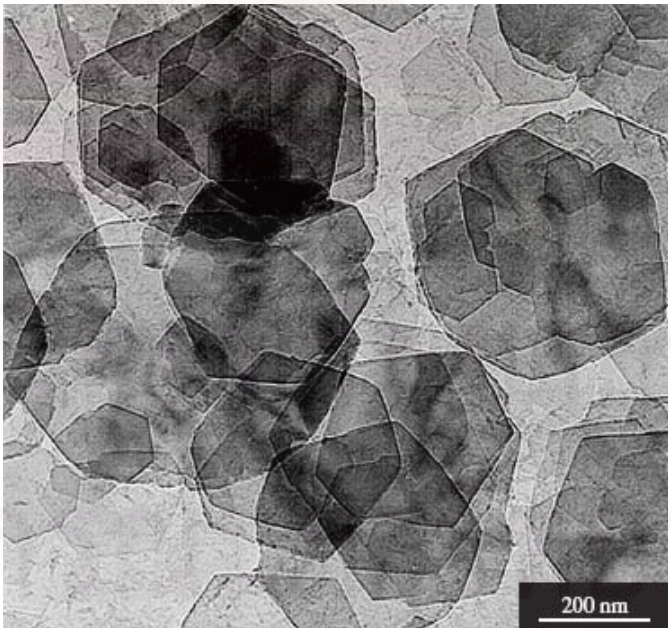

Figure 3.1 TEM of I-gibbsite

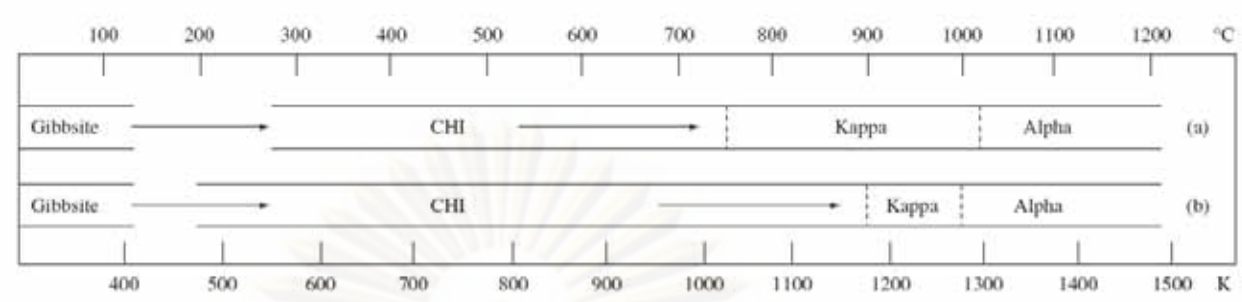

Figure 3.2 Thermal transformation series between Bayer gibbsite and I-gibbsite. (a) Bayer gibbsite (b) I-gibbsite

3.2 Effect of Al_2O_3 supported cobalt catalyst in Fischer-Tropsch synthesis

Xiong *et al*. (2005) presented effect of porosity of Al_2O_3 on the performance of Co/ Al_2O_3 for Fischer-Tropsch synthesis (FTS). γ-Al_2O_3 was calcined at various temperatures (450, 600, 800°C) to obtain the supports with different pore size. Co/Al_2O_3 was prepared by incipient wetness impregnation method. All catalysts contained 15% Co loading and were investigated by XRD, TPR, H_2-TPD. BET data showed that increasing calcination temperature, the surface area of supports decreased and pore size increased. Average Co_3O_4 diameter data for Co/Al_2O_3 catalysts was calculated from Scherrer equation. The Co_3O_4 diameter decreased with increasing calcination temperature of supports. TPR profile showed typical reduction behavior of Co/Al_2O_3 ($Co_3O_4 \rightarrow CoO \rightarrow Co$) of three kinds of catalysts. For the performance of catalysts on FTS, it can be seen that with increasing pore size, CO conversion and C_{5+} decreased as well as the formation of CH_4 increased.

Xu *et al*. (2005) studied FTS by using Co/Al_2O_3 and noble metal (Pt, Ru, and Pd) promoted Co/Al_2O_3. All catalysts were prepared by impregnation method and characterized by XRD, TPR, H_2-TPD. The catalytic activities of cobalt catalysts follow the order Co-Pt/ Al_2O_3> Co-Ru/ Al_2O_3> Co-Pd/ Al_2O_3> Co/ Al_2O_3. Compared with Ru/Al_2O_3, Pt/Al_2O_3, Pd/Al_2O_3, these catalysts displayed much lower CO conversion. It pointed out that the promoted Co/Al_2O_3 catalysts are attributed to the pronounced

catalytic synergistic effect between Co and noble metal. Moreover, the promoted catalysts resulted in decreasing the methane selectivity and increasing C_{5+} selectivity. The BET surface area data show that the addition of noble metal to Co/Al_2O_3 catalysts had higher surface area than Co/Al_2O_3. The TPR profile showed that the reduction temperature of both Co_3O_4 and Co surface species decreased when the noble metal was promoted in Co/Al_2O_3. H_2-TPD results indicated that the amount of chemisorbed hydrogen was enhanced and the bond strength of Co-H was weakened after the addition of noble metal.

Mikhailova *et al*. (2007) synthesized mixed oxides Co_xAl_yO with different ratios of Co/Al. They were used as catalysts for FTS and prepared by solid-state chemical reaction. The supports (Co_xAl_yO) were prepared by modifying gibbsite with various cobalt salts (acetate, nitrate, carbonate). All catalysts contained 20% Co loading and were prepared by double impregnation of support with an aqueous solution of cobalt nitrate. Only Co(20%)/Co_xAl_yO catalyst based on gibbsite and cobalt carbonate was modified by addition of Pd, Ru, and Re. The Co(30%)/Al_2O_3 catalyst was used as the reference catalyst. XRD patterns show that supports contained six reflections feature of crystalline Co_xAl_yO. Compared to the Co(30%)/Al_2O_3 catalyst, the presence cobalt in supports resulted in higher yield of hydrocarbons C_{5+} and selectivity. The highest yield of hydrocarbon C_{5+} was observed when cobalt carbonate was used as a modifying additive. When catalyst was modified with Pd, Ru, and Re, the catalysts promoted by Ru, Re increased the yield of hydrocarbons C_{5+} whereas the yield of the C_{5+} decreased in the Pd modified catalyst. Moreover, the introduction of Pd and Ru decreased the selectivity regarding hydrocarbons C_{5+} from 90 (absence of promoter) to 76 (modified with Pd) and 84% (modified with Ru), respectively. Thus, Re is the best promoter for this study. When catalyst was modified with various contents of Re (0.1, 0.3, 0.5, and 0.7wt%), yield of hydrocarbons C_{5+} and selectivity increased up to 0.3 wt% and declined at 0.5 wt%.

Tristantini *et al*. (2007) studied the FTS using different synthesis gas over Al_2O_3 supported Co catalyst with and without Re as a promoter. The catalysts containing 12wt% Co and 0 or 0.5%wt Re were prepared by wetness co-impregnation. The addition of Re resulted in increasing the dispersion and decreasing BET surface area. Besides, they presented effect of inlet H_2/CO varied (1.0, 1.5, 2.1) in feed on reaction. For catalysts Co/γ-Al_2O_3 (A) and Co-Re/ γ--Al_2O_3 (B), the conversion of CO and syngas conversion to HCs increased with increasing H_2/CO ratio and with reducing GHSV. The space time yield (mol CO/g $_{cat}$, h) decreased when ratio was shifted from 2.1 to 1.5. A smaller activity decrease was observed when shifting from 1.5 to 1.0 for both catalysts. The Re-promoted catalyst is more active than the un-promoted any inlet H_2/CO ratio.

Burakorn *et al.* (2008) studied effect of mixed nano-Al_2O_3-ZrO_2 supports on the dispersion of Co for CO hydrogenation. The nano-Al_2O_3-ZrO_2 were prepared by the solution mixing and varied weight ratios between 0 to 100%. The XRD patterns showed peaks of mixed nano-Al_2O_3-ZrO_2 . TEM illustrated that size of Al_2O_3 was larger and less uniform whereas the size of ZrO_2 was smaller and more uniform. In the reaction study, the presence of ZrO2 in the mixed supports could result in the low number of active Co metal atoms as detected using H_2 chemisorption due to a strong support interaction. However, the chain growth probability was found to increase with the presence of the nano-ZrO_2 in the mixed nano-Al_2O_3–ZrO_2 support. The TPR profiles indicated that Co oxides dispersed on the pure Al_2O_3 showed the lowest reduction temperature than those on mixed nano-Al_2O_3–ZrO_2 support.

Pansanga *et al*. (2008) studied effect of mixed γ- and χ- crystalline phases in nanocrystalline Al_2O_3 on the dispersion of Co on alumina for CO hydrogenation. Al_2O_3 supports (γ-Al_2O_3, mixed γ- and χ- Al_2O_3) were synthesized by decomposition of aluminum isopropoxide (AIP) under solvothermal conditions. The catalysts were characterized by XRD, N_2 physisorption, TEM, and H_2 chemisorption. It

was found that when lower amounts of AIP (10 and 15 g in 100 cm^3 of 1-butanol) were used, only γ-alumina was observed by calcinations. χ-Al_2O_3 was formed when higher amounts of AIP (25 and 35 g in 100 cm^3 of 1-butanol) were used. The mixed γ- and χ-crystalline phases were happened in this condition and the samples contained χ-phase 33% and 57%, respectively. The BET surface areas increased with increasing amount of AIP. Increasing Co loading from 5 to 20 wt% for the mixed phase Al_2O_3-supported Co catalysts resulted in higher dispersion of Co and higher CO hydrogenation activities. However, for γ- Al_2O_3 support, Co dispersion increased up to 15 wt% and declined at 20 wt%.

Rojanapipatkul *et al*. (2008) synthesized of Co on cobalt-aluminate via solvothermal method. The catalyst was prepare using the mixture of AIP and cobalt (II) acetyacetonate that depended on Co/Al molar ratio (0.5, 1, 2) and varied holding time (1, 2h). The result showed that the surface area increased with increasing Co/Al molar ratio, it was due to agglomeration of the larger amounts of cobalt oxide formed. The holding time during solvothermal made a little effect on surface area. SEM micrograph showed that Co was well distributed on the catalyst surface. The degree of dispersion decreased with increasing holding time as well as increased Co/Al. TPR profiles of samples (Co/Al=2, holding time=1, 2h) showed one reduction peak below 400°C and assigned to the overlap of two steps of reduction $Co_3O_4 \rightarrow CoO \rightarrow Co$. The reduction peak at high temperature (>600°C) can be assigned to the reduction of non-stoichomertric cobalt-aluminate. However, the lower Co/Al molar ratio, reduction peak below 400°C did not be observed. Thus, increased Co/Al molar ratios resulted in increasing Co_3O_4 species. No significant change on the reaction behaviors on changing the holding time was observed. For CO hydrogenation, increased Co/Al molar ratios of Co on cobalt-aluminate catalyst resulted in increased activity without changing the product selectivity whereas the holding time seemed to have only little effect on the activites on the high molar ratio Co/Al. Nevertheless, at Co/Al=0.5, the increased holding time can result in decreased activity.

Bae et al.(2009) studied effect of phosphorous modification of γ-Al_2O_3 support (P-Al_2O_3). They varied different concentration of phosphorous from 0 to 5%wt. Then, 20%wt.cobalt was load on P-Al_2O_3. The BET surface area increased with increasing phosphorous content. The maximum value was 222.1 m^2/g when phosphorous content was 2%wt. The cluster size of Co_3O_4 decreased and TPR profile showed that the first peak shifted toward lower temperature when phosphorous content increased. From FTS activity showed that the cobalt-impregnated catalyst on P- Al_2O_3 support with an appropriate amount of phosphorous (1-2%) showing a high activity (CO conversion and C_{5+} selectivity). It was attributed to the good dispersion of cobalt species with high reducibility and their homogeneous distribution. The phosphorous content resulted in the low interaction between cobalt and phosphorous-modified surface by the partial transformation of γ-Al2O3 surface to aluminum phosphate and the suppressed sintering phenomena of redispersed cobalt species by the localized presence of aluminum phosphate.

3.3 Comments on previous studies

In our previous works, alumina was used as catalysts and supports. In CO hydrogenation, the mixed γ- and χ- phase Al_2O_3, pure phases (γ) were used as supports for preparationa of Co/Al_2O_3 catalysts. Nevertheless, the alumina in the work mentioned above was prepared by solvothermal method. In this method, this technique required high pressure reactor and long reaction time. However, the χ- Al_2O_3 prepared by thermal decomposition of gibbsite required lower pressure, short reaction time and produced large amount of product.

The particle size of starting material has shown effect on phase transformation from gibbsite to χ-Al_2O_3. It is interesting to study the effect of grinding of gibbsite and on the formation of χ- Al_2O_3. In this study, χ-alumina was synthesized by thermal decomposition of gibbsite. χ-alumina has high surface area (>100 m^2/g) and good thermal stability, then, it may be suitable for support in order to disperse catalytic material.

CHAPTER IV

EXPERIMENTAL

4.1 Chemicals

The chemicals used in this experiment are specified as follows:

1. Fine gibbsite available from Merck.
2. Cobalt (II) nitrate hexahydrate 98% available from Aldrich.
3. Aluminium isopropoxide (AIP) available from Aldrich.
4. Toluene available from Fisher Scientific.
5. Calcium fluoride available from Merck.
6. γ-Al_2O_3 available from Sumitomo Aluminium Smelting Co. Ltd.

4.2 Catalyst Preparation

4.2.1 Preparation of χ-Al_2O_3 by grinding method

Fine gibbsite was used as a starting material. The fine gibbsite 100 g and water 300 ml were mixed in plastic pot and milled in attrition mill for 12 h and 24 h, using alumina balls as grinding media. Alumina balls were weighted before and after milling as well as filled to a half volume of the milling pot. Cooling water was fed continuously in attrition mill in order to remove heat. Rotational speed of the mill was fixed at 500 rpm. The sample was collected by using a pipet every 2 h and dried at 105°C overnight in an oven to remove water. The dried sample was subsequently milled in a mortar to deagglomerate. The samples were calcined in a tube furnace in air (95ml/min) by heating to a desired temperature at a rate of 10°C/min and hold at that

temperature for 4 h. Then, the samples were cool down to room temperature in N_2 (75ml/min).

4.2.2 Cobalt loading

The catalysts were prepared by incipient wetness impregnation with aqueous solution of cobalt (II) nitrate hexahydrate. The certain amount of cobalt (20 wt% loading) will be dissolved de-ionized water and then impregnated into the support. The cobalt solution is dropped slowly to the support and then the catalyst is dried in the oven at 110 ^{o}C for 12 h. The catalyst is calcined in air at 300 ^{o}C for 2 h using a ramp rate of 1°C/min.

4.2.3 Preparation of χ-Al_2O_3 from solvothermal method

The alumina preparation by solvothermal method requires an autoclave (**Figure 4.1**) reactor with the following specifications.

Autoclave reactor

- Made from stainless steel
- Volume of 200 cm^3
- Maximum temperature of 350°C
- Pressure gauge in the range of 0-300 bar
- Relief valve used to prevent runaway reaction
- Test tube was used to contain the reagent and solvent
- A temperature program controller was connected to a thermocouple attached to the reagent in the autoclave.
- Electrical furnace (heater) supplied the required heat to the autoclave for the reaction.
- Nitrogen was set with a pressure regulator (0-150 bar) and needle valves are used to release gas from autoclave.

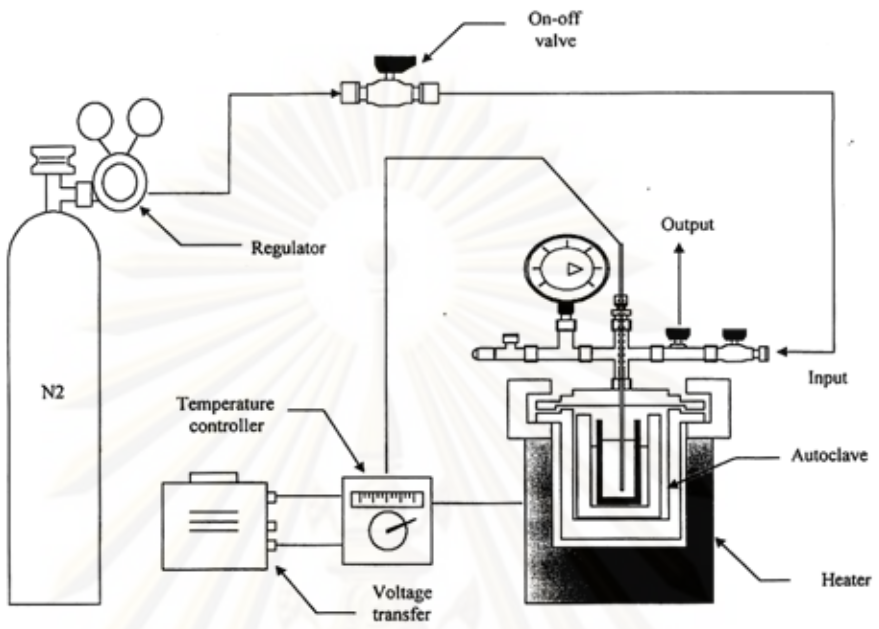

Figure 4.1 Autoclave reactor and gas controlling system

χ-Al_2O_3 was used as catalyst support. In this experiment, χ-Al_2O_3 was synthesized by solvothermal method. It was prepared by aluminium isopropoxide, 15.0 g. The starting materials was suspended in 100 mL of toluene in a beaker, and then set up in 300 mL autoclave. In the gap between the beaker and autoclave wall, 30 mL of toluene was added. After the autoclave was completely purged with nitrogen, the suspension was heated to 300 ^{o}C at the rate of 2.5 ^{o}C/min and will hold at that temperature for 2 h. Autogenous pressure during the reaction gradually increased as temperature was raised. Then the autoclave was cooled to room temperature. The resulting products were washed repeatedly with methanol by centrifugation and dried at 110°C for 24 hrs. The calcination of the obtained product was carried out in a furnace. The product was heated at the rate of 10 ^{o}C/min to 600°C and was hold at that temperature for 6 h.

4.2.4 Catalyst Nomenclature

The products from the thermal decomposition of fine gibbsite are designed as FG**h***C where the first two asterisks represent the milling time and the latter three asterisks represent temperature of calcination. The abbreviation of FG is fine gibbsite (starting material) and products from solvothermal method are designed as χ-solvothermal .

4.3 Catalyst Characterization

4.3.1 X-ray diffraction (XRD)

XRD was performed to determine the bulk phase of catalysts by SIEMENS D 5000 X-ray diffractometer using CuK_{α} radiation with Ni filter in the 2θ range of 10-80 degrees resolution 0.04°. The crystallite size was calculated from Scherrer's equation.

4.3.2 N_2 Physisorption

The catalyst 0.1 gram was study BET surface area, pore volume and pore diameter were measured by N_2 adsorption–desorption isotherm at liquid nitrogen temperature (-196 ˚C) using a Micromeritics ASAP 2020. The surface area and pore distribution were calculated according to Brunauer-Emmett-Teller (BET) and Barret-Joyner-Halenda (BJH) methods, consecutively.

4.3.3 CO-Pulse Chemisorption

The active sites and the relative percentages dispersion of cobalt catalyst were determined by CO-pulse chemisorption technique using Micromeritics ChemiSorb 2750 (pulse chemisorption system) and ASAP 2101C V.3.00 software. It was

carried out using 10 mg of a sample and reduced in H_2 flow rate at 50 ml/min with heated from room temperature to 350°C at rate 10°C/min and held at this temperature for 3 h after the cooled down to room temperature in a He flow. Desorbed CO was measured using thermal conductivity detector. Pulsing was continued until no further carbon monoxide adsorption was observed.

4.3.4 Temperature-programmed reduction (TPR)

TPR was used to determine the reduction behaviors of the samples using a Micrometritics Chemisorb 2750.

1. The catalyst sample 0.1 g used in the sample cell.
2. Prior to operation, the catalysts were heated up to 200°C in flowing nitrogen and held at this temperature for 1 h.
3. After the catalyst sample was cooled down to room temperature, the carrier gas was 5% H_2 in Ar (30 CC/min) were ramping from 35 to 800°C at 10°C/min.
4. A cold trap was placed before the detector to remove water produced during the reaction.
5. A thermal conductivity detector (TCD) was used to determine the amount of hydrogen consumption during TPR.

4.3.5 X-ray photoelectron spectroscopy (XPS)

The XPS analysis was performed originally using an AMICUS spectrometer equipped with a Mg Ka X-ray radiation. For a typical analysis, the source was operated at voltage of 15 kV and current of 12 mA. The pressure in the analysis chamber was less than 10^{-5} Pa. The AMICUS system is computer controlled using the AMICUS “VISION 2”software.

4.3.6 Transmission Electron Microscopy (TEM)

The morphology and size of the catalyst was observed using JEOL JEM 2010, operating at 200 kV.

4.3.7 Laser Diffraction Particle Size Analysis

The particle size distributions of the milled powders were performed by means of a laser diffraction granulometer (Malvern Mastersizer). The proportion of each particle class in the sample was expressed as number percentage. The average size, d_{50}, corresponding to a cumulative frequency of 50%, was also determined.

4.3.8 Thermal Gravimetric Analysis (TGA)

Thermal gravimetric analysis (TGA) and differential thermal analysis (DTA) were performed using an SDT Analyzer Model Q600 from TA Instruments, USA. The TGA/DTA analysis of the spent catalysts were carried out from room temperature to 1000ºC at a heating rate of 10ºC/min in oxygen.

4.3.9 Temperature Programmed Desorption of Ammonia (NH_3-TPD)

The acid properties of prepared catalysts were observed by Temperature Programmed Adsorption of Ammonia (NH_3-TPD) equipment by using Micromeritics chemisorp 2750 Pulse Chemisorption System. In an experiment, about 0.10 g of the catalyst sample was placed in a quartz tube and pretreated at 200 °C in a flow of helium. The sample was saturated with 15%NH_3/He. After saturation, the physisorbed ammonia was desorped in a helium gas flow about 1.0 h. Then the sample was heated from 40 to 800 °C at a heating rate 10 °C /min. The amount of ammonia in effluent was measured via TCD signal as a function of temperature.

4.3.10 Atomic adsorption spectroscopy (AAS)

AAS is a technique for determining the concentration of Co element in the bulk of catalysts using a Varian Spectra A800 atomic adsorption Spectrometer at the Department of Science Service Ministry of Science and Technology.

4.4 Isothermal kinetic measurements

Samples were heated at three different temperatures in the range of 450 to 600°C with different holding times. The activation energy for transformation of gibbsite to χ-Al_2O_3 was estimated by isothermal experiments according to Arrhenius method (Macêdo). First of all, the value of rate constant (*k*) was calculated by the Johnsom-Mehl-Avrami (JMA) equation (**eq.4.1**) (Macêdo).

$$x(t) = 1 - \exp\left[-(kt)^n\right] \quad (4.1)$$

where x is the phase fraction of χ-Al_2O_3 at time (*t*) and *n* is the reaction exponent. For analyzing the equation 1, it can be rewritten in the form of follow **equation** 4.2.

$$\ln(-\ln(1-x)) = n\ln k + n\ln t \quad (4.2)$$

The value of *k* and *n* can be calculated from slope and interception of a linear plot of ln *t* and ln(-ln(1-*x*)). After the value of *k* is obtained, the activation energy (E_a) can be estimated by Arrhenius equation (**eq.4.3**).

$$\ln k = \ln A - \frac{E_a}{RT} \quad (4.3)$$

where A is constant, R is gas constant ($8.314 J.K^{-1}.mol^{-1}$) and T is the working temperature. The value of E_a can be calculated from slope of a linear plot of ln k and l/T.

The fraction of χ-Al_2O_3 was determined by quantitative XRD analysis, using CaF_2 as an internal standard. A 0.2000±0.0001 g of sample was placed in a porcelain dish. One tenth of the sample weight of CaF_2 was weighted and mixed with the sample for 5 minutes. The analysis was calculated by ratio of the integrated intensities of the 43° (Cu-K_α 2θ) of χ-Al_2O_3 and integrated intensities of the 28.1° (Cu-K_α 2θ) of CaF_2. Their ratios were compared against a standard χ -Al_2O_3/CaF_2 calibration curve. The calibration curve was determined by using mixture of χ -alumina and the same amount of CaF_2, spanning the range of 20 to 90 wt% χ -alumina.

4.5 Reaction study in CO hydrogenation

4.5.1 Materials

The reactant gas used for the reaction study was the carbon monoxide in hydrogen feed stream as supplied by Thai Industrial Gas Limited (TIG). The gas mixture contained 9.73 vol % CO in H_2 (22 CC/min). The total flow rate was 30 CC/min with the H_2/CO ratio of 10/1. Ultra high purity hydrogen (50 CC/min) and high purity argon (8 CC/min) manufactured by Thai Industrial Gas Limited (TIG) were used for reduction and balanced flow rate.

4.5.2 Apparatus

Flow diagram of CO hydrogenation system is shown in **Figure 4.2**. The system consists of a reactor, an automatic temperature controller, an electrical furnace and a gas controlling system.

4.5.2.1 Reactor

The reactor was made from a stainless steel tube (O.D. 3/8”). Two sampling points were provided above and below the catalyst bed. Catalyst was placed between two quartz wool layers.

4.5.2.2 Automation Temperature Controller

This unit consisted of a magnetic switch connected to a variable voltage transformer and a solid-state relay temperature controller model no. SS2425DZ connected to a thermocouple. Reactor temperature was measured at the bottom of the catalyst bed in the reactor. The temperature control set point is adjustable within the range of 0-800°C at the maximum voltage output of 220 volt.

4.5.2.3 Electrical Furnace

The furnace supplied heat to the reactor for CO hydrogenation. The reactor could be operated from temperature up to 800°C at the maximum voltage of 220 volt.

4.5.2.4 Gas Controlling System

Reactant for the system was each equipped with a pressure regulator and an on-off valve and the gas flow rates were adjusted by using metering valves.

4.5.2.5 Gas Chromatography

The composition of hydrocarbons in the product stream was analyzed by a Shimadzu GC14B (VZ10) gas chromatograph equipped with a flame ionization detector. A Shimadzu GC8A (molecular sieve 5A) gas chromatography equipped with a thermal conductivity detector was used to analyze CO and H_2 in the feed and product streams. The operating conditions for each instrument are shown in the **Table 4.1**.

Table 4.1 Operating condition for gas chromatograph

Gas Chromagraph	SHIMADZU GC-8A	SHIMADZU GC-14B
Detector	TCD	FID
Column	Molecular sieve 5A	VZ10
- Column material	SUS	-
- Length	2 m	-
- Outer diameter	4 mm	-
- Inner diameter	3 mm	-
- Mesh range	60/80	60/80
- Maximum temperature	350 ^{o}C	80 ^{o}C
Carrier gas	He (99.999%)	H_2 (99.999%)
Carrier gas flow	40 cc/min	-
Column gas	He (99.999%)	Air, H_2
Column gas flow	40 cc/min	-
Column temperature		
- initial (^{o}C)	60	70
- final (^{o}C)	60	70

Table 4.1 Operating condition for gas chromatograph (cont.)

Injector temperature (^{o}C)	100	100
Detector temperature (^{o}C)	100	150
Current (mA)	80	-
Analysed gas	Ar, CO, H_2	Hydrocarbon C_1-C_4

4.5.3 Procedures

1. Using 0.1 g of catalyst packed in the middle of the stainless steel microrector, which is located in the electrical furnace.

2. A flow rate of Ar = 8 CC/min, 9% CO in H_2 = 22 CC/min and H_2 = 50 CC/min in a fixed-bed flow reactor. A relatively high H_2/CO ratio was used to minimize deactivation due to carbon deposition during reaction.

3. The catalyst sample was re-reduce *in situ* in flowing H_2 at 350 ^{o}C for 3 h prior to CO hydrogenation.

4. CO hydrogenation was carried out at 220 ^{o}C and 1 atm total pressure in flowing 9% CO in H_2.

5. The effluent was analyzed using gas chromatography technique. [Thermal conductivity detector (TDC) was used for separation of carbon monoxide (CO) and methane (CH_4) and flame ionization detector (FID) were used for separation of light hydrocarbon such as methane (CH_4), ethane (C_2H_6), propane (C_3H_8), etc. In all cases, steady-state was reached within 6 h.

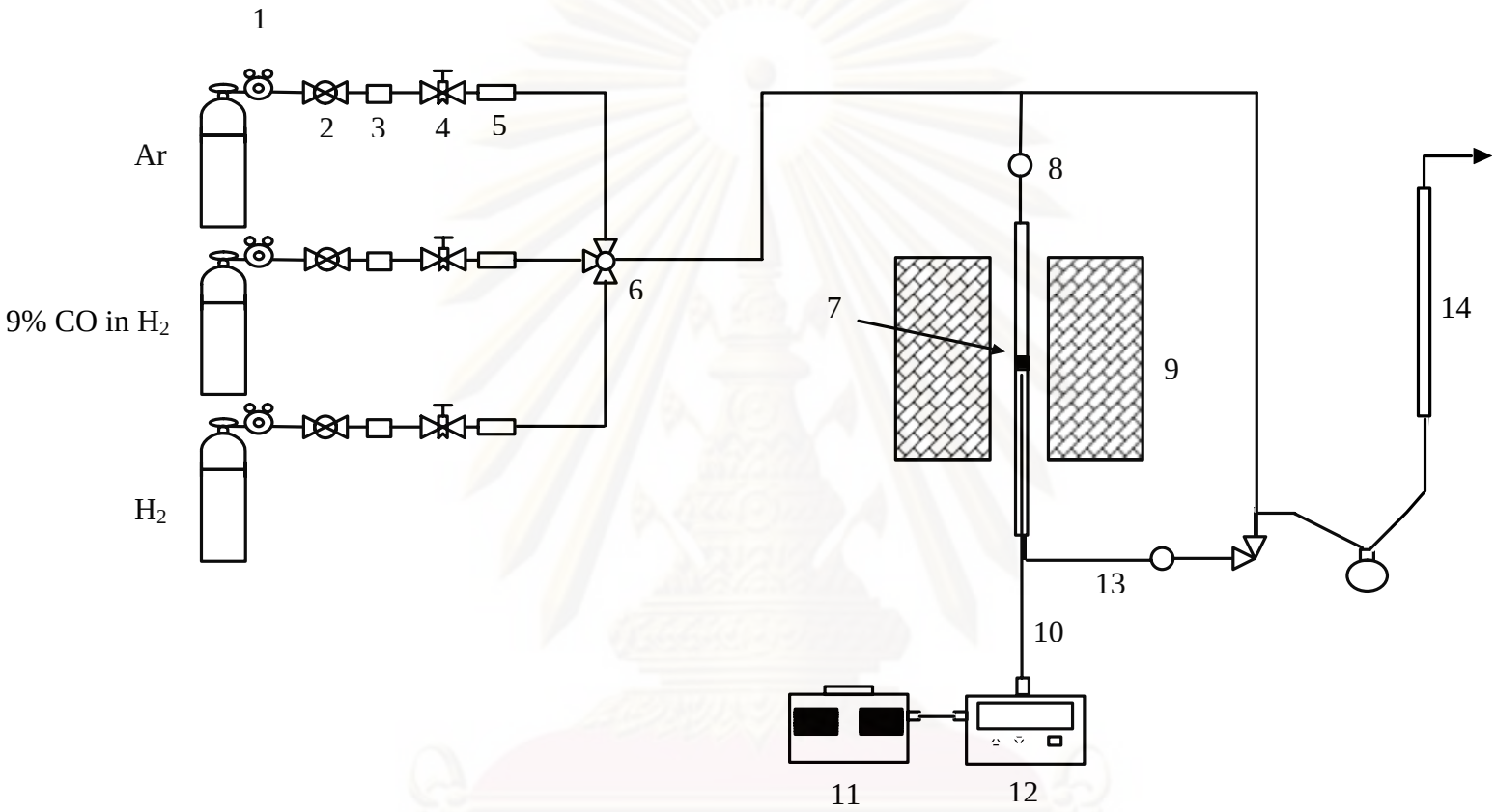

1. Pressure Regulator
2. On-Off Value
3. Gas Filter
4. Metering Valve
5. Back Pressure
6. 3-way Valve
7.Catalyst Bed
8. Sampling point
9. Furnace
10. Thermocouple
11. Variable Voltage Transformer
12. Temperature Controller
13. Heating Line
14. Bubble Flow Meter

Figure 4.2 Flow diagram of CO hydrogenation system

CHAPTER V

RESULTS AND DISCUSSION

Supported Co catalysts are preferred for Fischer-Tropsch synthesis. The catalysts with 20 wt% Co loading were used in this study. This chapter is divided into three sections: 5.1) the study of preparation of -Al_2O_3 from gibbsite, 5.2) measurement of isothermal kinetic for phase transformation from gibbsite to chi-alumina and 5.3) Comparison catalytic activity between Co catalyst on - Al_2O_3 prepared from thermal decomposition of gibbsite and solvothermal method. This section consists of catalyst characterization and CO hydrogenation study.

For catalyst characterization, the catalysts were characterized by several techniques such as laser diffraction-based size analyzer, TG-DTA, XRD, BET, TEM, TPR, CO-pulse chemisorption, AAS, and NH_3-TPD. For CO hydrogenation, the reaction was carried out at 220°C and 1 atm, $CO/H_2/Ar$ = 20/2/8.

5.1 The study of preparation of -Al_2O_3 from gibbsite

5.1.1 Particle size distribution

Figure 5.1 shows the particle size distribution of gibbsite milled for various times. The median particle size (d_{50}) decreased from 13 μm to 3 μm and 0.6 μm after milling for 12 h and 24 h, respectively. It was found that the unimodal size distribution in the starting gibbsite changed to bimodal distribution after milling for 24 h. These results are in agreement with that of Alex *et al*. They have shown that during milling, the evolution of the distributions of gibbsite is lower, and the mean size decreased. Moreover, the particle size distribution of samples did not come from alumina balls because weight loss of balls was less than 1 % (initial weight 761.9 g and after milling 759.9 g). Milling run of the alumina balls for 24 h in pure water without

gibbsite was carried out in order to determine the typical mean particle size of the wear debris (possible alpha seeds and abrasives coming from the grinding media). The result is also shown in Figure 2 and the typical mean particle size was determined to be 24 μm.

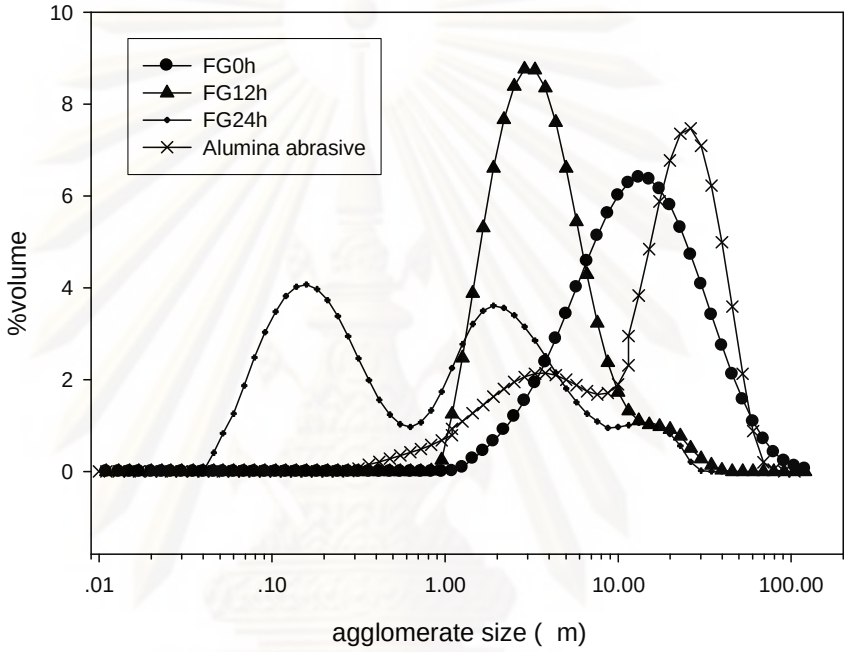

Figure 5.1 The particle size distribution of unmilled, milled gibbsite, and alumina abrasive at various milling time.

5.1.2 Characterization by XRD and TGA/DTA data

Figure 5.2 and **5.3** shows the results from the thermogravimetric analysis, i.e. TGA and DTA plots, of all gibbsite powders prepared by milling at various times. Two weight processes were detected corresponding on two endothermic and one exothermic processes. The decrease in mass at around 150-600°C, accompanied by the endothermic peaks in DTA signal, is attributed to the dehydration of gibbsite to form alumina. It was found that the endothermic peak shifted toward lower temperature with increasing milling time. This would by due to the acceleration of the dehydration of gibbsite by milling process (Du, 2009). The overall weight losses of all samples were

approximately around 35% which were in good agreement with the calculated value of 34.6% for the dehydration reaction (eq. 5.1):

$$2Al(OH)_3 \quad Al_2O_3 \quad 3H_2O \quad (5.1)$$

The dehydration of FG0h (Figure 4a) in first endothermic step (236 C) was due to loss of water in sample. The second endothermic peak (306 C) is corresponding to a weight loss of 22.5%, XRD measurements of FG0h treated at 400 C also showed peak at 2 =14.4 (**Figure 6d**). It points out that boehmite formed at in this range of temperature. In addition, endothermic peak at around 526 C indicated that boehmite transforms to alumina. **Figure 6b** showed that diffraction peaks of mixed phases of alumina were observed at 500 C. However, this endothermic peak disappeared when milling time increased, indicating that the milling conditions make affects the transformation sequence of gibbsite (Jang, 2000).

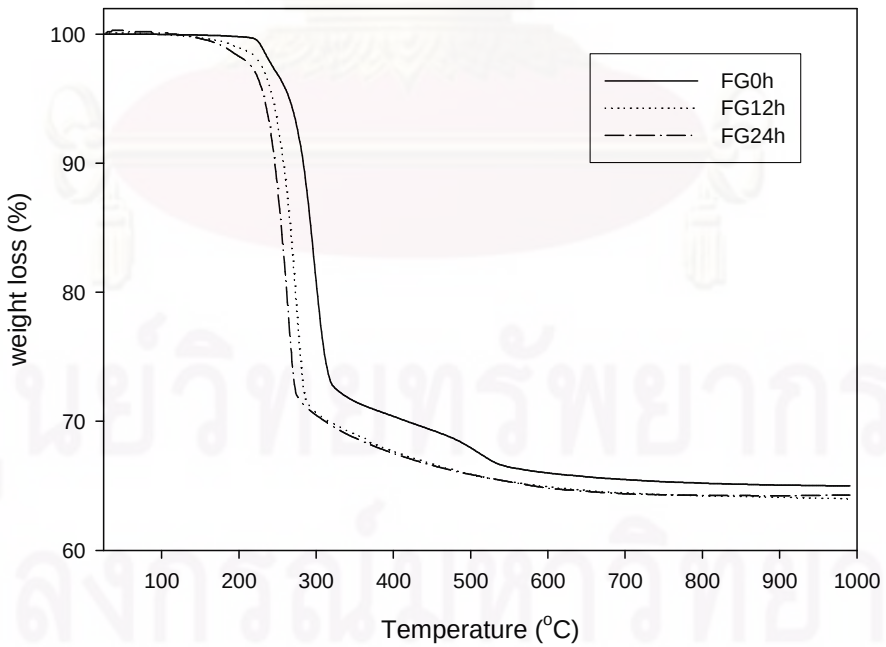

Figure 5.2 TG curves of unmilled and milled gibbsite at various milling time.

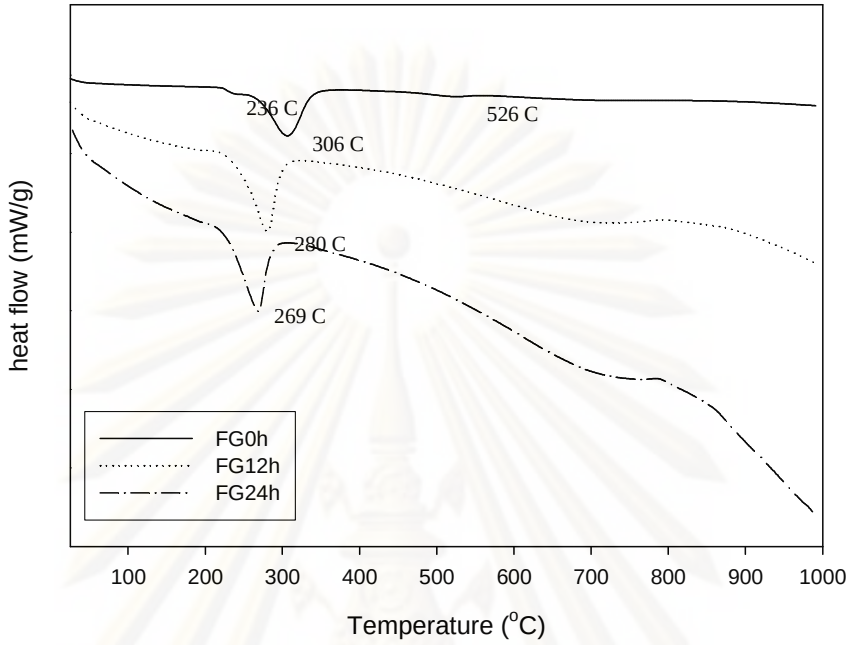

Figure 5.3 DTA curves of unmilled and milled gibbsite at various milling time.

XRD data was undertaken to study the transformation phases from gibbsite at various temperatures. XRD patterns of FG0h, FG12h and FG24h are shown in Figure 5.4, respectively. The intensities of XRD peaks decreased and became wider as milling time increased. It is due to decreasing of the particle size of gibbsite. However, the patterns remained crystallite because the wet milling would reduce size of particle. It did not destroy structure of gibbsite. Figure 5.5, 5.6 and 5.7 show the XRD patterns of calcined FG0h, FG12h and FG24h at various temperatures. For calcined FG12h, the mixture between boehmite and χ-phases was found at 400 C and the -phase was observed at higher calcinations temperature. In the case of prolong milling (FG24h), the transformation of gibbsite to -alumina was complete at 350 C. This implies that the small particle sizes are effective for reduction in the transformation temperature (Kano, 2000) of gibbsite to -alumina.

In the past, alpha-seeding has been shown to influence phase development and transformation kinetics of alumina. It may be possible that the gamma peaks in Figures 5.6-5.7 could have been enhanced by such seeding effect. However,

in the present study, the contamination from abrasives appeared to have very little impact on the reduction of transformation temperature of gibbsite to -alumina due to the very small amount presented. The amounts of wear debris obtained by milling the alumina balls in water for 24 h with and without gibbsite were only 2 and 3 wt% of the gibbsite weight, respectively. According to the literature, the effect of alpha-seeding was dependent not only on the size of the seeds but also on the amount of the seeds presented. For examples, Kano et al. (2000) showed that the presence of 50wt.% α-alumina seeding reduced the transformation temperature of gibbsite to α-alumina by 120°C (from 1030 C to 910 C), whilst for 5wt.% α-alumina seeding, the transformation temperature decreased only about 30 C. Similarly, Xie et al. (2003) reported that $Al(OH)_3$ can be transformed to α-Al_2O_3 at a relatively lower temperature (1100°C) with the help of seeds by wet grinding of high-purity Al_2O_3 balls when the seed concentration was increased to more than 10 wt.%. Moreover, the average particle size of the abrasives in this study was much larger than those reported in the literature for reduction in the transformation temperature of gibbsite powder (i.e., 24 μm (this work) as compared to 0.6 μm in Xie's work).

When particle size of gibbsite is small, dominant peak (2 =14.4) of boehmite would be reduced (**Figure. 5.6d, 5.7d**). As a result, -alumina occurred from the small particle size of gibbsite. It has been known that the dehydration sequence of gibbsite in air is affected by its particle size. In small gibbsite particles (<10μm), boehmite is rarely formed, but in the case of larger particles (>100μm), boehmite is formed because the water formed by the decomposition of the gibbsite cannot rapidly escape from the larger particles (Gitzen, 1970; Jang, 2000; Bhattacharya, 2004; Misra,1986). Consequently, transformation of gibbsite occurred through route 1 (**Figure 1.1**). However, boehmite phase may be observed from small particle size of gibbsite, if gibbsite particle is crystal (Bhattacharya, 2004). Bhattacharya *et al*. (2004) found that crystal gibbsite (0.25μm) can produce boemite at 400 C. Nevertheless, Jang *et al*. (2000) used ground gibbsite losing crystalline structure, boehmite was not observed at low temperature. When FG0h was heated, boehmite was observed at 400 C and -

alumina was formed at 450 C. However, -alumina was not the only phase of alumina occurred at this temperature, the peak of -alumina was also observed. For the micrometer sizes, both transition routes (Figure 1.1) may possibly take place which depend on the heat treatment conditions (Chang, 2009). The large particle of gibbsite (LG, d_{50}=20μm) was heated, mixed phase (- and -) started at 450 C (**Figure 5.9**). However, fraction of -alumina of this sample was lower than that in FG0h600C.

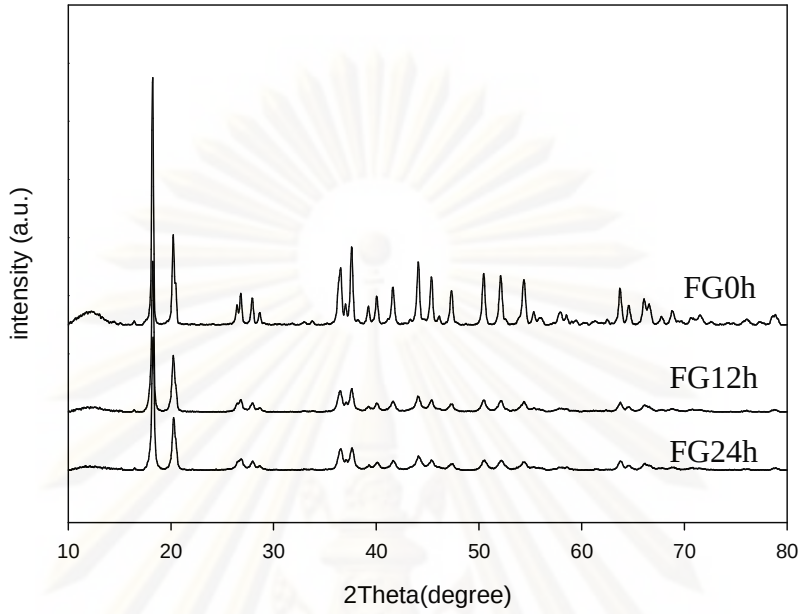

Figure 5.4 XRD patterns of unmilled and milled gibbsite at various milling time.

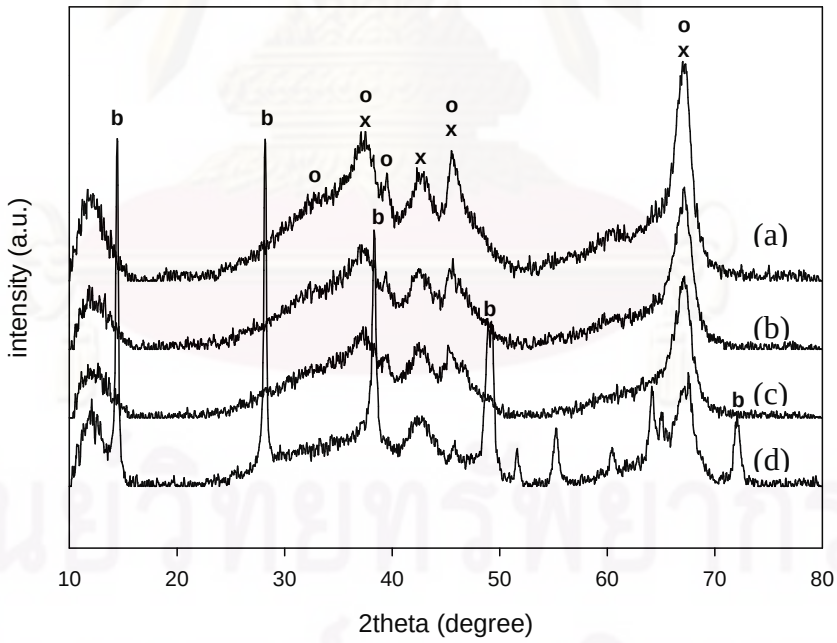

Figure 5.5 XRD patterns of FG0h calcined at various temperatures, b=boehmite, x= - Al_2O_3, o= - Al_2O_3 (a) 600 C (b) 500 C (c) 450 C (d) 400 C

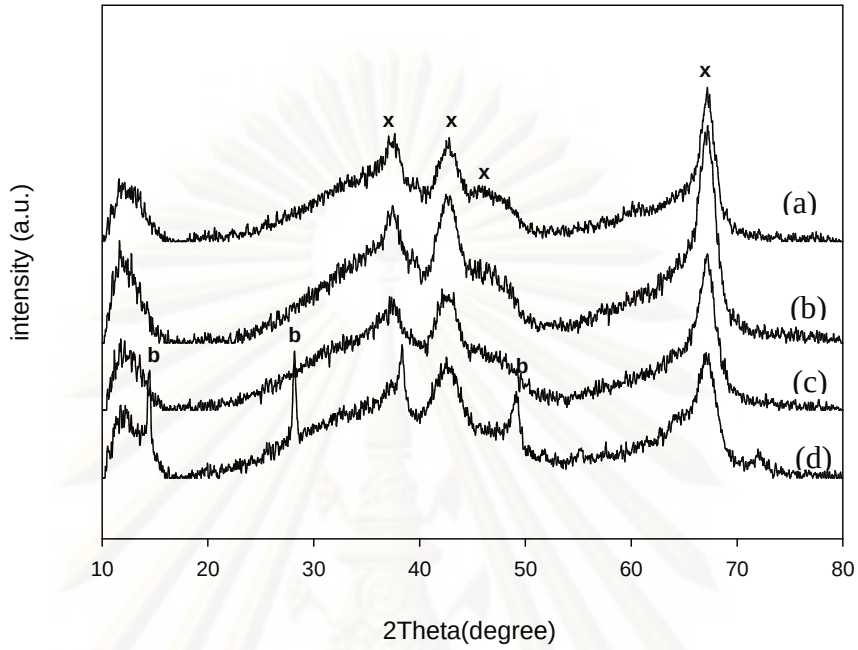

Figure 5.6 XRD patterns of FG12h calcined at various temperatures, b=boehmite, x= -Al_2O_3 (a) 600 C (b) 500 C (c) 450 C (d) 400 C

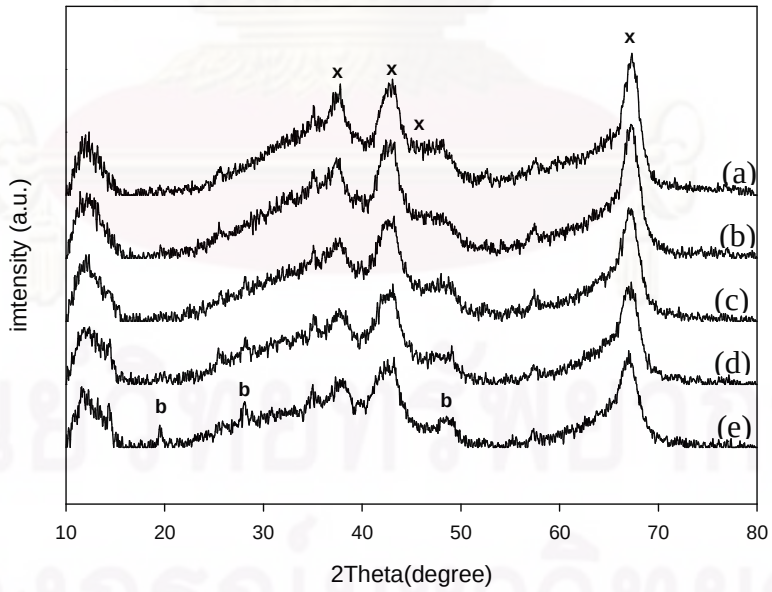

Figure 5.7 XRD patterns of FG24h calcined at various temperatures, b=boehmite, x= -Al_2O_3 (a) 600 C (b) 500 C (c) 400 C (d) 350 C (e) 300 C

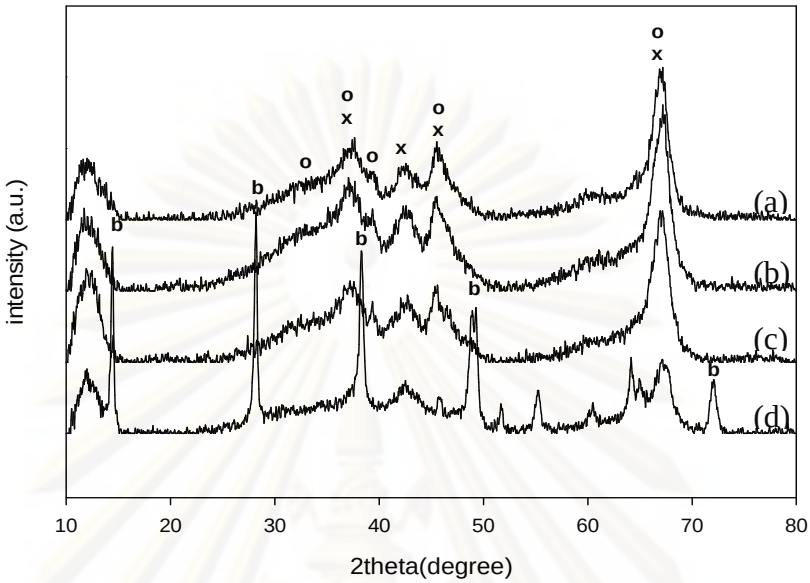

Figure 5.8 XRD patterns of LG calcined at various temperatures, b=boehmite, x= - Al_2O_3, o= - Al_2O_3 (a) 600 C (b) 500 C (c) 450 C (d) 400 C

5.1.3 BET surface area

The BET surface area of calcined samples is summarized in **Table 5.1**. FG0h has small surface area. After the calcination the structure of gibbsite was destroyed, which resulted in surface area and pore volume of calcined samples dramatically increased. In the same temperature of calcinations, the highest surface area is 183.4 m^2/g of FG24h600C. The increasing of surface area is due to its small particle size. The pore size of products was similar values (4nm), indicating that milling did not affect the pore size of products. Nevertheless, the pore volume of products increased with increasing the milling time. These results are in agreement with that of Ogata *et al.* They used gibbsite as starting material and found that the specific surface area increased when the calcinations temperature increased.

Table 5.2 summarizes the crystallite size (d_{XRD}) and the fraction of - phase of the calcined samples. It can be seen that increasing calcination temperature, crystallite size increased. In the same calcinations temperature, crystallite size of

FG24h was smaller than that in FG12h and FG0h. The fraction of -alumina increased with increasing the calcinations temperature. It indicated that high purity -alumina can form at the higher temperature. Macêdo *et al*. (2007) found that the high fraction of α-alumina can be produced from -alumina when calcinations temperature increased from 750 C to 900 C. Du *et al.* (2009) synthesized α-alumina from bayerite, the fraction of α-phase increased with increasing calcinations temperature. At low temperature (450 C), the fraction of -alumina rapidly increased from 0.58 to 0.89. It implied that mechanical activation affected the formation of -alumina. At every constant temperature, the fraction of -alumina increased when particle size decreased. It confirmed that small particle size of gibbsite can produce high purity of -alumina.

Table 5.1 BET surface area, pore volume and pore size data of gibbsite, samples after calcinations.

Samples	phase	Surface area (m^2/g)	Pore volume(cm^3/g)	Pore size(nm)
FG0h	-	5.3	0.0059	8.35
FG0h600C	and	125.6	0.23	4.88
FG12h600C		169.7	0.29	4.26
FG24h600C		183.4	0.34	4.82

Table 5.2 d_{XRD} of samples after calcinations and fraction of χ-phase.

samples	T (°C)	d_{XRD} [a] (nm)	Fraction of χ-phase [b]
FG0h	450	3.8	0.58
	500	4.1	0.72
	600	4.4	0.88
FG12h	450	3.7	0.68
	500	3.8	0.94
	600	4.2	0.95
FG24h	450	3.3	0.89
	500	3.7	0.99
	600	3.8	1

[a] calculated by Scherrer equation.

[b] calculated by quantitative XRD and based on FG24h600C as 100%χ.

5.1.4 TEM observation

The effect of grinding on the morphology of gibbsite and χ-Al_2O_3 were studied by TEM observation. **Figure 5.9** showed the TEM micrographs of unmilled (a and b) and milled (c and d) gibbsite powder. The unmilled fine gibbsite clearly consisted of pseudohexagonal plates, while the irregular and flaky particles were observed for milled samples. It revealed that the milling changed effectively morphology of gibbsite and reduced particle size. **Figure 5.10a** and **5.10b** show the TEM micrographs of FG0h400C and FG0h600C, respectively. Figure 5.10a showed that the structure is a strip. It was due to the formation of boehmite. However, this structure disappeared when gibbsite was milled for 12h and calcined at the same temperature (**Figure 5.10c**). It was probably due to the decreasing of boehmite phase in calcined samples. **Figure 5.10d,** and **5.10e** exhibited the TEM micrographs of FG12h600C, and FG24h600C, respectively. Figure 5.10d and 5.10e indicated that the dispersed χ-

alumina with narrow size distribution was obtained from milled gibbsite, whereas the larger particle of mixed phase (χ, γ) was obtained from unmilled one (Figure 5.10b). Besides, the morphology of samples is similar to that of gibbsite treated by mechanically.

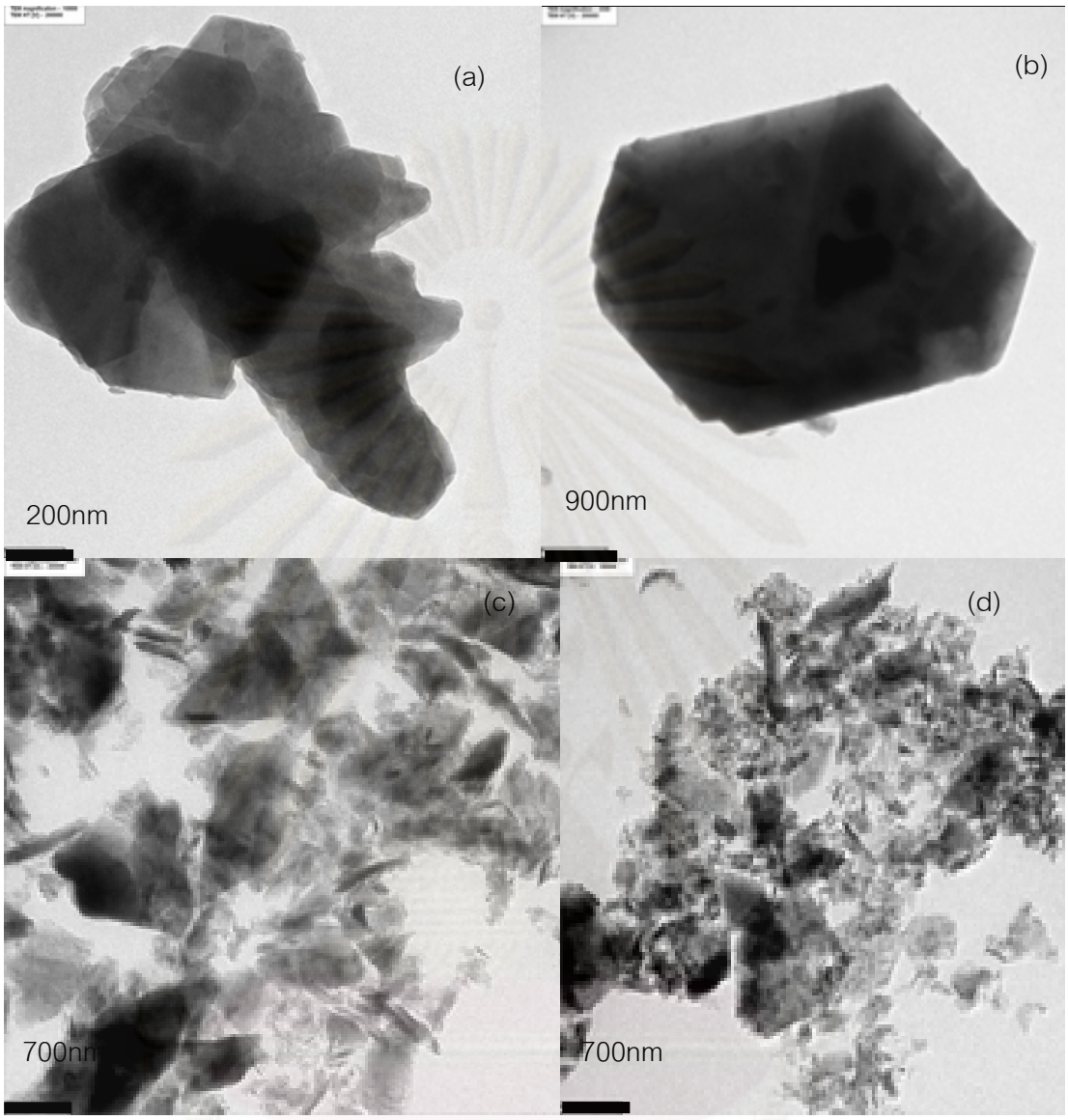

Figure 5.9 TEM micrographs of the FG0h (a, b), FG12h (c), FG24h (d).

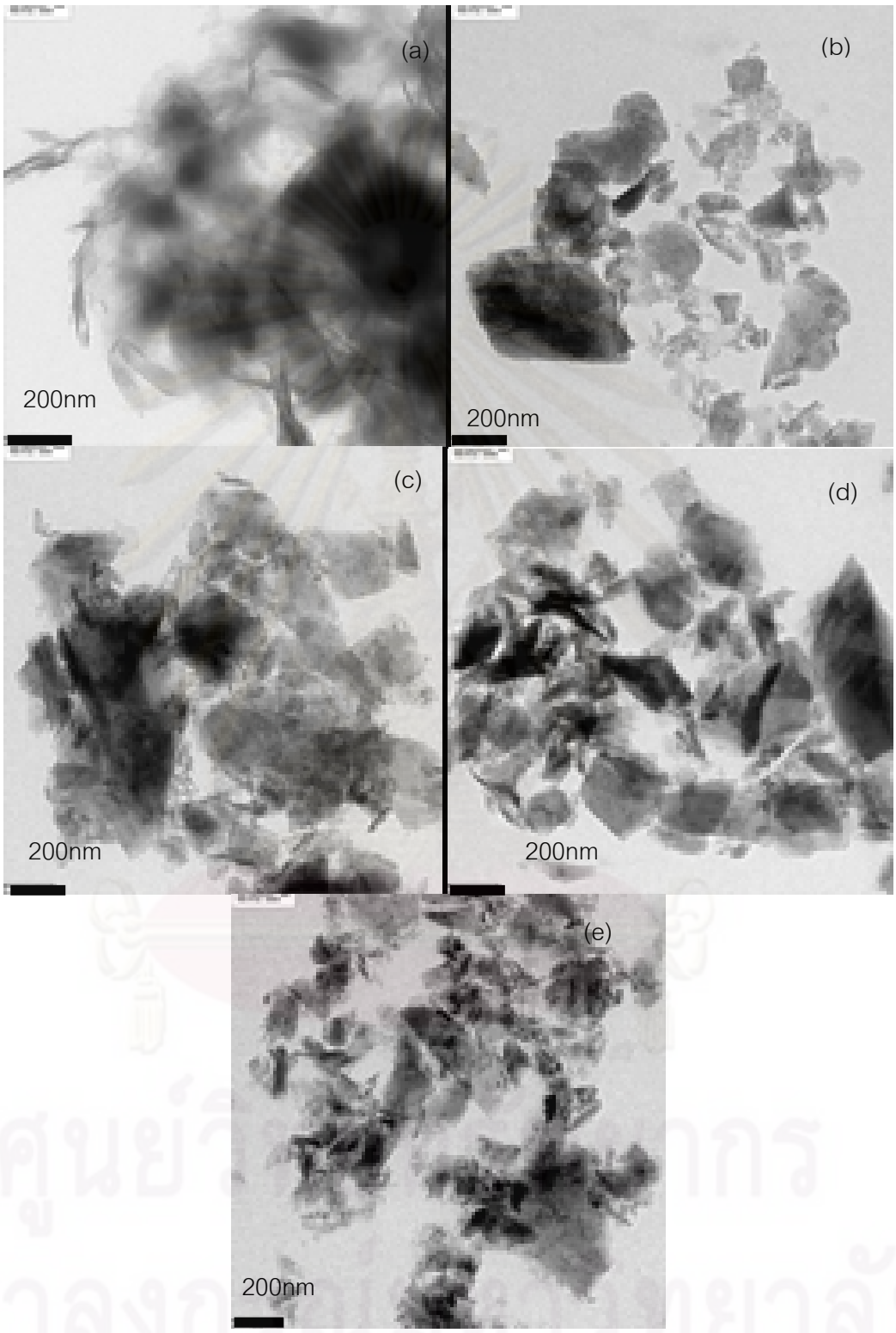

Figure 5.10 TEM micrographs of the FG0h400C (a), FG0h600C (b), FG12h400C (c), FG12h600C (d), FG24h600C(e).

5.2 Kinetic result

Table 5.3 summarizes the transformation rate constants (*k*) of milled and unmilled gibbsite at different temperatures. At every constant temperature, *k* increased with increasing the milling time. The milling can increase *k* at low temperature more significantly. For example, activation of the sample for 24h increased the reaction rate constant 5.7 times (compared with sample for 0 h) at 450°C, but it is only 2.5 at 600°C. Panchula *et al.* (1997) synthesized □-alumina from milled and unmilled γ-alumina. They found that *k* increased with increasing calcination temperature and the milling time increased from 30 min to 120 min. **Table 5.4** shows activation energy for phase transformation of milled and unmilled gibbsite to χ-alumina. The activation energy decreased from 20.6 to 14.7 and 6.8 kJ/mol after milling for 12h and 24h, respectively. It is indicated that the activation energy decreased with decreasing particle size of the starting gibbsite. In general, reducing the particle size allows to increase the surface energy of particle (Chang, 2009). It results in the decreasing of activation energy for phase transformation and transformation temperature as shown in the DTA profile (Chang, 2009). The XRD patterns also confirmed that the transformation temperature of gibbsite to χ-alumina reduced from 450°C to 350°C after milling for 24 h. It may be attribution to the fact that gibbsite grows to the critical size of phase transformation and then transform to χ-alumina at a lower temperature (Yang, 2007; Chang, 2009). Moreover, the milling of gibbsite for 12h and 24h can be up to 28% and 67% of activation energy compared with that of the unmilled gibbsite. Several researchers observed kinetic of transition aluminas. Macêdo *et al.* (2007) studied kinetic of γ to □-alumina. They found that the activation energy of this phase transformation was 201$\pm$4 kJ/mol. Chang *et al.* (2009) studied size effect of χ-alumina to □-alumina. The activation energy reduced from 506 to 321 kJ/mol when d_{50} of χ-alumina decreased from 155 to 40, respectively. Yang *et al.* (2007) presented formation during θ- Al_2O_3 to □-Al_2O_3 transformation. They used three kinds of θ-powder (as-received,

homogenized, homogenized and additionally unaxial-pressed compact) as the starting material. The activation energy was 299, 189, 148 kJ/mol, respectively. Candela and Perlmutter (1992) studied kinetics of boehmite formation by thermal decomposition of gibbsite under water vapor pressure from 100 to 3200 Pa. The activation energy was 142±10 kJ/mol. In our work, the value of activation energy was lower than those in the mention above. It was due to lower transformation temperature.

Table 5.3 Rate constant (*k*) for milled and unmilled gibbsite at different temperature

Milling time (h)	k (min^{-1})
T=600°C	
0	0.0142
12	0.0178
24	0.0359
T=500°C	
0	0.0110
12	0.0153
24	0.0248
T=450°C	
0	0.0033
12	0.0054
24	0.0188

Table 5.4 Activation energy of milled and unmilled gibbsite

Sample	E_a (kJ/mol)
FG0h	20.6
FG12h	14.7
FG24h	6.8

5.3 Reaction study

The reaction study was carried out in CO hydrogenation to determine the overall activity of the catalyst samples. First, the catalysts were reduced in H_2 at 350°C for 3 h in a fixed-bed flow reactor. Then, the reaction test was carried out with flow rate of H_2/CO/Ar = 20/2/8 cm^3/min. The supports from the thermal decomposition of fine

gibbsite are designed as ***χ-FG where the three asterisks represent the percent of χ-alumina

5.3.1 Characterization of the Catalysts

5.3.1.1 X-ray Diffraction (XRD)

XRD patterns of supports and Co based catalysts with different supports are shown in **Figure 5.11** and **5.12**, respectively. The scans were recorded in the 2θ range of 10-80°. The sharp peak at 2θ=47.5° in the solvothermal sample indicates the presence of χ-Al_2O_3 without contamination of Na^+ ions. According to Mekasuwandumrong *et. al.* (2004), gibbsite is usually contaminated with a small amount of Na^+ and thermal decomposition of gibbsite to χ-Al_2O_3 cannot eliminate the Na^+ ion from the matrix. The 100χ-FG and 95χ-FG, on the other hand, show the broad peaks at 2θ=47.5° in the XRD patterns.

All the alumina supported cobalt catalysts exhibited XRD peaks at 18.9°, 31.3°, 36.8°, 44.9°, 59.3° and 65.3° which can be assigned to Co_3O_4 (Xu, 2005). The diffraction peak at 68° corresponded to the alumina supports. **Table 5.5** and **5.6** shows the crystalline size of supports (2θ=68°) and Co_3O_4 (2θ=36.8°) calculated by using the Scherrer equation. The crystallite sizes of Co_3O_4 were similar for all the catalysts (7-9 nm). However, the crystallite sizes of Co_3O_4 should be correlated with the support pore diameter (Borg, 2008). In this study, Co_3O_4 crystalline sizes might be secondary particle. They did not depend on support pore diameter.

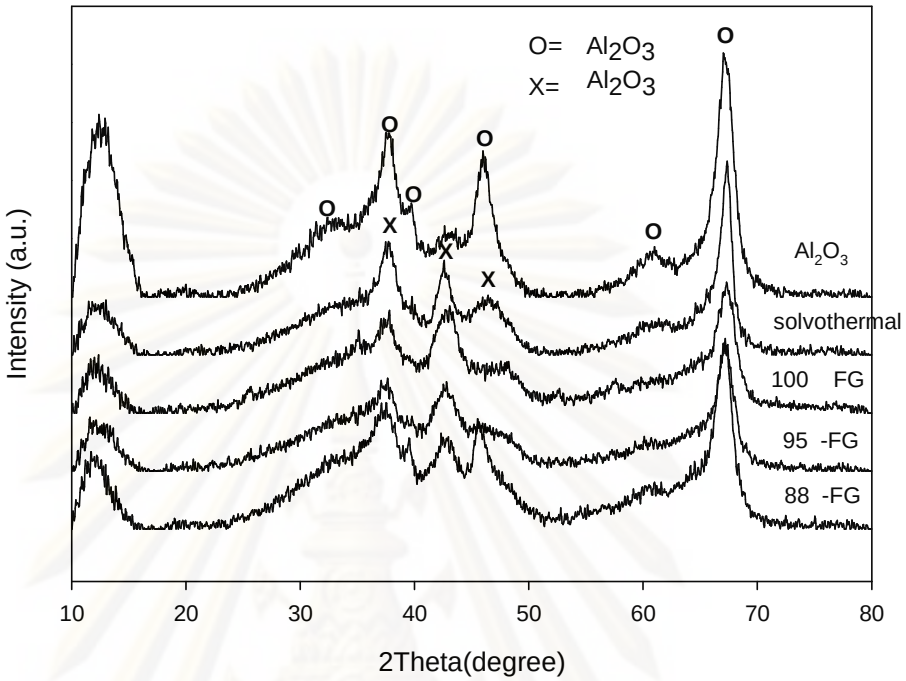

Figure 5.11 XRD patterns of different supports.

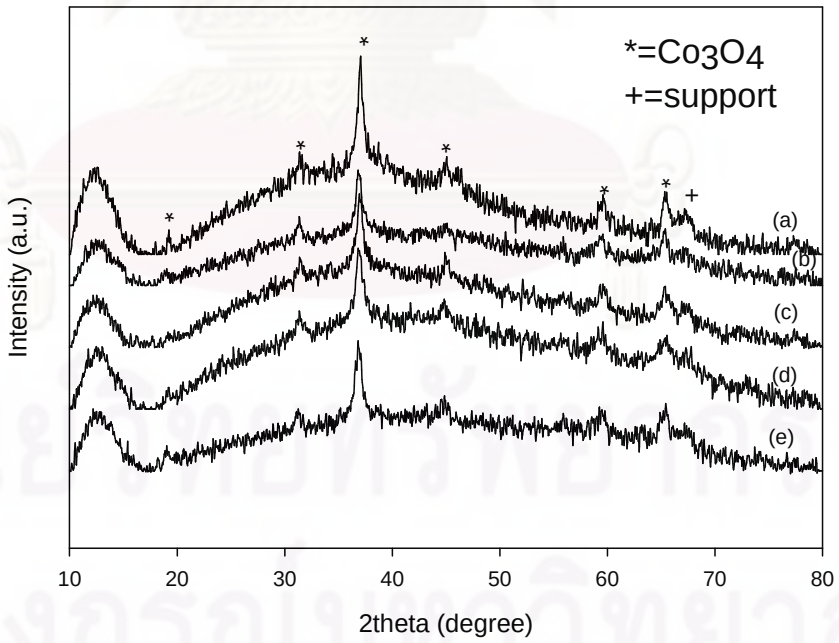

Figure 5.12 XRD patterns of Co catalyst with different supports. (a) Co/ -Al_2O_3 (b) Co/ -solvothermal (c) Co/88 -FG (d) Co/95 -FG (e) Co/100 -FG.

Table 5.5 crystallite sizes of different supports

Catalyst	crystallite sizes (nm)
-solvothermal	5.5
100 -FG	3.8
95 -FG	4.2
88 -FG	4.4
-Al_2O_3	4.9

Table 5.6 Co_3O_4 crystallite sizes of different catalysts

Catalyst	Co_3O_4 crystallite sizes (nm)
Co/ -solvothermal	8.0
Co/100 -FG	9.1
Co/95 -FG	7.2
Co/88 -FG	6.7
Co/ -Al_2O_3	7.8

5.3.1.2 BET surface areas

The most common procedure for determining surface area of a solid is based on adsorption and condensation of nitrogen at liquid nitrogen temperature. This method is also called BET (Brunauer Emmett Teller) method.

BET surface areas of gibbsite samples after calcination and Co catalysts area shown in **Table5.7**. The surface areas of100 -FG, -solvothermal, and -Al_2O_3 were quite similar. For cobalt catalyst, the surface areas and pore volume decreased in all catalysts, indicating that some pore blockage by cobalt oxide clusters occurred. **Figure 5.13a** illustrates the adsorption-desorption isotherms of different supports. All alumina in this study exhibited a type IV isotherm characteristic of a mesoporous solid. **Figure 5.13b** shows the pore size distribution of supports. It was found that the unimodal pore size distribution was in -solvothermal and -Al_2O_3 whereas bimodal size distribution was

observed in 88 -FG, 95 -FG and 100 -FG. Besides, the bimodal size distribution was apparently observed when milling time increased. From this figure, it was observed that the pore size of -Al_2O_3 was larger than those of the others. Impregnation, drying and calcination did not change pore size distribution of cobalt catalysts, but reduced the nitrogen uptake (Borg, 2009).

Table 5.7 BET surface area data of gibbsite, samples after calcinations and Co catalysts.

Samples	Fraction of -phase[a]	Surface area (m^2/g)	Pore volume(cm^3/g)	Pore size(nm)
-solvothermal	1	170.7	0.63	10.40
88 -FG	0.88	125.6	0.23	4.88
95 -FG	0.95	169.7	0.29	4.26
100 -FG	1	183.4	0.34	4.82
-Al_2O_3	-	188.0	0.49	6.75
Co/ -solvothermal	-	117.3	0.38	9.24
Co/88 -FG	-	81.8	0.13	4.35
Co/95 -FG	-	106.5	0.16	4.04
Co/100 -FG	-	134.9	0.23	4.86
Co/ -Al_2O_3	-	147.6	0.35	5.69

[a] Determined by quantitative XRD.

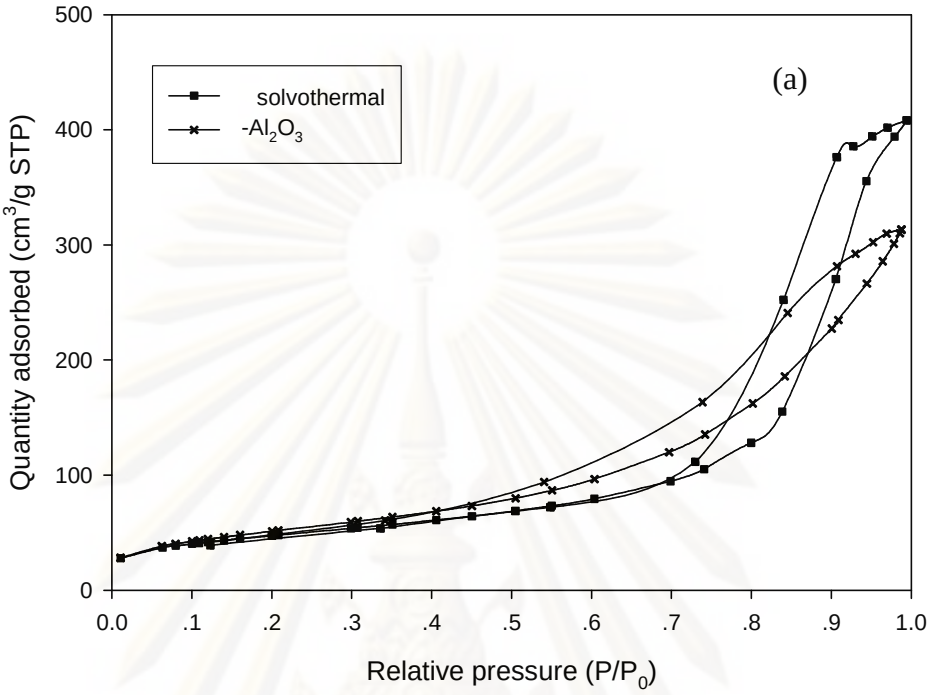
500
400
300
200
100
0
0.0
.1
.2
.3
.4
.5
.6
.7
.8
.9
1.0
Quantity adsorbed (cm3/g STP)
Relative pressure (P/P0)
solvothermal
-Al2O3
(a)

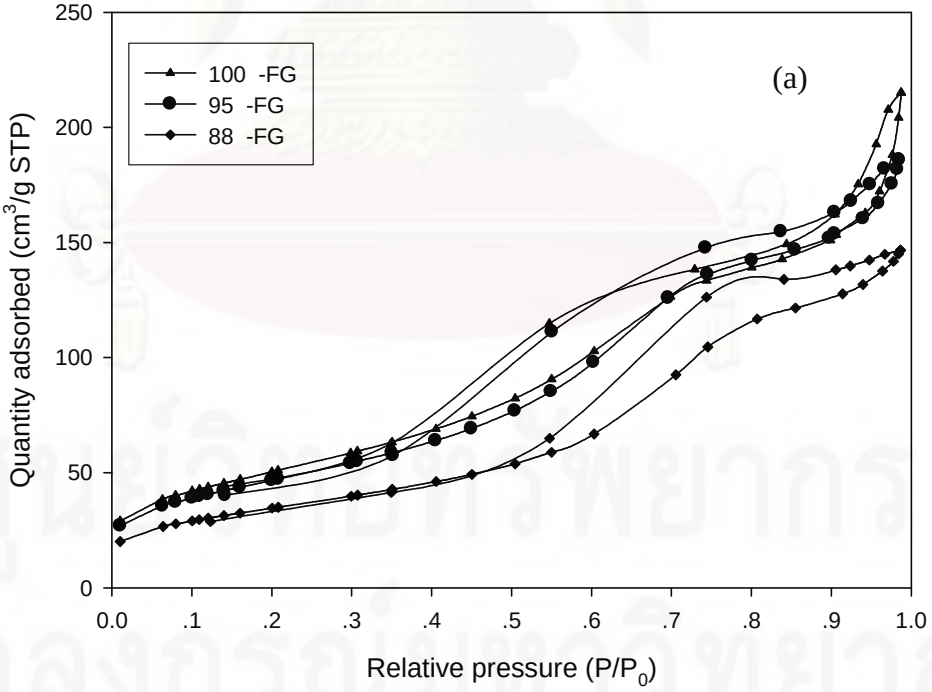
250
200
150
100
50
0
0.0
.1
.2
.3
.4
.5
.6
.7
.8
.9
1.0
Quantity adsorbed (cm3/g STP)
Relative pressure (P/P0)
100 -FG
95 -FG
88 -FG
(a)

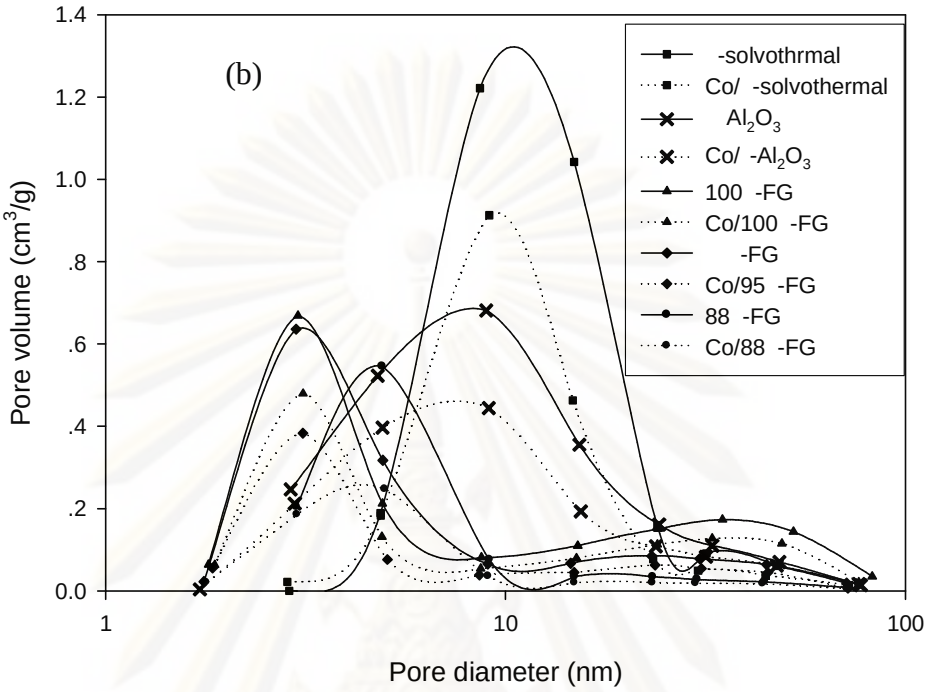

Figure 5.13 The N_2 adsorption-desorption isotherms of different supports (a), Pore size distribution of supports and Co catalysts (b).

5.3.1.3 Temperature Programmed Reduction (TPR)

The TPR profiles for all samples are shown in **Figure 5.14** TPR was performed to determine the reduction behaviors of the samples. Reduction was observed for all the catalyst samples as shown by two major peaks. They were located at 300 to 400 C and 550 to 750 C. The reduction temperature peak of Co/ -Al_2O_3 (195 C) and Co/100 -FG (250 C) was reduction of residual cobalt nitrate remaining after calcination (Kogelbauer, 1996). Prolonged calcination or reduction and recalcination resulted in completed decomposition of any cobalt nitrates present (Kogelbauer, 1996). For all the Co catalysts, the first major broad reduction peak located at 300 to 400 C. The broad peak was related to a two-step reduction of Co_3O_4 to CoO, and then to Co metal (Pansanga, 2007). The two reaction steps (**eq. 5.2 and 5.3**) may not be observed

as separated peaks. The reduction peak located at 300 to 400 C of Co/ -solvothermal showed higher reduction temperature than that of others. It pointed out that interaction between cobalt species and -solvothermal was higher than that on other supports.

$$H_2 \quad Co_3O_4 \quad H_2O \quad 3CoO \quad (5.2)$$
$$3H_2 \quad 3CoO \quad 3H_2O \quad 3Co \quad (5.3)$$

Moreover, it has been often found that the highest temperature peak represented the incomplete reduction of Co_XO_Y-support due to interactions between Co_3O_4 and support materials. For all the cobalt catalysts, the second major broad reduction peaks located at 550 to 750 C were the reduction of cobalt aluminate. The high temperature reduction peak of Co/ -solvothermal shifted toward lower temperatures compared to the catalysts (except for Co/ -Al_2O_3). It is indicated that -solvothermal resulted in a decrease in the concentration of hardly reducible cobalt aluminate. For Co/100 -FG, Co/95 -FG and Co/88 -FG, the temperature in first major peak of Co/100 -FG and Co/95 -FG was lower than that of Co/88 -FG. It is revealed that the higher amount of -phase resulted in higher reducibility of these catalysts. Pansanga *et al*. (2007) revealed that the support contained the higher amount of -phase could decrease temperature in TPR profiles. However, for Co/100 -FG and Co/95 -FG, TPR profiles appeared to be not significantly different, suggesting that particle size of supports (or milling time) had little impact on the interaction of cobalt and support.

For Co/ -Al_2O_3, the temperatures of the two major peaks of TPR profile were lower than those of all catalysts because it has larger pore size. Borg *et al*. (2009) used Co/ -Al_2O_3 and CoRe/ -Al_2O_3 with different pore sizes of supports. They found that the reduction peaks of both of them moved to lower temperatures with increasing pore size of supports.

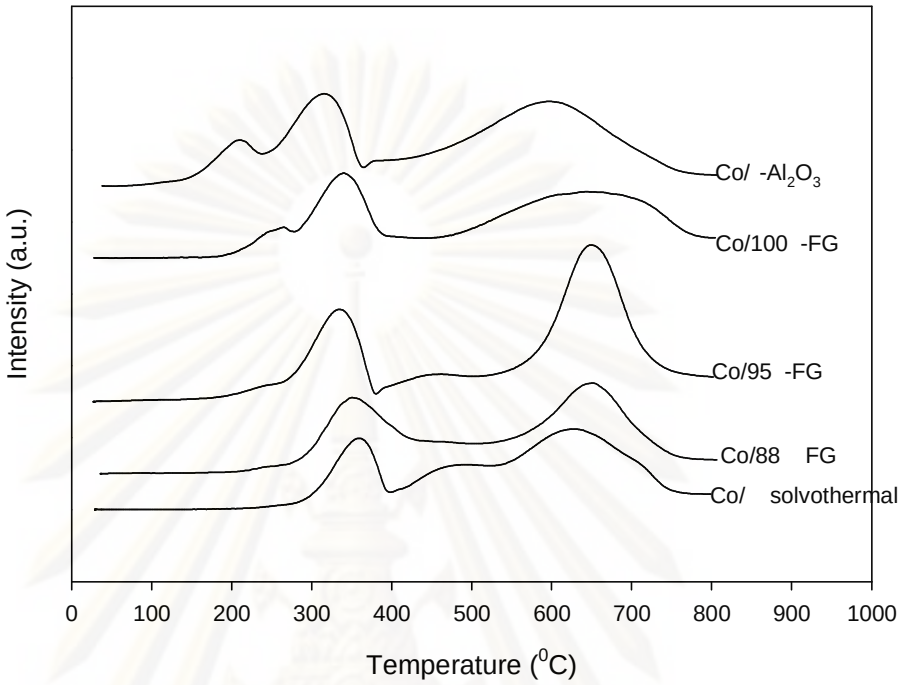

Figure 5.14 TPR profiles of Co catalysts with different supports.

5.3.1.4 CO-Pulse Chemisorption

The characterization results of CO chemisorption for the catalyst samples are illustrated in **Table 5.8**. The cobalt catalysts prepared from thermal decomposition of gibbsite (Co/100 -FG, Co/95 -FG, Co/88 -FG) and Co/ -solvothermal exhibited the amount of CO uptake on catalytic phase within the range of 0.5 to 0.86 μmol CO/ g of catalyst, indicating the higher overall Co dispersion. These values were higher than that of Co/ -Al_2O_3. It was found that the presence of -phase in support resulted in higher dispersion of cobalt. Consequently, in order to eliminate the effect of BET from the effect of crystallite size, the data reported in term of CO chemisorption per unit surface area. It was found that CO chemisorption/BET of Co/100 -FG, Co/95 -FG and Co/88 -FG and Co/ -solvothermal were higher than that of Co/ -Al_2O_3.

Table 5.8 CO chemisorption results of cobalt catalysts

Sample	CO chemisorption					
	Co content (wt%)[a]	Active site ($x10^{-19}$ site/g.cat)	Total CO chemisorption (μmol CO/g.cat)	% Co Dispersion	Active metal surface area (m^2/g.metal)	CO chemisorption/ BET surface area ($x10^{-3}$ μmol CO /g.cat/m^2)
Co/ - solvothermal	20	2.2	0.50	1.1	6.7	4.2
Co/100 -FG	22	3.1	0.86	1.4	8.4	6.3
Co/95 -FG	20	5.7	0.86	2.8	17.0	8.1
Co/88 -FG	17	2.2	0.65	1.3	8.6	7.9
Co/ -Al_2O_3	19	1.9	0.34	1.0	7.7	2.3

[a]= determined by AAS

5.3.1.5 X-ray Photoelectron Spectroscopy (XPS)

XPS analysis were carried out to examine the surface species on the cobalt catalysts and also to determine the relative amount of element on the surface. The samples were analyzed in the Co 2p, Al 2s, O1s with regards to the binding energy regions. For cobalt in an oxide state, the XPS results indicate that Co $2p_{3/2}$ in Co_3O_4 has lower binding energy than that in $CoAl_2O_4$. The binding energies of Co $2p_{3/2}$ in catalysts reflect the total values for that of both Co_3O_4 and of surface phase (Zang, 2003). The binding energy, the ratio of percentages of atomic concentration, and FWHM of Co $2p_{3/2}$ and Al 2s are also given in **Table 5.9**. The ratios of atomic concentrations of Co/Al in Co/ -solvothermal, Co/100 -FG, Co/95 -FG and Co/88 -FG were lower than that of Co/ -Al_2O_3, indicating the higher dispersion of cobalt on alumina supports (Pansaga, 2008). The binding energies of $Co2p_{3/2}$ for all the catalysts were matched with that of Co_3O_4. This observation was consistent with XRD patterns which showed the peaks of Co_3O_4 for all catalysts.

Table 5.9 The binding energy, the ratio of percentages of atomic concentration, and FWHM of various elements.

Sample	Co(II) $2p_{3/2}$		Al 2s		Atomic Conc%	
	B.E. (eV)	FWHM	B.E. (eV)	FWHM	Al/O	Co/Al
Co/ -solvothermal	780.4	3.505	118.2	3.050	0.45	0.031
Co/100 -FG	780.6	3.431	118.6	2.853	0.44	0.064
Co/95 -FG	780.55	3.406	118.8	2.814	0.46	0.021
Co/88 -FG	779.85	3.377	118.3	2.952	0.42	0.045
Co/ -Al_2O_3	780.45	3.368	119.1	2.994	0.42	0.072
[a]Co_3O_4	780 0.7					
[a]$CoAl_2O_4$	781.9 0.5					
[a]Co	778.1 0.1					

[a]Z. Zsoldos and L. Guczi, 1992

5.3.1.6 Transmission Electron Microscopy (TEM)

TEM is a useful tool for determining crystallite size and size distribution of supported metals. It allows determination of the micro-texture and microstructure of electron transparent samples by transmission of a focused parallel electron beam to a fluorescent screen with a resolution presently better than 0.2 nm.

TEM micrographs of the two kinds of support (-Al_2O_3, -solvothermal) and different cobalt catalysts are shown in **Figure 5.15** and **Figure 5.16**. For the supports, they apparently illustrated that -solvothermal and -Al_2O_3 showed spherical structure and wrinkled sheet, respectively. For cobalt catalysts, the dark spots represented cobalt oxide species dispersing on the different supports after calcination of samples. It was found that the dispersion of cobalt oxide species was good. The crystallite size of cobalt was very small (less than 10 nm) and agglomerated as the polycrystals. However, cobalt oxide appeared to be more agglomerated on the -Al_2O_3 than on the other catalysts as shown by the appearance of larger cobalt oxide granules.

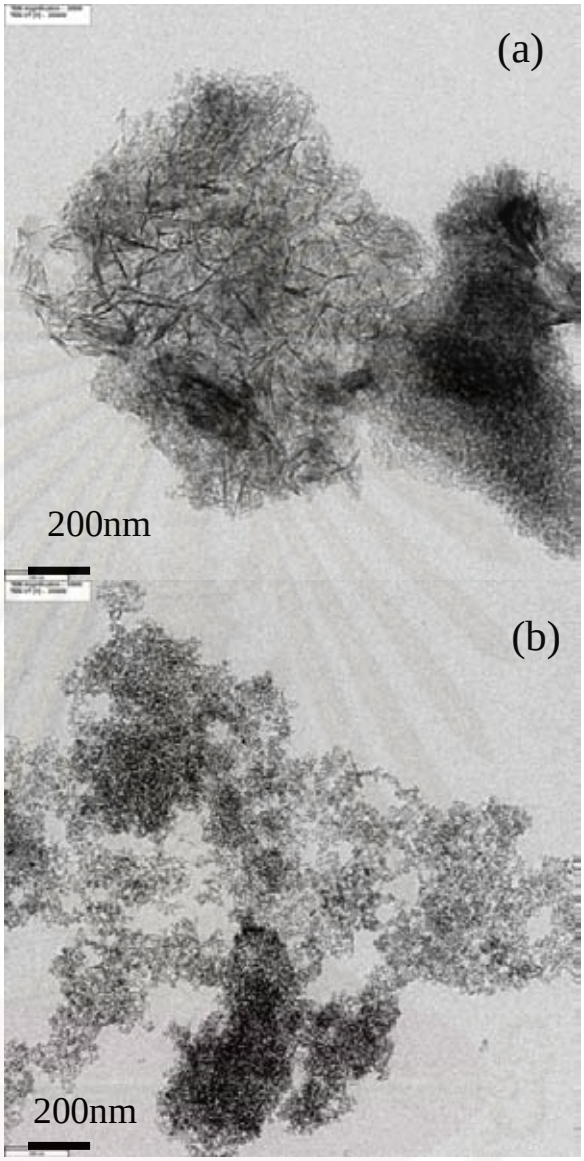

Figure 5.15 TEM micrographs of the -Al_2O_3(a), -solvothermal(b).

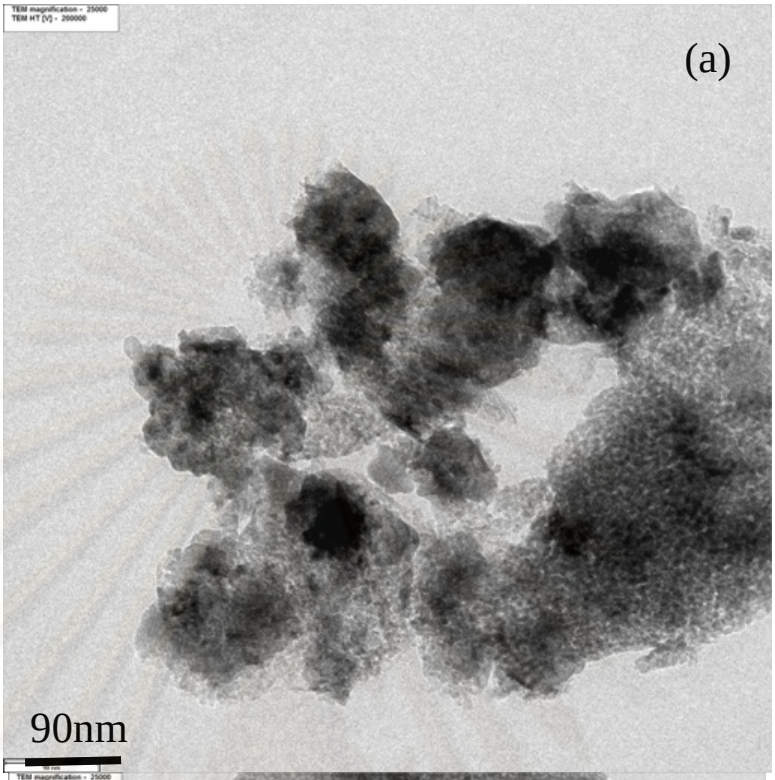
(a)
90nm

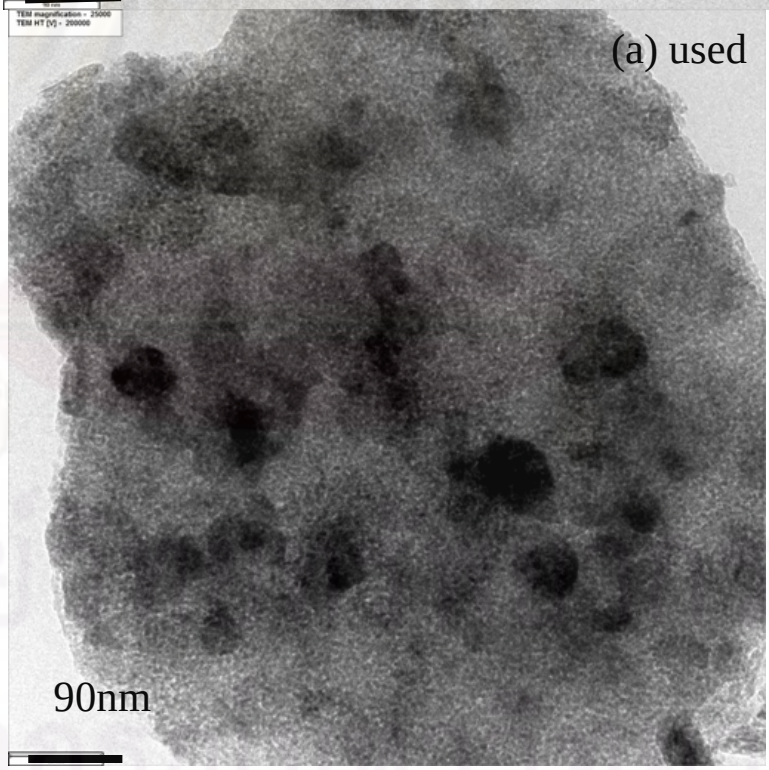
(a) used
90nm

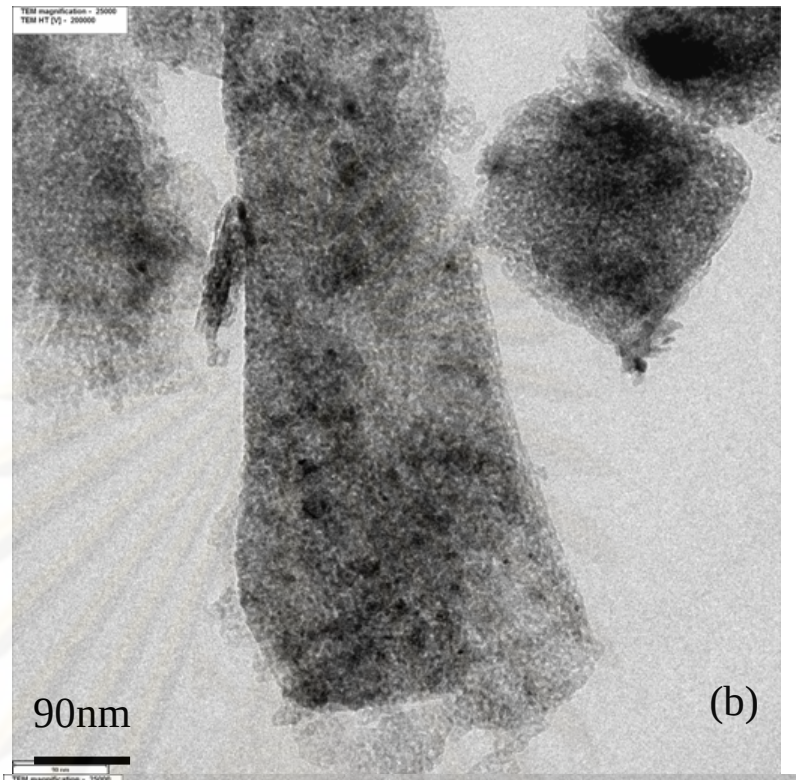
90nm
(b)

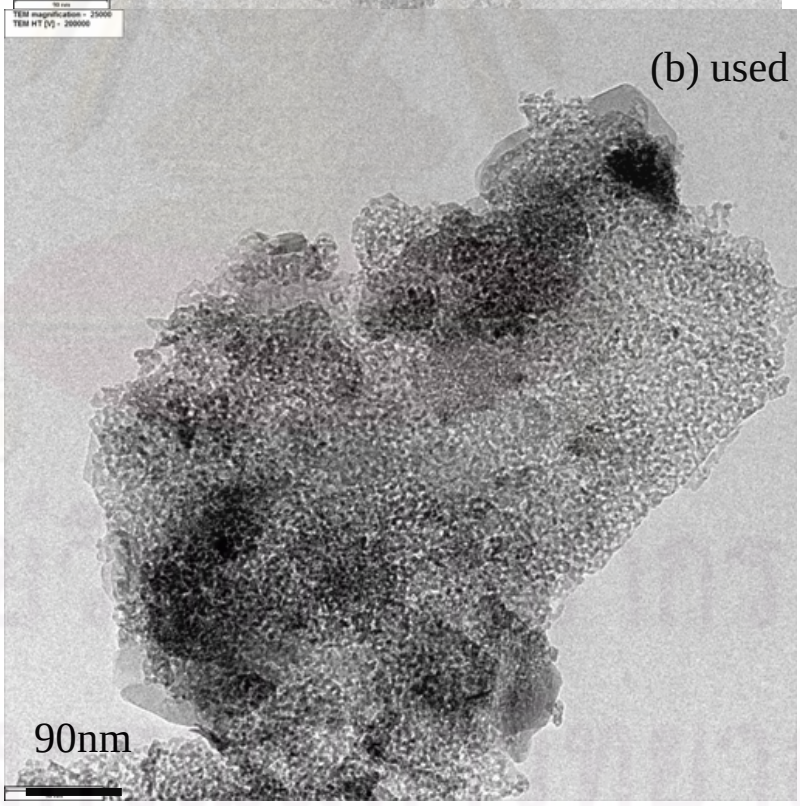
(b) used
90nm

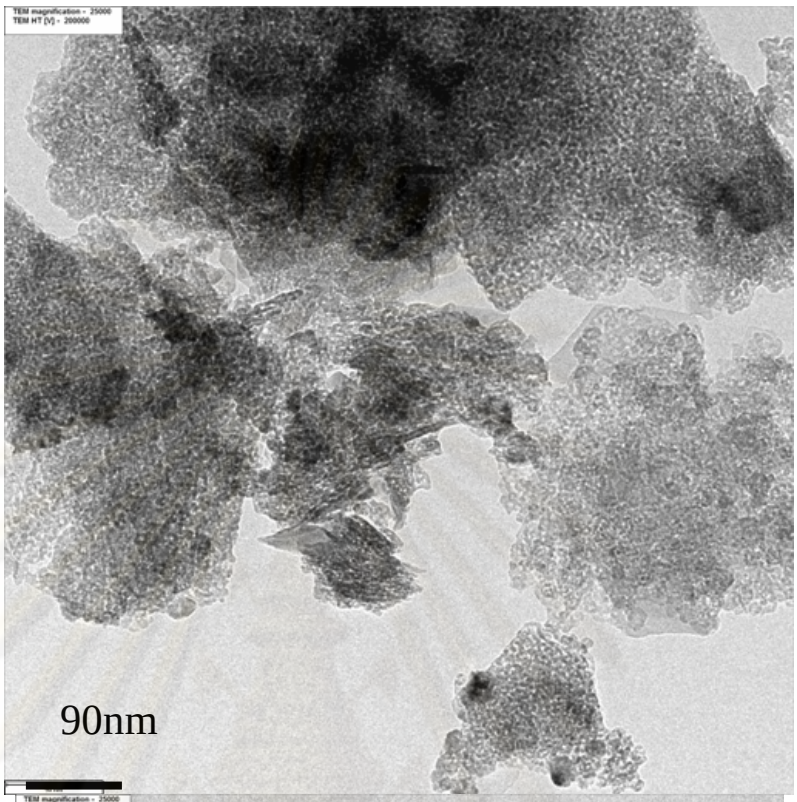

(c)

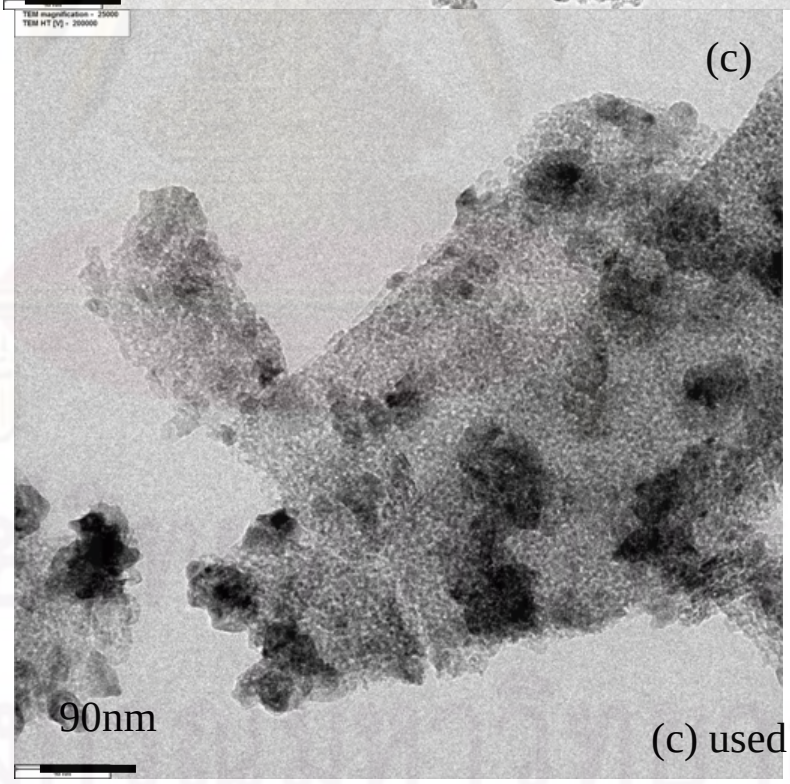

(c) used

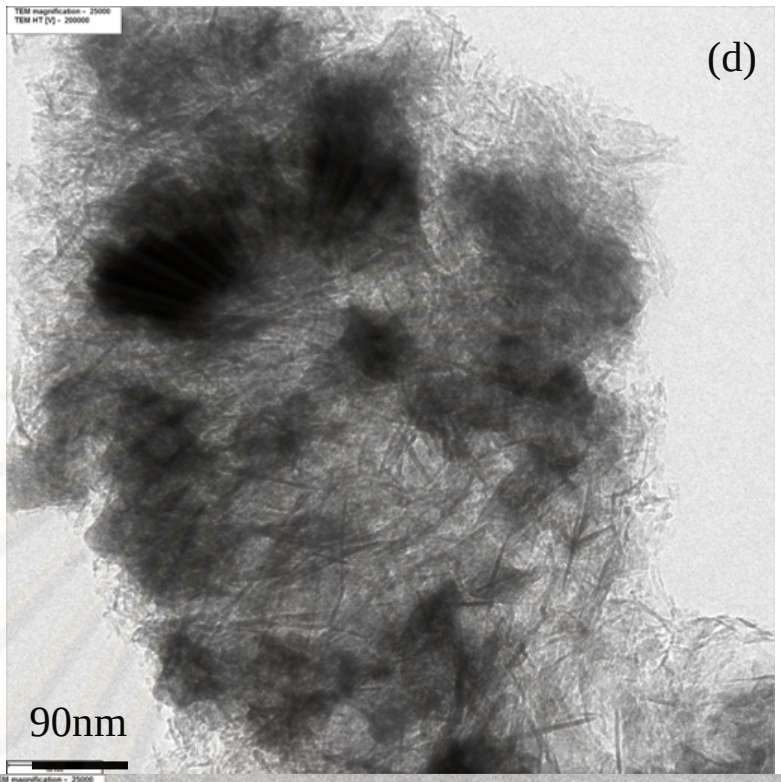
(d)
90nm

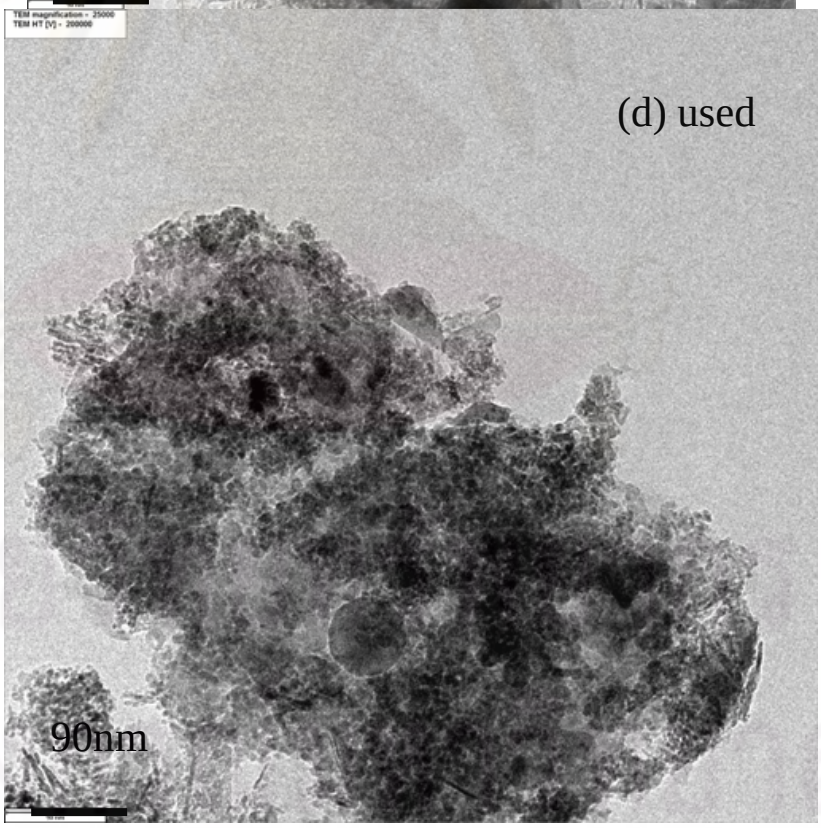
(d) used
90nm

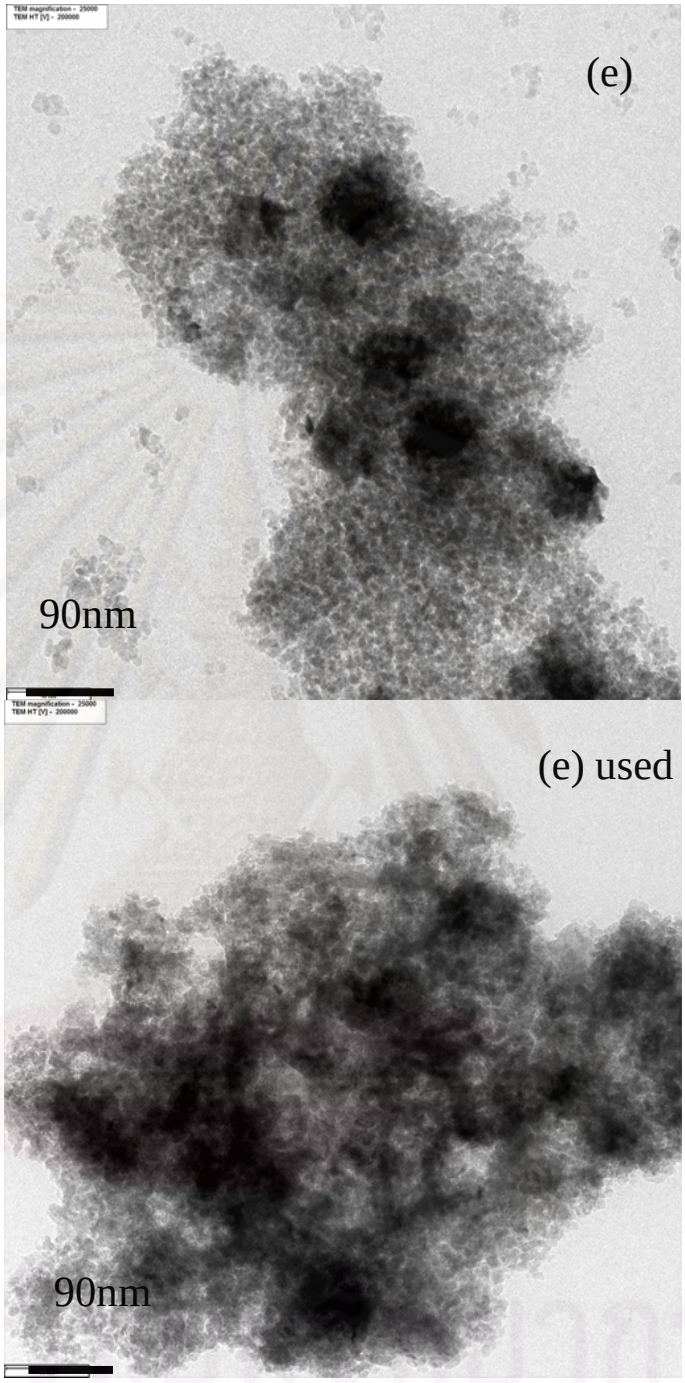

Figure 5.16 TEM micrographs of fresh and used catalysts. Co/88 -FG (a), Co/95 -FG (b), Co/100 -FG (c), Co/ -Al_2O_3 (d), Co/ -solvothermal (e).

5.3.2 Activities of CO hydrogenation

The conversion, reaction rate, TOF (based on the number of reduced surface cobalt atoms measured from CO chemisorption), and product selectivity during CO hydrogenation at steady-state are given in **Table 5.10**. The conversion of the Co catalysts on supports prepared from thermal decomposition of gibbsite changed when gibbsite at different milling times was used. The rate of these catalysts increased with increasing milling time, and slightly decreased in C_1 selectivity. However, for Co/100 -FG and Co/95 -FG, the activities appeared to be not significantly different, suggesting that particle size of supports (or milling time) had little impact on the activities. For Co/ -Al_2O_3, the conversion and the rate of reaction were lower than those of other catalysts. It can be attributed to lower number of active sites. Nevertheless, the C_2-C_4 selectivity of this catalyst showed the highest values. The rate vs. time on stream of the Co catalysts is illustrated in **Figure 5.17**. The rate of cobalt catalysts on supports prepared from thermal decomposition of gibbsite was lower than that of Co/ -solvothermal. The increased activity for Co catalysts on supports prepared from thermal decomposition of gibbsite can be attributed to the dispersion of Co metal on the catalysts as seen from CO chemisorption and TPR results. For Co/100 -FG and Co/95 -FG, the activities had similar trend because the physicochemical properties of these catalysts were similar. However, the activity of most catalysts was lower than that of Co/ -solvothermal. Typically, the activity of cobalt catalysts on Al_2O_3 (Bae, 2009), SiO_2 (Yan, 2009), TiO_2 (Duvenhage, 2005) and mixed supports (Jongsomjit, 2006) usually decreases with increasing time on steam because heat and water occurred during the reaction results in sintering of catalysts as well as active cobalt may rearrange on support surface. However, the Co/ -solvothermal performed the good activity and stable rate because high thermal stability (Mekasuwandumrong, 2006) and single spherical structure. From TPR profile of Co/ -solvothermal, the interaction of cobalt particles and -solvothermal was stronger than that on other catalysts. These properties might provide high stability of cobalt particles without altering the electronic property of Co_3O_4 (as seen from XPS

data). In addition, the larger average pore size and pore volume of Co/ -solvothermal and -solvothermal (table 5.7) resulted in good properties of active cobalt. The cobalt particles can be effectively dispersed on the surface and/or in pore of support. When considered the difference in rate between the cobalt catalysts of supports prepared thermal decomposition of gibbsite (Co/100 -FG, Co/95 -FG and Co/88 -FG). It is indicated that milling method (physical improvement) could increase activity of CO hydrogenation. TEM observation of the spent catalysts is showed in **Figure 5.16**. Morphology of the spent Co/ -solvolthermal, Co/88 -FG, Co/95 -FG and Co/100 -FG was similar to the starting catalyst (Figure 5.16), while the structure of Co/ -Al_2O_3 was changed. The wrinkled sheet structure of -Al_2O_3 disappeared. In addition, the irregular and flaky particles of -Al_2O_3 produced from thermal decomposition of gibbsite may result in lower stability of cobalt particles on surface compared to CO/ -solvothermal. The total acidity concentration as determined by NH_3-TPD in mmol NH_3/g cat. revealed that acidity of -solvolthermal (8.8 mmol NH_3/g cat.) was lower than that of 100 -FG (9.7 mmol NH_3/g cat.). The alumina with weaker acidity has shown to result in higher Co/alumina activity because the formation of inactive surface cobalt aluminate decreased (Zhang, 2003).

Since CO hydrogenation is a structure insensitive reaction, therefore the catalytic activity depends only on the number of reduced Co metal surface atoms available for catalyzing the reaction. The calculated TOFs at steady state of the samples are summarized in Table 5.10. They are in the range of 1×10^{-2} s^{-1}-typical of Co catalyst under these conditions (Kogelbauer, 1996, Jongsomjit, 2002, Kittiruangrayab, 2008). Considering the TOFs calculated based on CO chemisorption of the catalysts, it was found that TOFs of Co catalysts on all the alumina supports were essentially similar. Since TOF can be derived from the intrinsic rate by definition, the intrinsic activity of the samples remained constant.

Table 5.10 The conversion, reaction rate, TOF and product selectivity during CO hydrogenation at initial and steady-state conditions

Samples	Conversion[a] (%)		Rate[c] (10^{-2}g CH_2/g.cat h)	TOF[d] (10^3 s^{-1})	Product selectivity[c] (%)	
	Initial[b]	Steady state[c]			C_1	C_2-C_4
Co/ -solvothermal	84.1	78.8	59	10.2	99.5	0.5
Co/100 -FG	87.2	60.9	46	6.6	99.3	0.7
Co/95 -FG	87.2	60.9	46	5.9	99.3	0.7
Co/88 -FG	91.6	55.3	41	6.8	98.5	1.5
Co/ -Al_2O_3	67.6	46.6	35	5.7	98.3	1.7

[a] CO hydrogenation was carried out at 220 C, 1 atm, and H_2/CO/Ar = 20/2/8, GSHV= 11400 h^{-1}.

[b] After 5 min of reaction.

[c] After 6 h of reaction.

[d] The TOF calculation was based on CO chemisorption

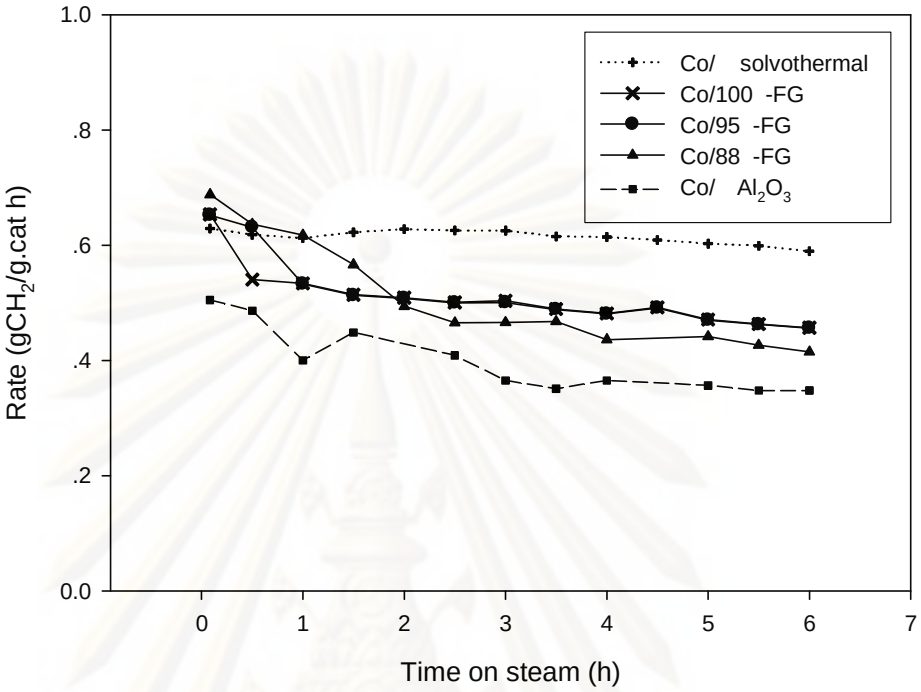

Figure 5.17 The rate vs. time on stream of the cobalt catalysts.

CHAPTER VI

CONCLUSIONS AND RECOMMENDATIONS

6.1 Conclusions

The present work revealed the physicochemical properties of χ-Al_2O_3 prepared from thermal decomposition of milled fine gibbsite and cobalt on χ-Al_2O_3 supported catalysts. It can be concluded as follows:

1. High purity nanocrystalline χ-alumina was produced from milled gibbsite (FG12h and FG24h). The transformation temperature of gibbsite to χ-alumina decreased from 450 to 350°C when milling time of fine gibbsite was increased from 12 to 24 h, respectively. For the unmilled gibbsite (FG0h), the mixed phases between χ and γ-phase Al_2O_3 were formed at 450°C.

2. The fraction of χ-alumina increased with increasing milling time and calcination temperature. The activation energy for phase transformation of gibbsite to χ-Al_2O_3 also decreased with reducing particle size of the starting gibbsite.

3. The Co/100χ-FG, Co/95χ-FG, and Co/88χ-FG showed higher activity at initial conditions because of the higher number of active sites. Nevertheless, at steady state conditions, the activity of Co/χ-solvothermal showed the highest performance. It was due to high thermal stability and stable cobalt particles on surface. Moreover, the activity of Co/γ-Al_2O_3 was lower than that of Co/100χ-FG, Co/95χ-FG, and Co/88χ-FG, and Co/χ-solvothermal.

6.2 Recommendations

1. The residual fraction of χ-Al_2O_3 prepared from thermal decomposition of milled fine gibbsite should be investigated.

2. The properties of cobalt on χ-solvothermal and χ-Al_2O_3 prepared from thermal decomposition of milled fine gibbsite should be studied by EXAFS (Extended X-ray Absorption Fine Structure) technique in order to investigate the cobalt coordination number, O_2 titration to find %reducibility and IR spectra in order to study the mechanism of adsorbed CO.

3. The effect of seeding on phase transformation of gibbsite to χ-Al_2O_3 should be investigated.

REFERENCES

Ahmad, A.L. and Muatafa, N.N.N. Sol-gel synthesized of nanocomposite palladium-alumina ceramic membrane for H_2 permeability: Preparation and characterization. International Journal of Hydrogen Energy 32 (2007): 2010-2021.

Alex, T., C.; Kumar, R.; Roy, S., K. and Mehrotra, S., P. Stirred bead mill grinding of gibbsite: surface and morphological change. Advanced powder technology 19 (2008): 483-391.

Bae, W., J.; Kim, M., S.; Lee, J.,Y.; Lee, J.,M. and Jun, W., K. Enhanced Fischer–Tropsch activity on Co/P–Al2O3 catalyst: Effect of phosphorous content. Catalysis Communications 10 (2009): 1358-1362.

Bhattacharya, I. N.; Das, S. C.; Mukherjee, P. S.; Paul, S. and Mitra P. K. Thermal decomposition of precipitated fine aluminium trihydroxide. Scandinavian Journal of Metallurgy 33 (2004): 211-219.

Borg, Ø. et al. Electron microscopy study of -Al_2O_3 supported cobalt Fischer-Tropsch synthesis catalysts. Catalysis Letter 126 (2008): 224-230.

Borg, Ø et al. Fischer-Tropsch synthesis over un-promoted and Re-promoted -Al_2O_3 support cobalt catalyst with different pore size. Catalysis Today 142 (2009): 70-77.

Boumaza, A et al. Transition alumina phases induced by heat treatment of boehmite: An X-ray diffraction and infrared spectroscopy study. Journal of solid state Chemistry 182 (2009): 1171-1176.

Brindley, W., G. and Choe, O., J. The reaction series, gibbsite to chi alumina to kappa alumina to corundum. Journal of the Mineralogical society of America 46 (1961).

Burakorn, T.; Panpranot, J.; Mekasuwandumrong, O.; Chaisuk, C.; Praserthdam, P. and Jongsomjit, B. Characterization of cobalt dispersed on the mixed nanoscale alumina and zirconia supports. Journal of Materials Processing Technology 206 (1961): 352-358.

Candela, L. and Perlmutter, D., D. kinetics of boehmite formation by thermal decomposition of gibbsite. Industrial & Engineering Chemistry Research 31 (1992): 694-700.

Chang, L. P.; Wu, C. Y.; Lai, J. S. and Yen, S. F. Size effects on the -to α-Al_2O_3 phase transformation. Journal of European Ceramic Society 29, 16 (2009): 3341-3348.

Church, S., J.; Cant, W., N. and Trimm, L., D. Stailisation of aluminas by rare earth and alkaline earth ions. Applied catalyst 101 (1993): 105-116.

Du, X.; Su, X.; Wang, Y. and Li, J. Thermal decomposition of grinding activated bayerite. Material Research Bulletin 44 (2009): 660-665.

Duvenhageand, D., J. and Coville, N., J. Fe:Co/TiO_2 bimetallic catalysts for the Fischer–Tropsch reaction: Part 3: The effect of Fe:Co ratio, mixing and loading on FT product selectivity. Applied Catalysis A: General 289 (2005): 231-239.

Dynys, F. W. and Halloran, J. W. Alpha alumina Formation in Alum-Deriver Gamman Alumina. Journal of American Ceramic Society 65 (1982): 442-448.

Gitzen, H.; W. Alumina as a ceramic material. Westerville, Ohio: The American Ceramic Society, 1970.

He, J.; Liu, W.; Zhu, H., L. and Huang, W., Q. Phase transformation behaviors of aluminum hydroxides to alpha alumina in air and molten salt. Journal of Materials Science 40 (2005): 3259-3260.

Hill, R., M.; Bastow, J., T.; Celotto, S. and Hill, J., A. Integrated study of the calcination cycle from gibbsite to corundum. Chemistry of Materials 19 (2007): 2877-2883.

Jang, W., S.; Lee, Y., H.; Lee, M., S.; Lee, W., S. and Shim, B., K. Mechanical activation effect on the transition of gibbsite to α-alumina. Journal of Materials Science Letters 19 (2000): 507-510.

Jongsomjit, B.; and Goodwin Jr., J. G. Co-support compound formation in Co/Al_2O_3 catalysts: effect of reduction gas containing CO. Catalysis Today 77 (2002): 191-204.

Jongsomjit, B.; Wongsalee, T. and Praserthdam, P. Catalytic behaviors of mixed TiO_2-SiO_2-supported cobalt Fischer–Tropsch catalysts for carbon monoxide hydrogenation. Materials Chemistry and Physics 97 (2006): 343-350.

Kano, J.; Saeki, S.; Saito, F.; Tanjo, M. and Yamazaki, S. Application of dry grinding toreduction in transformation temperature of aluminum hydroxides. International Journal of Mineral Processing 60 (2000): 91-100.

Kittiruangrayab, S.; Burakorn, T.; Jongsomjit, B. and Praserthdam, P. Characterization of Cobalt Dispersed on Various Micro- and Nanoscale Silica and Zirconia Supports. Catalysis Letter. 124 (2008): 376-383.

Kogelbauer, A., Goodwin Jr., J. G., and Oukaci, R. Ruthenium Promotion of Co/Al_2O_3 Fischer–Tropsch Catalysts. Journal of Catalysis. 160 (1996): 125-133.

Kraum, M. and Baerns, M. Fischer–Tropsch synthesis: the influence of various cobalt compounds applied in the preparation of supported cobalt catalysts on their performance. Applied Catalysis A: General 186 (1999): 189-200.

Lacroix, M.; Pajonk, M., G. and Teichner, J., S. Silica and alumina catalysts, activated by hudrogen spillover, for the conversion of n-heptane at 270 C. Journal of catalysis 101 (1986): 314-322.

MacKenzie, K.J.D. and Okada, J., T. Thermal decomposition of mechanically activated gibbsite. Thermochimica Acta 327 (1999): 103-108.

Macêdo, F., I., M.; Bertran, A., C. and Osawa, C., C. Kinetic of the α-alumina phase transformation by quantitative X-ray diffraction. Journal of Materials Science 42 (2007): 2830-2836.

Mekasuwandumrong, O.; Kominami, H.; Praserthdam, P. and Inoue, M. Synthesis of thermally stable -alumina by thermal decomposition of aluminum isopropoxide in toluene. Journal of American Ceramic Society 87 (2004): 1543-1549.

Mekasuwandumrong, O.; Pavarajarn, V.; Inoue, M and Praserthdam, P. Preparation and phase transformation behavior of -alumina via solvothermal synthesis. Materials Chemistry and Physics 100 (2006): 445-450.

Mekasuwandumrong, O.; Tantichuwet, P.; Chaisuk, C. and Praserthdam, P. Impact of concentration and Si doping on the properties and phase transformation behavior of nocrystalline alumina prepared via solvothermal synthesis. Materials Chemistry and Physics 107 (2008): 208-214.

Mikhailova, V., Ya.; Sviderskii, A., S.; Mishin, V., I. and Mordkovich, Z., V. Effect of epitaxial growth on the formation of the cobalt catalysts of the Fischer-Tropsch synthesis. Rassian Chemical Bulletin, International Edition 56, 9 (2007) :1922-1926.

Misra, C. Industrial Alumina Chemicals. Washington DC: American Chemical Society, 1986.

Okabe, K., Li, X., Wei, M., and Arakawa, H. Fischer–Tropsch synthesis over Co–SiO_2 catalysts prepared by the sol–gel method. Catalysis Today 89 (2004): 431-438.

Ogata, F., Kawasaki, N., Kabayama, M., Nakamura, T. and Tanada, S. Structure transformation of gibbsite by calcinations. e-Journal of Surface Science and Nanotechnology 4 (2006): 267-259.

Othmer, K. Encyclopedia of chemical technology. Vol 6. 4th ed. New York: A Wiley Interscience Publication, John Wiley&Son, 1991.

Panchula, L., M. and Ying, Y., J. Mechanical synthesis of nanocrytalline α-Al_2O_3 seeds for enhanced transformation kinetics. Nanostructured Materials 9 (1997): 161-164.

Pansanga, K.; Panpranot, J.; Mekasuwandumrong, O.; Satayaprasert, C. and Praserthdam, P. Synthesis of nanocrystalline alumina by thermal decomposition of aluminum isopropoxide in 1-butanol and their application as cobalt catalyst support. Korean Journal of Chemical Engineering 24 (2007): 397-402.

Pansanga, K.; Panpranot, J.; Mekasuwandumrong, O.; Satayaprasert, C.; Goodwin, G.; J. and Praserthdam, P. Effect of mixed - and -crystalline phases in nanocrystalline Al_2O_3 on the dispersion of cobalt on Al_2O_3. Catalysis Communications 9 (2008): 207-212.

Rojanapipatkul, S. and Jongsomjit, B. Synthesis of cobalt on cobalt-aluminate via solvothermal method and its catalytic properties for carbon monoxide hydrogenation. Catalysis Communications 10 (2008): 232-236.

Santos, S., P.; Santos, S., H. and Toledo, S.P. Standard transition aluminas. Electron microscopy studies. Materials Research 3, 4 (2000): 104-114.

Shinohara, K., Golman, B., Uchiyama, T., and Otani, M. Fine-grinding characteristics of hard materials by attrition mill. Powder Technology 103 (1999): 292–296.

Stumpf, H., C.; Russell, S., Allen.; Newsome, W., J. and Tucker, M. Thermal Transformations of Aluminas and Alumina Hydrates - Reaction with 44% Technical Acid. Industrial and Engineering Chemistry 42(7) (1950): 1398-1403.

Tauster, S. J., Fung, S. C., and Garten, R. L. Strong Metal-Support Interactions. Group 8 Noble Metals Supported on TiO_2. Journal of American Ceramic Society 100 (1978): 170-175.

Tonejc, A.; Stubicar, M.; Tonejc, A., M.; Kosanovic, K.; Subotic, B. and Smit, I. Transformation of -AlOOH (boehmite) and $Al(OH)_3$ (gibbsite) to α-Al_2O_3 (corundum) induced by high energy ball milling. Journal of Materials Science Letters 13 (1994): 519-520.

Tristantini, D.; LÖgdberg, S.; Gevert, B.; Borg, Ø. and Holmen, A. The effect of synthesis gas composition on the Fischer-Tropsch synthesis over Co/ -Al_2O_3 and Co-Re/ -Al_2O_3 catalyst. Fuel Processing Technology 88 (2007): 643-649.

Tsvigunov, A., N.; Khotin, V., G.; Krasikov, S., A.; Valasov, S., A. and Svetlov, S., B. Synthesis of new modification of aluminium oxide with the spinel structure under shock-wave action on gibbsite. Glass and Ceramics 56 (1999): 16-18.

Vieira Coelho, A., C.; Souza Santos, H.; Kiyohara, P., K.; Pinto Marcos, K., N. and Souza Santos, P. Surface area, crystal morphology and characterization of transition alumina powders from a new gibbsite precursor. Materials Research 10, 2 (2007): 183-189.

Xie, Z., -P.; Lu, J., -W.; Huang, Y. and Cheng, Y., –B. Influence of α-alumina seed on morphology of grain growth in alumina ceramics from Bayer aluminum hydroxide. Materials Letter 57 (2003): 2501-2508.

Xiong, H.; Zhang, Y.; Wang, S. and Li, J. Fischer-Tropsch synthesis: the effect of Al_2O_3 porosity on the performance of Co/Al_2O_3 catalyst. Catalysis Communications 6 (2005): 512-516.

Xu, D.; Li, W.; Duan, H.; Ge, Q. and Xu, H. Reaction performance and characterization of Co/Al_2O_3 Fischer-Tropsch catalysts promoted with Pt, Pd and Ru. Catalysis Letters 102 (2005): 229-235.

Yan, Z.; Wang, Z.; Bukur, D., B. and Goodman, D., W. Fischer–Tropsch synthesis on a model Co/SiO_2 catalyst. Journal of Catalysis 268 (2009) 196-200.

Yang, J., R.; Yen, S., F.; Lin, M., S. and Chen, C., C. Microstructure-controlled effects on temperature reduction of α-Al_2O_3 crystallite formation. Journal of Crystal Growth 299 (2007): 429-445

Young, R.S. COBALT: Its Chemistry, Metallurgy, and Uses. New York: Reinhold Publishing Corporation, 1960.

Zhang, J.; Chen, J.; Ren, J.; Li, Y. and Sun, Y. Support effect of Co/Al_2O_3 catalysts for Fischer-Tropsch synthesis. Fuel 82 (2003): 581-586.

Zolotovskii, P., B.; Krivoruchko, P., O.; Buyanov, A., R.; Kriger, A., T. and Krjukova, N., G. Study of the effect of the size of hydrargillite crystals on the peculiarities of its thermal decomposition and formation of the phase composition of Al (III) oxide. Reaction Kinetic and Catalytic Letter 22 (1983): 153-157.

Zsoldos, Z. and Guczi, L. Structure and catalytic activity of alumina supported platlnum-cobait blmetalllc catalysts. 3. effect of treatment on the interface layer. The Journal of Physical Chemistry 96 (1992): 9393-9400.

APPENDICES

APPENDIX A

CALCULATION FOR CATALYST PREPARATION

Preparation of 20%Co/Al_2O_3 is shown as follows:

Calculation for the preparation of cobalt loading catalyst (20%Co/Al_2O_3)

Example calculation for the preparation of 20%Co/Al_2O_3

Based on 100 g of catalyst used, the composition of the catalyst will be as follows:

Cobalt = 20 g

Al_2O_3 = 100-20 = 80 g

For 1 g of Al_2O_3

Cobalt required = $1 \times (20/80)$ = 0.25 g

Cobalt 0.25 g was prepared from $Co(NO_3)_2 \cdot 6H_2O$ and molecular weight of Co is 58.93

$$Co(NO_3)_2 \cdot 6H_2O \text{ required} = \frac{MW\ of\ Co(NO_3)_2 \cdot 6H_2O \times cobalt\ required}{MW\ of\ Co}$$

$$= (291.03/58.93) \times 0.25 = 1.23 \text{ g}$$

APPENDIX B

CALCULATION OF THE CRYSTALLITE SIZE

Calculation of the crystallite size by Scherrer equation

The crystallite size was calculated from the half-height width of the diffraction peak of XRD pattern using the Debye-Scherrer equation.

From Scherrer equation:

$$D = \frac{K\lambda}{\beta \cos \theta} \qquad \text{(B.1)}$$

where D = Crystallite size, Å

K = Crystallite-shape factor = 0.9

λ = X-ray wavelength, 1.5418 Å for CuKα

θ = Observed peak angle, degree

β = X-ray diffraction broadening, radian

The X-ray diffraction broadening (β) is the pure width of a powder diffraction free of all broadening due to the experimental equipment. Standard α-alumina is used to observe the instrumental broadening since its crystallite size is larger than 2000 Å. The X-ray diffraction broadening (β) can be obtained by using Warren's formula.

From Warren's formula:

$$\beta^2 = B_M^2 - B_S^2 \qquad \text{(B.2)}$$

$$\beta = \sqrt{B_M^2 - B_S^2}$$

Where B_M = The measured peak width in radians at half peak height.

B_S = The corresponding width of a standard material.

Example: Calculation of the crystallite size of Co_3O_4 on χ-solvothermal

The half-height width of peak = 1.07^{o} (from Figure B.1)

= (2¶ x 1.07)/360

= 0.019 radian

The corresponding half-height width of peak of α-alumina = 0.0041 radian

The pure width = $\sqrt{B_M^2 - B_S^2}$

= $\sqrt{0.019^2 - 0.0041^2}$

= 0.018 radian

β = 0.018 radian

2θ = 36.9^{o}

θ = 18.45^{o}=0.322 radian

λ = 1.5418 Å

The crystallite size = $\frac{0.9 \times 1.5418}{0.018 \cos 0.322}$ = 81.3 Å

= 8.1 nm

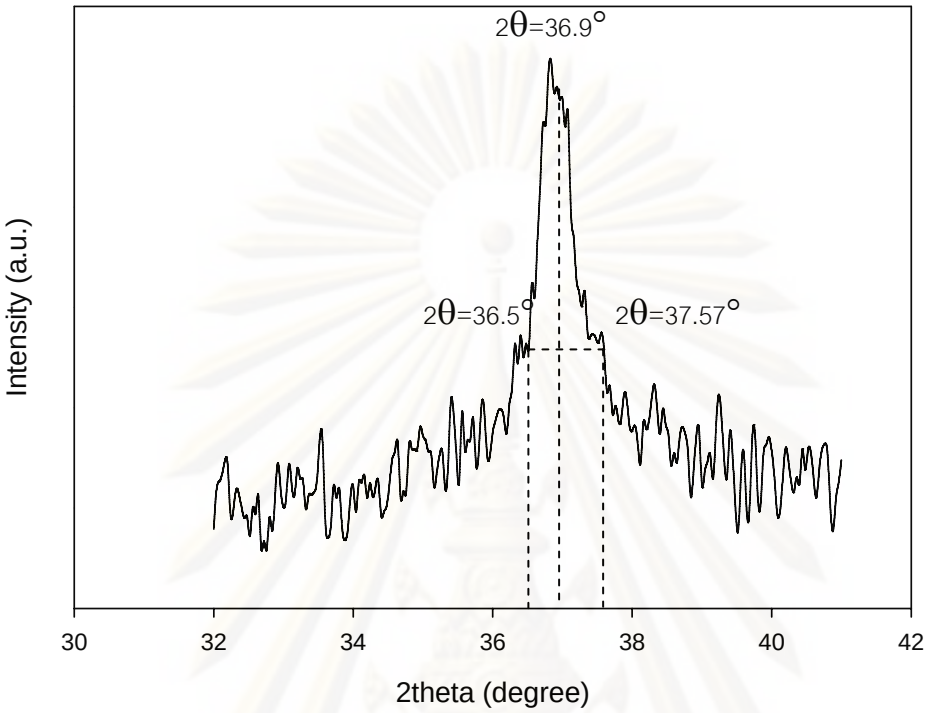

Figure B.1 The measured peak of Co/χ-solvothermal to calculate the crystallite size.

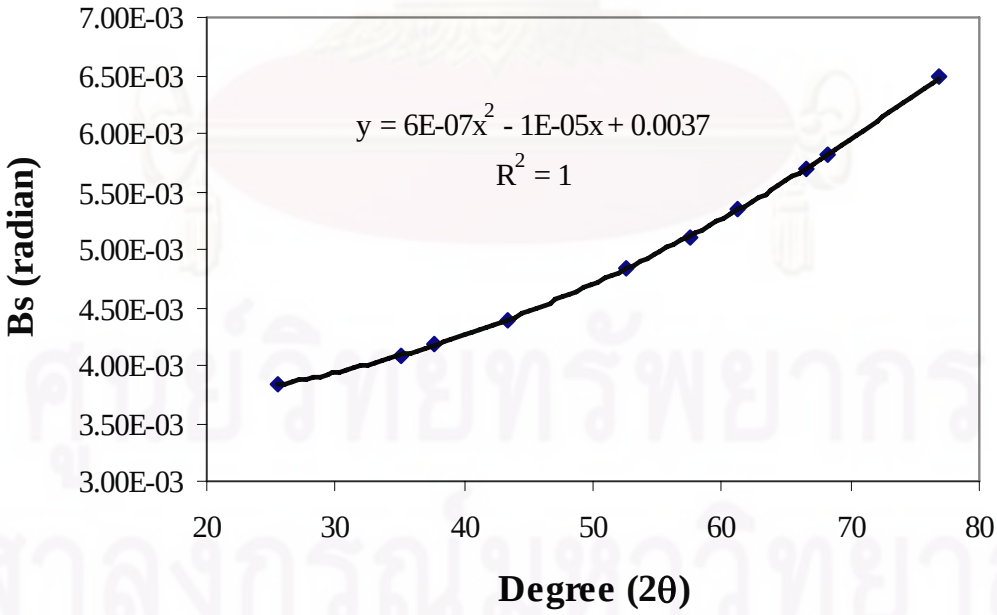

Figure B.2 The plot indicating the value of line broadening due to the equipment. The data were obtained by using α-alumina as standard.

APPENDIX C

CALCULATION FOR TOTAL CO CHEMISSORPTION AND DISPERSION

Calculation of the total CO chemisorption and metal dispersion of the catalyst, a stoichiometry of CO/Co = 1, measured by CO chemisorption is as follows:

Let the weight of catalyst used	=	W	g
Integral area of CO peak after adsorption	=	A	unit
Integral area of 50 µl of standard CO peak	=	B	unit
Amounts of CO adsorbed on catalyst	=	B-A	unit
Concentration of Co	=	C	%wt
Volume of CO adsorbed on catalyst	=	$50 \times [(B-A)/B]$	µl
Volume of 1 mole of CO at 30°C	=	24.86	µl
Mole of CO adsorbed on catalyst	=	$[(B-A)/B] \times [50/24.86]$	µmole

Molecule of CO addorbed on catalysts =

$$[(B-A)/B] \times [50/24.86] \times [6.02 \times 10^{23}] \text{ µmole}$$

Total CO chemisorption (Metal active site)

$$= [(B-A)/B] \times [1.21 \times 10^{24}] \times [1/W] \text{ µmole/g cat}$$

Molecular weight of cobalt = 58.993

Calculation of %metal dispersion

Definition of % metal dispersion :

Metal dispersion (%) = 100×[molecules of Co from CO adsorption/molecules of Co loaded]

In this study, the formula from Chemisorb 2750 Operator's Manual can used for determined the % metal dispersion as follow:

$$\%D = S_f \times [\frac{Vads}{Vg}] \times [\frac{m.w.}{\%M}] \times 100\% \times 100\% \text{.....(C.1)}$$

Where

%D	=	%metal dispersion
S_f	=	stoichiometry factor, (CO on Co* =1)
V_{ads}	=	volume adsorbed (cm^3/g)
V_g	=	molar volume of gas at STP = 22414 (cm^3/mol)
m.w.	=	molecular weight of the metal (a.m.u.)
%M	=	%metal loading

<u>Example: %Dispersion of Co/χ-solvothermal</u>

- Calculation Volume Chemisorbed (V_{ads})

$$V_{ads}(cm^3/g) = [\frac{Vinj}{m}] \times \sum_{i=1}^{n}(1-\frac{Ai}{Af}) \text{.....(C.2)}$$

Where:

V_{ing}	=	volumn injected (cm^3) = 45.2 μL=0.452 cm^3
m	=	mass of sample (g)
Ai	=	area of peak i
Af	=	area of last peak

To replace values in equation (1) and (2);

$$V_{ads} = [\frac{0.452}{0.0509}] \times [(1-\frac{0.00192}{0.00870}) + (1-\frac{0.00836}{0.00870}) + (1-\frac{0.00854}{0.00870}) + (1-\frac{0.00859}{0.00870})]$$

$$= 0.751\ cm^3/g$$

$$\%D = 1 \times [\frac{0.75}{22414}] \times [\frac{58.993}{20}] \times 100\% \times 100\%$$

$$= 0.98\%$$

%Co dispersion is 0.98%

APPENDIX D

CALIBRATION CURVES

This appendix showed the calibration curves for calculation of composition of reactant and products in CO hydrogenation reaction. The reactant is CO and the main product is methane. The other products are linear hydrocarbons of heavier molecular weight that are C_2-C_4 such as ethane, ethylene, propane, propylene and butane.

The thermal conductivity detector, gas chromatography Shimadzu model 8A was used to analyze the concentration of CO by using Molecular sieve 5A column.

The VZ10 column are used with a gas chromatography equipped with a flame ionization detector, Shimadzu model 14B, to analyze the concentration of products including of methane, ethane, ethylene, propane, propylene and butane. Conditions uses in both GC are illustrated in Table D.1.

Mole of reagent in y-axis and area reported by gas chromatography in x-axis are exhibited in the curves. The calibration curves of CO, methane, ethane, ethylene, propane, propylene and butane are illustrated in the following figures.

Table D.1 Conditions use in Shimadzu modal GC-8A and GC-14B.

Parameters	Condition	
	Shimadzu GC-8A	Shimadzu GC-14B
Width	5	5
Slope	50	50
Drift	0	0
Min. area	10	10
T.DBL	0	0
Stop time	8	20
Atten	2	2
Speed	10	3
Method	1	1
Format	1	1
SPL.WT	100	100
IS.WT	1	1

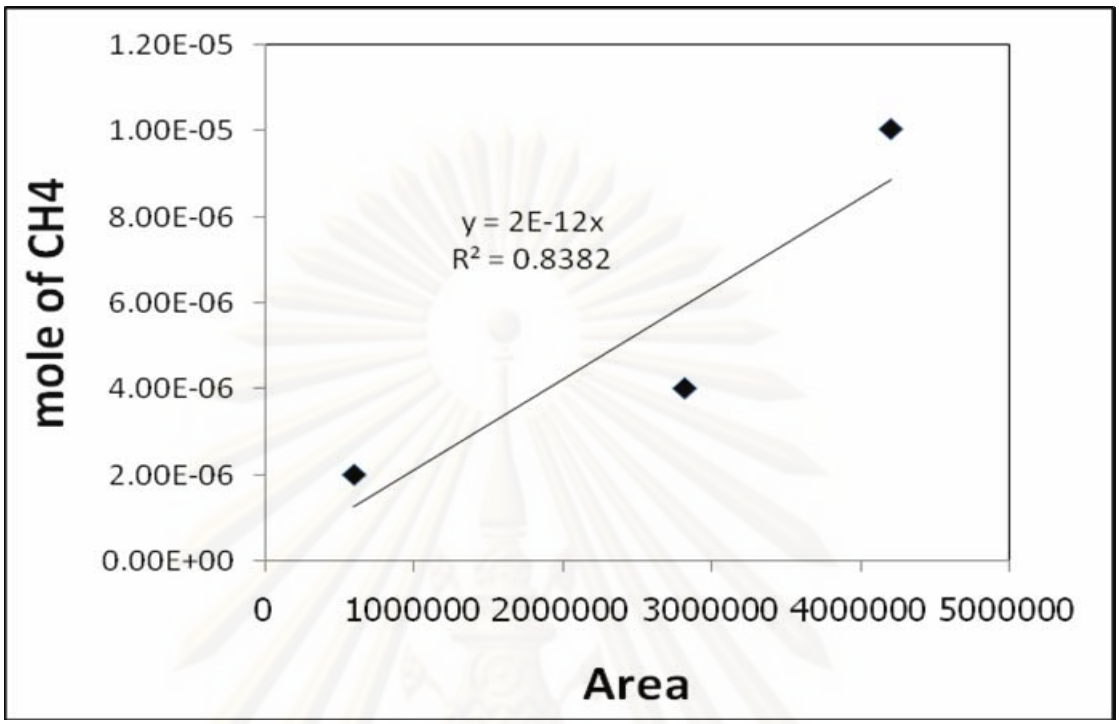

Figure D.1 The calibration curve of methane

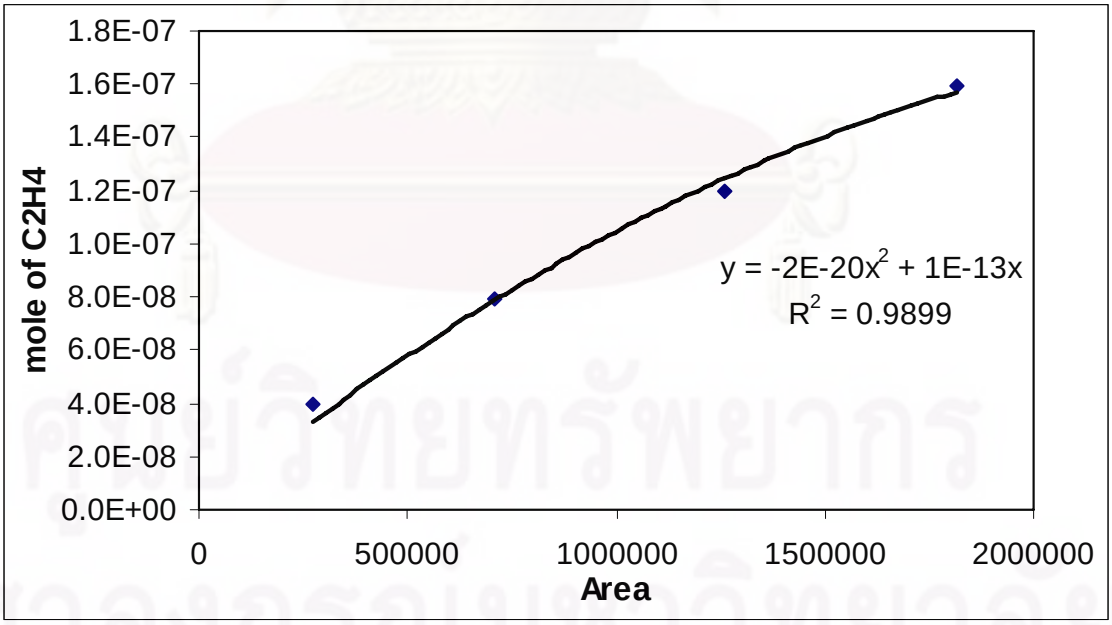

Figure D.2 The calibration curve of ethylene

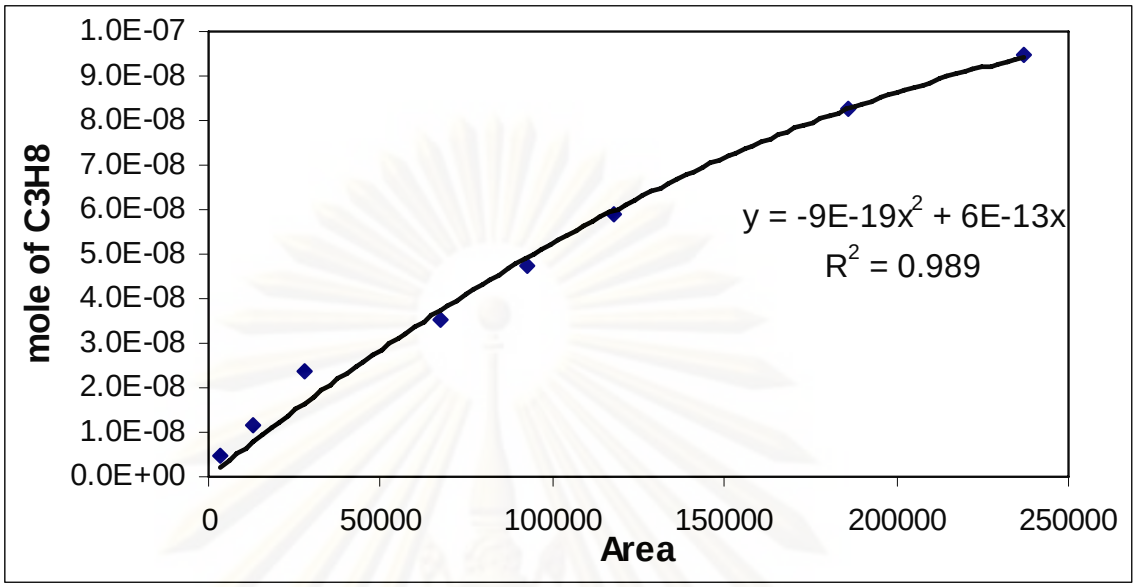

Figure D.3 The calibration curve of propane

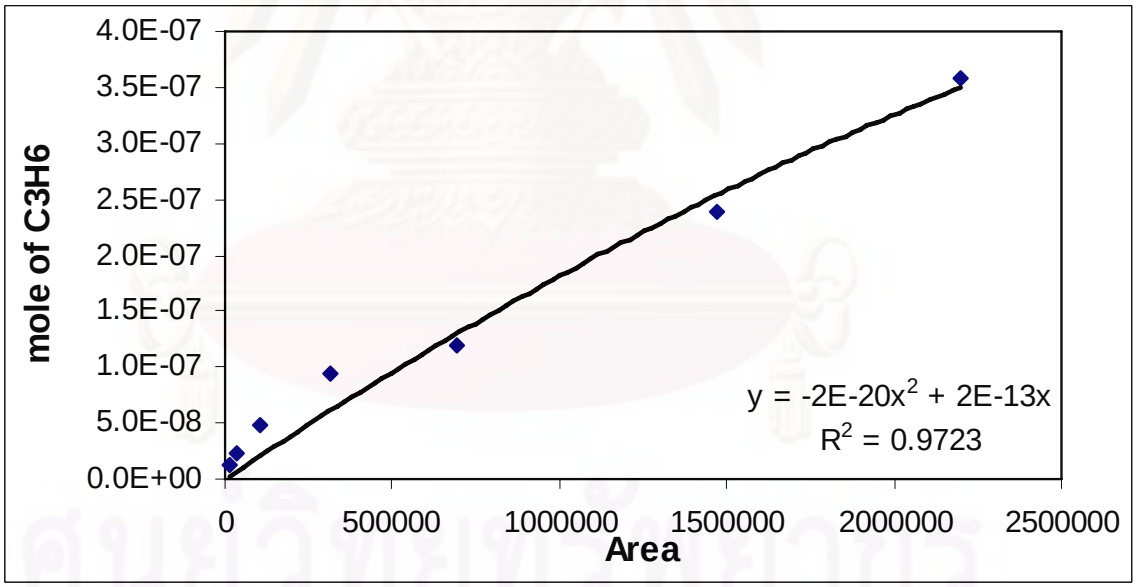

Figure D.4 The calibration curve of propene

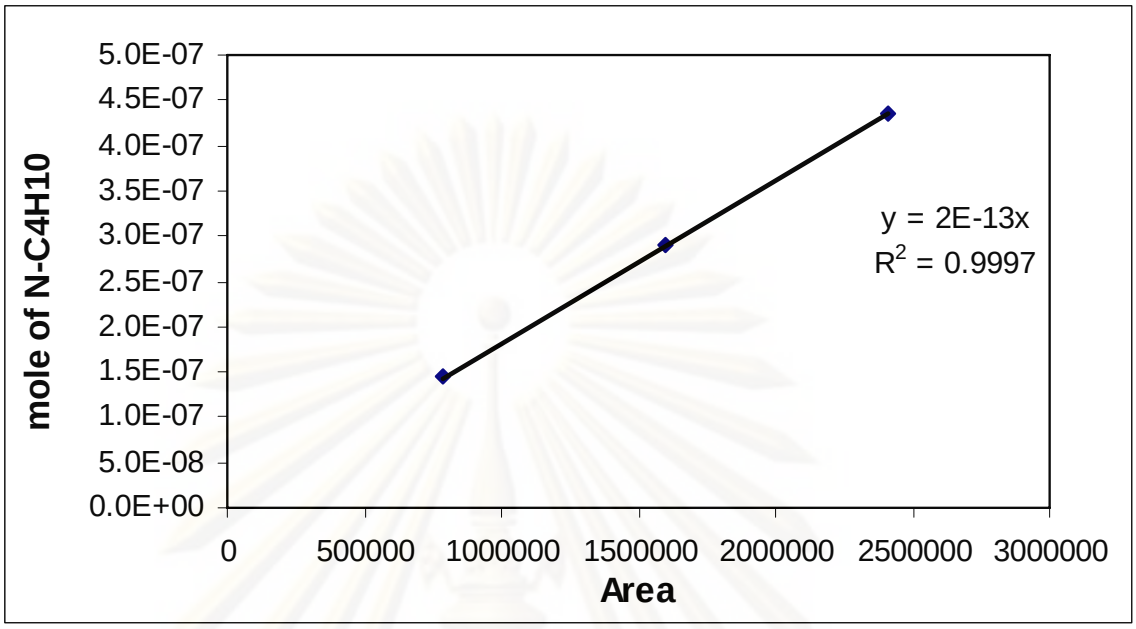

Figure D.5 The calibration curve of butane

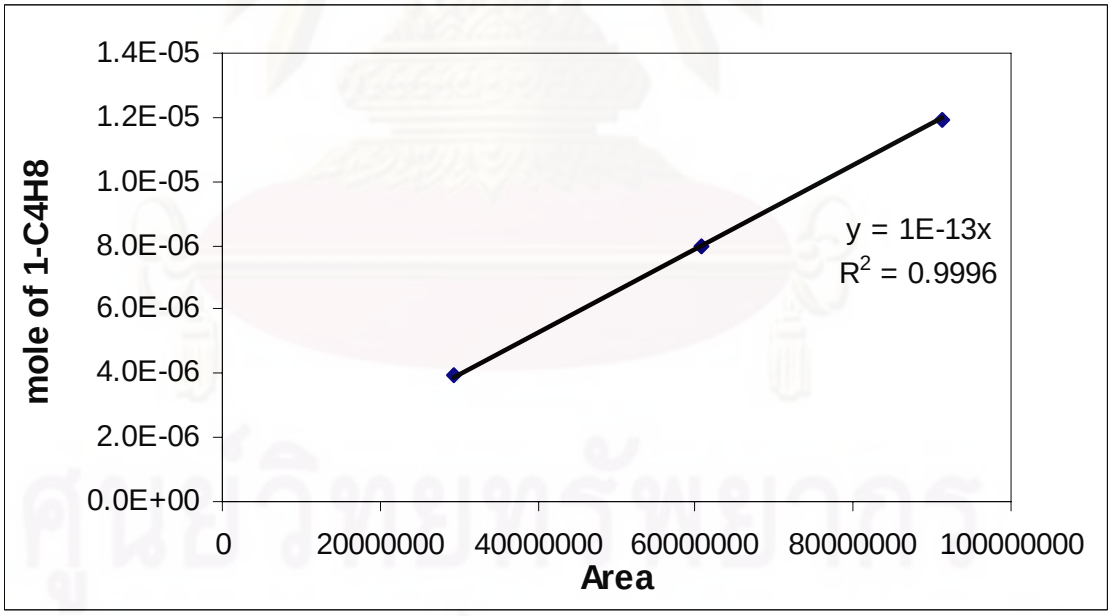

Figure D.6 The calibration curve of butene

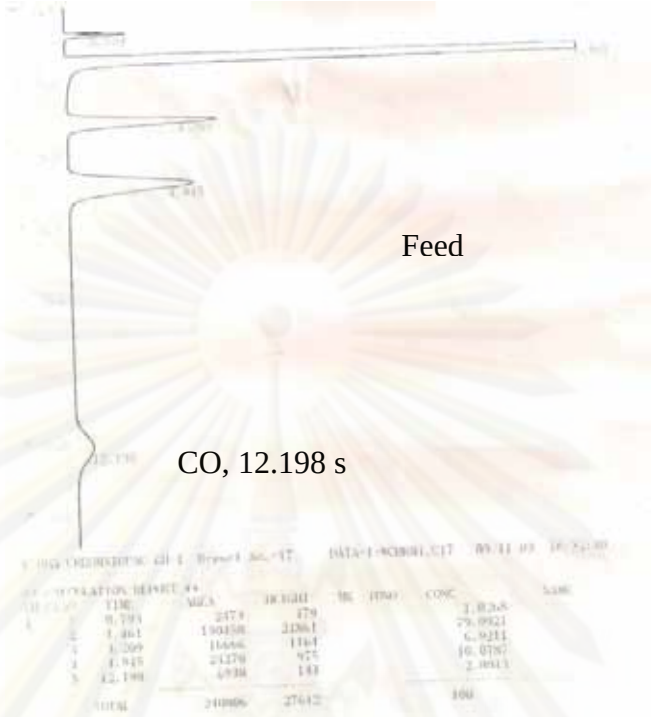

Figure D.7 The chromatograms of catalyst sample from thermal conductivity detector, gas chromatography Shimadzu model 8A (Molecular sieve 5A column)

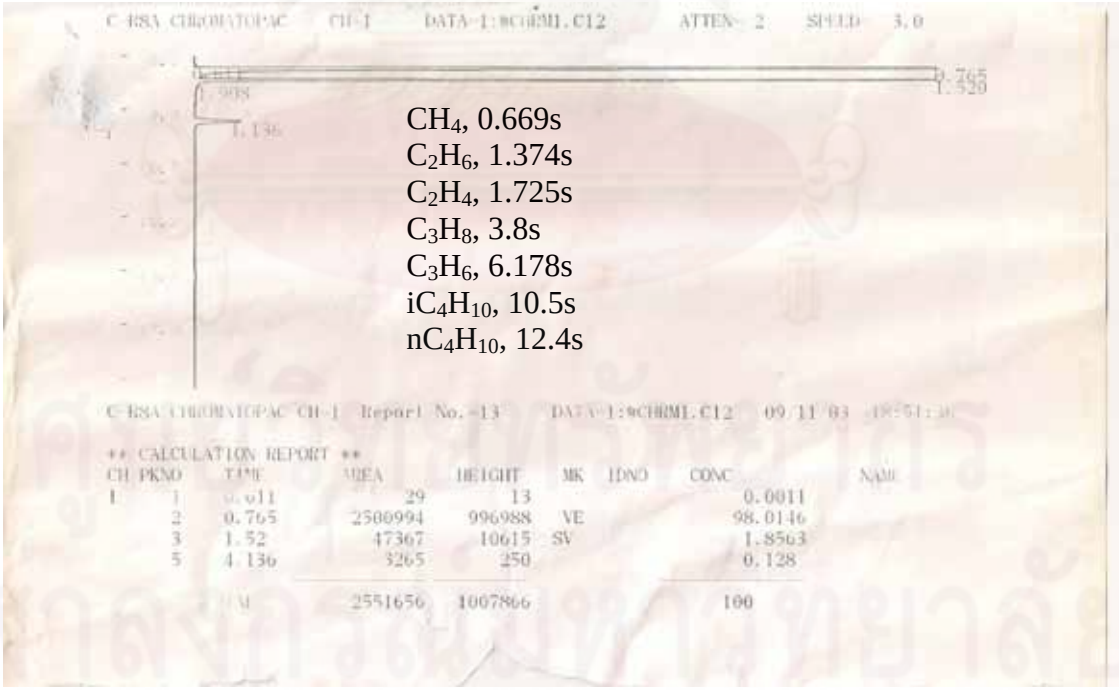

Figure D.8 The chromatograms of catalyst sample from flame ionization detector, gas chromatography Shimadzu model 14B (VZ10 column)

APPENDIX E

CALIBRATION CURVE OF CHI PHASE PERCENT

This appendix showed the calibration curves for calculation of chi phase percent in alumina catalysts which derived from the quantitative XRD of physical mixtures between pure γ- alumina, χ- alumina (CaF_2 as an internal standard) with various contents.

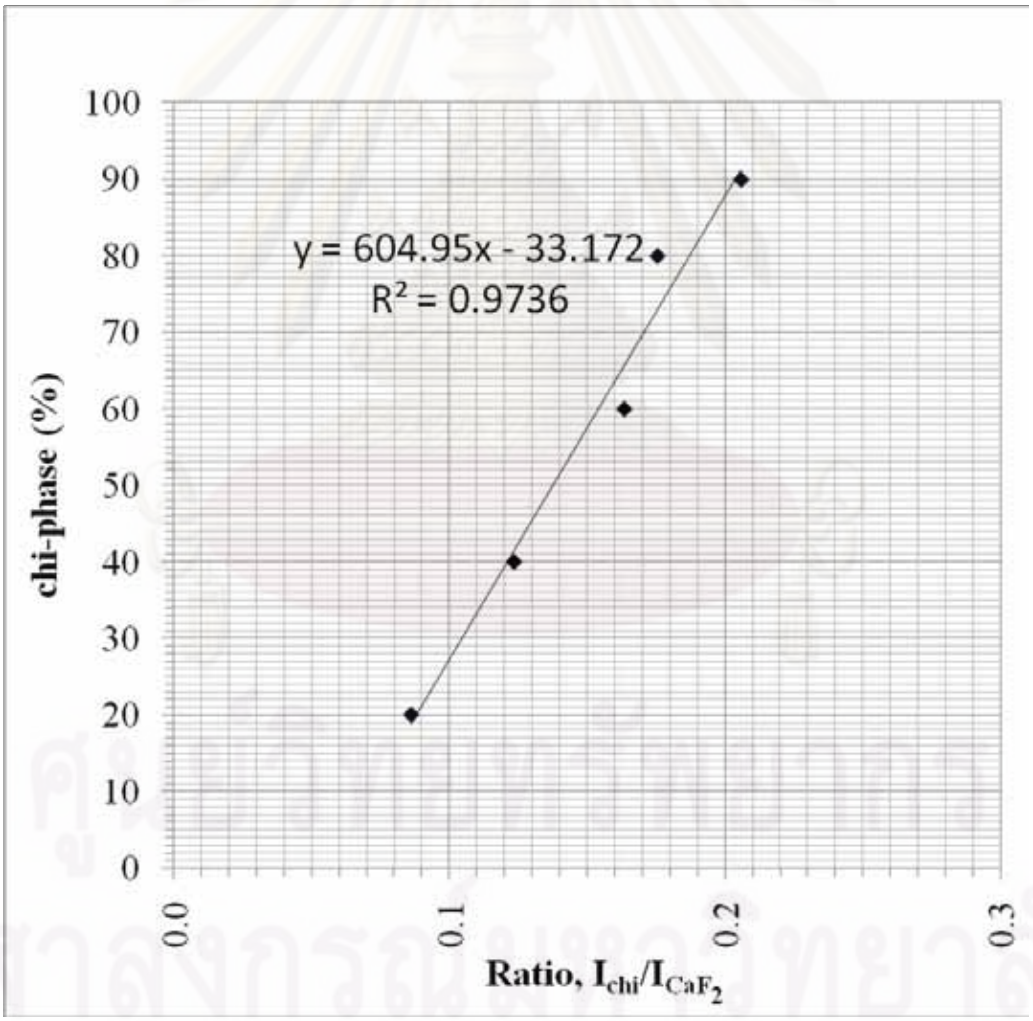

Figure E.1 The calibration curve of chi phase percent in alumina.

APPENDIX F

CALCULATION OF CO CONVERSION, REACTION RATE AND SELECTIVITY

The catalyst performance for the CO hydrogenation was evaluated in terms of activity for CO conversion rate and selectivity.

Activity of the catalyst performed in term of carbon monoxide conversion and reaction rate. Carbon monoxide conversion is defined as moles of CO converted with respect to CO in feed:

$$\text{CO conversion (\%)} = \frac{100 \times [mole\,of\ CO\,in\ feed - mole\,of\ CO\,in\ product]}{mole\,of\ CO\,in\ feed} \quad \text{(i)}$$

Reaction rate was calculated from CO conversion that is as follows:

Let the weight of catalyst used	=	W	g
Flow rate of CO	=	2	cc/min
Reaction time	=	60	min
Weight of CH_2	=	14	g
Volume of 1 mole of gas at 1 atm	=	22400	cc

$$\text{Reaction rate (g } CH_2\text{/g of catalyst)} = \frac{[\%\ conversion\,of\ CO/100] \times 60 \times 14 \times 2}{W \times 22400} \quad \text{(ii)}$$

Selectivity of product is defined as mole of product (B) formed with respect to mole of CO converted:

$$\text{Selectivity of B (\%)} = 100 \times [mole\,of\ B\ formed / mole\,of\ total\ products] \quad \text{(iii)}$$

Where B is product, mole of B can be measured employing the calibration curve of products such as methane, ethane, ethylene, propane, propylene and butane

mole of CH_4 = $(area\,of\ CH_4\ peak\ from\,\mathrm{int}egrator\ plot\,on\,GC - 14B) \times 8 \times 10^{12}$ (iv)

APPENDIX G

CALCULATION OF TURNOVER OF FREQUENCY

Metal active site = y molecule/g catalysts

$$\text{TOF} = \frac{\text{rate}}{(\text{number of active site})}$$

$$= \frac{[\text{molecule substrate conveted}]}{[\text{g cat.}][\text{min}]} \left| \frac{[\text{g cat.}]}{\text{y}\,[\text{active site}]} \right| \frac{[\text{min}]}{[\text{s}]}$$

$$= [\text{s}^{-1}]$$

APPENDIX H

DATA OF CALCULATION OF ACID SITE

Calulation of total acid sites

For example, χ-solvothermal sample, total acid site is calculated from the following step.

1. Conversion of total peak area to peak volume

conversion from Micromeritrics Chemisorb 2750 is equal to 77.5016 ml/area unit. Therefore, total peak volume is derived from

Example: χ-solvothermal catalyst give total peak area is 1.869548 units

Total peak volume = 77.5016 $\times$ total peak area

= 77.5016 $\times$ 1.869548

= 144.89 ml

2. Calculation for adsorbed volume of 15% NH_3

adsorbed volume of 15% NH_3 = 0.15 $\times$ total peak volume

= 0.15 $\times$ 144.89 ml

= 21.73 ml

3. Total acid sties are calculated from the following equation

$$\text{Total acid sites} = \frac{(\text{Adsorbed volume, ml}) \times 101.325\ \text{Pa}}{\left(8.314 \times 10^{-3}\ \frac{\text{Pa} \cdot \text{ml}}{\text{K} \cdot \mu\text{mol}}\right) \times 298\ \text{K} \times (\text{weight of catalyst, g})}$$

For χ-solvothermal catalyst sample 0.1004 g of this sample was measured, therefore

$$\text{Total acid sites} = \frac{21.73ml \times 101.325\ Pa}{\left(8.314 \times 10^{-3}\ \frac{Pa \cdot ml}{K \cdot \mu mol}\right) \times 298\ K \times (0.1004\ g)}$$

= 8,851.5 μmol H^+/g.

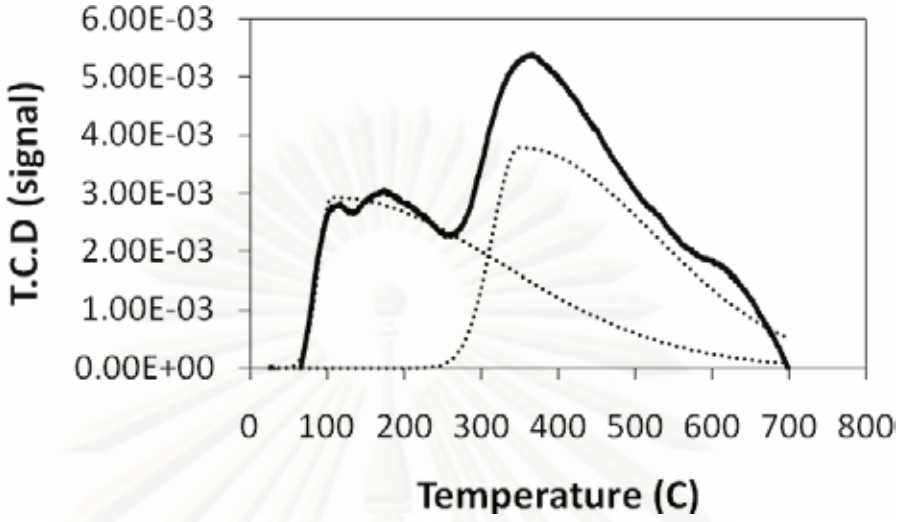

Figure H.1 The NH_3 TPD of χ-solvothermal.

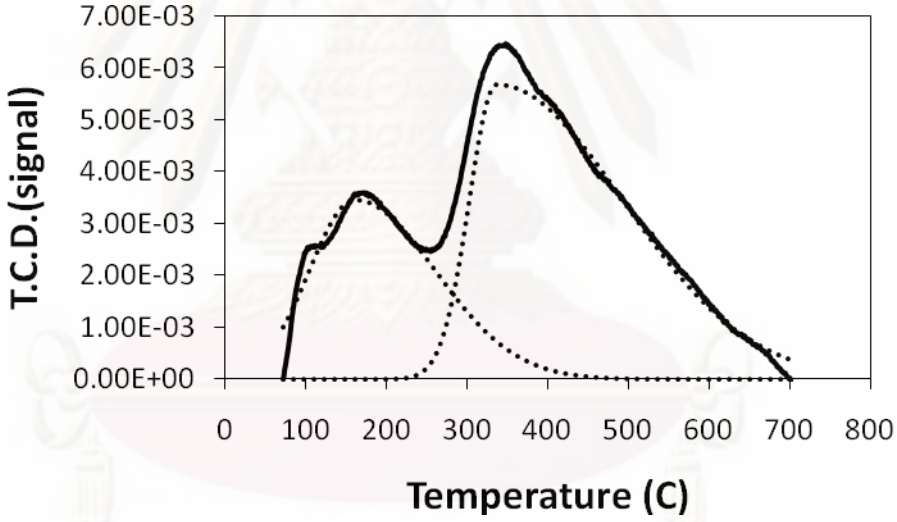

Figure H.2 The NH_3 TPD of FG24h600C (100χ-FG).

VITA

Mr. Wasu Chaitree was born on 31th May 1985, in Bangkok, Thailand. He received his Bachelor degree of Chemical Engineering (1st class honors) from Kasetsart University, Thailand in March 2007. Since May 27, 2008, he has been studying for his Master degree of Engineering from the department of Chemical Engineering, Chulalongkorn University.

List of plublications:

Wasu Chaitree, Sirithan Jiemsirilers, and Joongjai Panpranot, "EFFECT OF MILLING ON THE FORMATION OF χ-ALUMINA FROM GIBBSITE", Proceedings of the 19th Thailand Chemical Engineering and Applied Chemical Conference, Kanchanaburi, Thailand, Oct. 26-27, 2009.

Wasu Chaitree, Sirithan Jiemsirilers, Okorn Mekasuwandumrong, Piyasan Praserthdam, Thawatchai Charinpanitkul, and Joongjai Panpranot, "Effect of Milling on the Formation of Nanocrystalline χ-Al_2O_3 from Gibbsite" will be published in Journal of the American Ceramic Society, 2010.